5-8-2018

Investigation of the Effects of Heating & Quenching on the Mechanical Properties and Microstructure of 22MnB5 Steel Sheets

Jiakai Shi
University of Windsor

Investigation of the Effects of Heating & Quenching on the Microstructure & Mechanical Properties of 22MnB5 Steel Sheets

By

Jiakai Shi

A Thesis
Submitted to the Faculty of Graduate Studies
through the Department of **Mechanical, Automotive & Materials Engineering**
in Partial Fulfillment of the Requirements for
the Degree of **Master of Applied Science**
at the University of Windsor

Windsor, Ontario, Canada

2018

Investigation of the Effects of Heating & Quenching on the Mechanical Properties and Microstructure of 22MnB5 Steel Sheets

By

Jiakai Shi

APPROVED BY:

_____

A.T. Alpas
Mechanical, Automotive & Materials Engineering

_____

V. Stoilov
Mechanical, Automotive & Materials Engineering

_____

D.E. Green, Advisor
Mechanical, Automotive & Materials Engineering

April 30, 2018

Declaration of Originality

I hereby certify that I am the sole author of this thesis and that no part of this thesis has been published or submitted for publication.

I certify that, to the best of my knowledge, my thesis does not infringe upon anyone's copyright nor violate any proprietary rights and that any ideas, techniques, quotations, or any other material from the work of other people included in my thesis, published or otherwise, are fully acknowledged in accordance with the standard referencing practices. Furthermore, to the extent that I have included copyrighted material that surpasses the bounds of fair dealing within the meaning of the Canada Copyright Act, I certify that I have obtained a written permission from the copyright owner(s) to include material(s) in my thesis and have included copies of such copyright clearances to my appendix.

I declare that this is a true copy of my thesis, including any final revisions, as approved by my thesis committee and the Graduate Studies office, and that this thesis has not been submitted for a higher degree to any other University or Institution.

Abstract

Hot stamping of high-strength structural automotive components with tailored mechanical properties will help to reduce vehicle weight as well as improve crashworthiness. The purpose of this research is to establish the relationship between the quenching start temperature in a hot stamping process and the as-quenched mechanical properties and microstructures. A series of heating and quenching trials were carried out on 22MnB5 steel sheets having 2 different thicknesses, and final mechanical properties were determined from tensile tests and corresponding microstructures were analyzed. It was found that when the quenching start temperature is decreased to between 900°C and 720°C, the final strength of the as-quenched steel will rapidly decrease from about 1500 MPa to less than 570 MPa. The results of this research can be used to design structural automotive parts with tailored properties.

Acknowledgements

This thesis has become a reality with the kind support and help of many individuals, and I would like to extend my sincere thanks to all of them.

First, I would like to thank my advisor Dr. Daniel Green for giving me such an opportunity to get involved in this project, for his patience, invaluable supervision, guidance, continuing encouragement, intellectual discussions, thoughtful insights, and so generously taking his time to discuss all aspects of this research, and shared expertise in sheet metal forming throughout my graduate studies and research.

I would like to express my appreciation to my fellow colleagues Yang Song, Alexandra Rose, Mohammad Shirinzadeh Dastgiri, and Iman Sari Sarraf for their help in experimental setup, testing. They always give me valuable ideas and suggestions which inspired me in the process of the research.

Sincere thanks to the technicians at the Centre for Engineering Innovation, especially Andy Jenner for the care and expertise he demonstrated while making the many parts required for the experimental work. Andy helped me numerous times to formulate a plan to solve my problems and he spent a lot of time to make many components for me. The components Andy built were perfectly manufactured, which reflected positively on the University and me when I used them at the industrial partner's research facility. Andy always found a way to find time for my requests despite the many other projects he was working on.

Table of Contents

List of Tables

List of Figures

1 Introduction

1.1 Background

Approximately one-third of the greenhouse gas emissions in the United States come from the transportation sector. And approximately 60% of the transportation emissions are from light-duty vehicles. The United States government mandated a Corporate Average Fuel Economy (CAFE) policy and associated Greenhouse Gas Emission standard in response to the 1973 Oil Crisis. According to CAFE regulations, car manufacturers are required to either increase the fuel efficiency of their vehicles to reduce greenhouse gas emissions by a specific amount every year or pay a penalty, currently $5.50 per 0.1mpg under the standard [1]. The National Highway Traffic Safety Administration (NHTSA) regulates CAFE standards and the U.S. Environmental Protection Agency (EPA) measures vehicle fuel efficiency. As shown in Table 1, the goal for 2025 is to almost double the target for 2012. Historically, although the EPA encourages people to purchase more fuel-efficient cars, the NHTSA sets standards for the safety of the light-weight, fuel-efficient vehicles.

In Canada, similar regulations – the Canadian Environmental Protection Act 1999 (CEPA) were also established. The general approach to setting vehicle emissions standards in Canada is to harmonize them as much as possible with the US EPA federal standards for light-duty vehicles and for heavy-duty vehicles.

Manufacturers are therefore investigating every opportunity to meet the mandated emissions requirements while maintaining the necessary safety standards, by improving engine technology, drivetrain, aerodynamics, etc. One way to improve fuel efficiency is to reduce the vehicle weight by using higher strength materials. By using high-strength sheet materials, the vehicle body components can be thinner and lighter while having the same, or even better, crashworthiness. The safety of vehicles can be improved together with the

weight reduction by using advanced high-strength steels (AHSSs) and ultra-high-strength steels (UHSSs).

Model Year	Passenger Cars				Light Trucks			
	footprint: 41 sq ft (3.8 m^2) or smaller (e.g., 2011 Honda Fit)		footprint: 55 sq ft (5.1 m^2) or bigger (e.g., Mercedes-Benz S-Class)		footprint: 41 sq ft (3.8 m^2) or smaller (e.g., Chevy s10)		footprint: 75 sq ft (7.0 m^2) or bigger (e.g., Ford F-150)	
	CAFE	EPA Window Sticker	CAFE	EPA Window Sticker	CAFE	EPA Window Sticker	CAFE	EPA Window Sticker
2012	36	27	28	21	30	23	22	17
2013	37	28	28.5	22	31	24	22.5	17
2014	38	28	29	22	32	24	23	18
2015	39	29	30	23	33	25	23.5	18
2016	41	31	31	24	34	26	24.5	19
2017	44	33	33	25	36	27	25	19
2018	45	34	34	26	37	28	25	19
2019	47	35	35	26	38	28	25	19
2020	49	36	36	27	39	29	25	19
2021	51	37	38	28	42	31	25	19
2022	53	38	40	30	44	33	26	20
2023	56	40	42	31	46	34	27	21
2024	58	41	44	33	48	36	28.5	22
2025	60	43	46	34	50	37	30	23

Table 1 2011-2025 CAFE standards for each model year in miles per gallon [1]

As the tensile strength of AHSSs and UHSSs increases, however, their formability also decreases, which increases manufacturing challenges and costs. For instance, springback is an enormous challenge in the production of high-strength parts by cold stamping. Therefore, hot stamping has become a very attractive forming process to produce automotive parts with high-strength and complex geometries [2]. Hot stamped parts are usually structural components such as A-Pillars, B-Pillars, roof rails, door beams, tunnels as well as other parts, as shown in Figure 1.

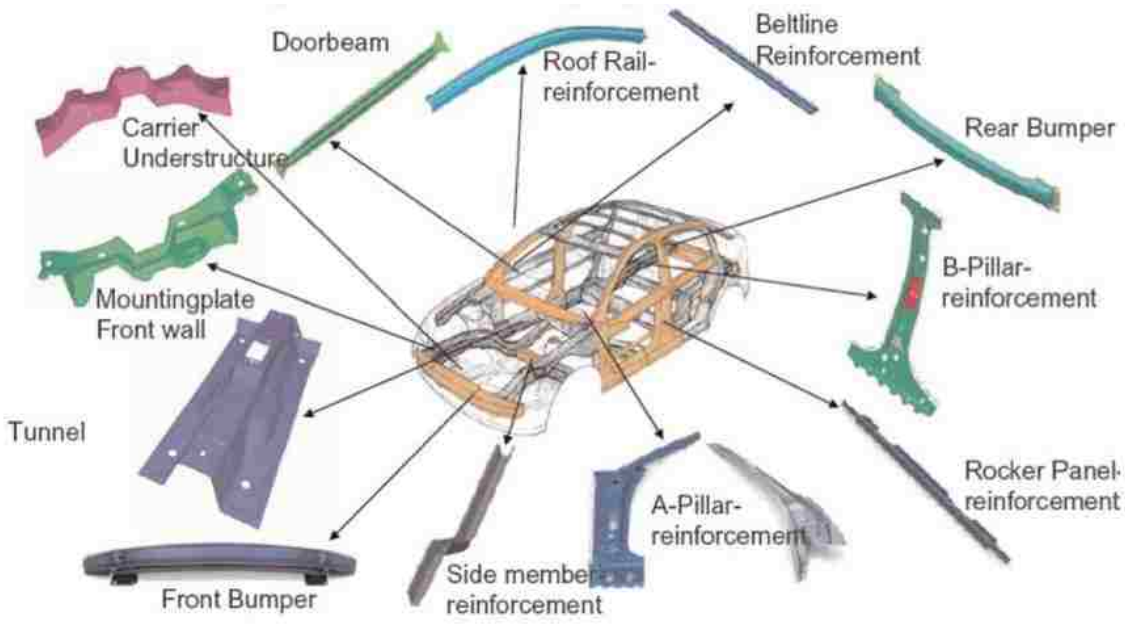

Figure 1 Hot Stamping Components in a Vehicle http://www.interlaken.com/hot-stamping

There are two different approaches to manufacturing hot stamped components: direct and indirect hot stamping [3]. In the direct hot stamping process, the blank is austenitized first in the furnace, then deformed and quenched simultaneously in the dies. In the indirect hot stamping process, the blank is pre-formed at room temperature, then austenitized and quenched [4] (Figure 2). In this thesis, the focus will be on direct hot stamping, since it is more widely used in the industry.

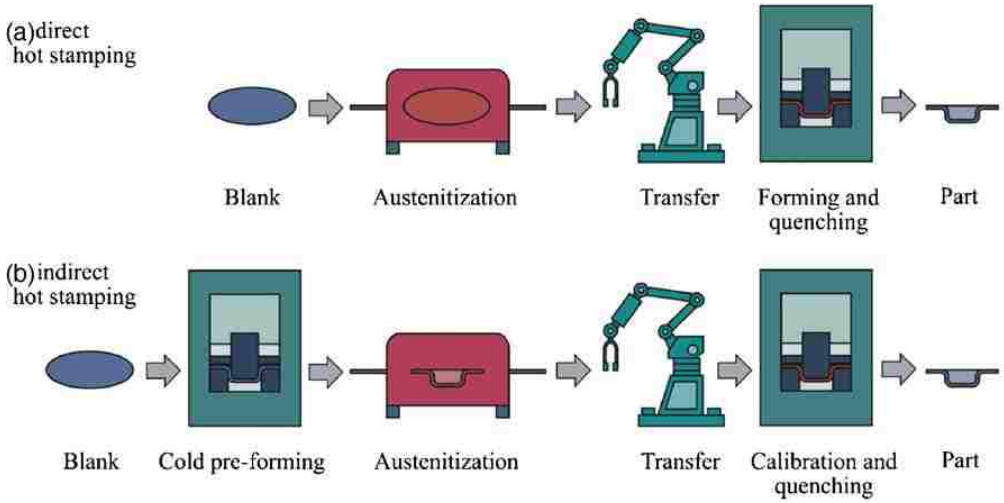

Figure 2 Direct and Indirect Methods of Hot Stamping [5]

1.2 Motivation

In order to further improve vehicle crashworthiness, hot-stamped structural components can be designed with different mechanical properties in different regions (tailored properties). One way to achieve this is to heat the blank in such a way that it has a gradient of temperature from one side to the other, and consequently to obtain different mechanical properties in different locations after quenching. Little research has been done in this area because of the cost and complexity of designing and building this kind of furnace.

Ford Research and Advanced Engineering purchased a customized electrical resistance furnace with three different heating zones and good insulation between each zone. This state-of-the-art furnace was located next to the hydraulic metal forming press in the Mechanical Testing Laboratory at the University of Windsor. The furnace was designed such that the temperature can be independently controlled in each heating zone. With this new flexible heating approach, it is possible to study the relationship among the initial temperature of the blank in the furnace, cooling speed, clamping pressure in the die, final as-quenched mechanical properties, and corresponding microstructures.

1.3 Research Objectives

The primary objective of this research is to establish relationships between starting temperatures and as-quenched mechanical properties for both 1.8 mm and 0.9 mm thickness 22MnB5 steel sheets.

1.4 Overview of the Thesis

The main subdivisions of this thesis are as follows: Chapter 2 is a review of the literature

on the sheet materials used for hot stamping applications, the effect of cooling rate in the quenching process, and the different methods to achieve tailored properties in a hot stamped part.

Chapter 3 describes the experimental procedures that were used to conduct hot stamping tests, tensile tests, microstructure observation and finite element simulations of the heating and quenching process.

Chapter 4 presents the experimental and numerical results that were obtained. The numerical predictions are also compared to the experimental results. The relations between starting temperature and mechanical properties and corresponding microstructure are established.

Chapter 5 discusses how the mechanical properties change with the starting temperature and the possible reasons for the trends that are observed. The mechanical properties and the corresponding microstructure of as-quenched sheets are also discussed.

Chapter 6 lists the conclusions of the research. The relationship between the starting temperature and mechanical properties has been established. Finally, suggestions for future research and improvement of the equipment setup are also presented.

2 Literature Review

2.1 Materials for Hot Stamping Sheet

Boron steel is typically used to produce hot stamped parts because of its high tensile strength and good hardenability. The alloying elements (i.e., Mn, Cr) have little effect on the strength after quenching, but they do have high influence on hardenability. This grade of steel is called boron steel because boron is the element that influences hardenability the most [6]. Naderi [7] tested ten different types of UHSS using a Schenck Press which allowed for either water cooling or nitrogen cooling of the punch. (Table 2). All the sheet steels Table 2 were hot stamped and quenched using both methods for cooling the punch.

Steel	Thickness-mm	C	Si	Mn	Cr	Ni	Al	Ti	B	N
8MnCrB3	3.5	0.07	0.21	0.75	0.37	0.01	0.05	0.048	0.002	0.006
20MnB5	2.7	0.16	0.40	1.05	0.23	0.01	0.04	0.034	0.001	-
22MnB5	1, 1.5, 2.8	0.23	0.22	1.18	0.16	0.12	0.03	0.040	0.002	0.005
27MnCrB5	3	0.25	0.21	1.24	0.34	0.01	0.03	0.042	0.002	0.004
37MnB4	3	0.33	0.31	0.81	0.19	0.02	0.03	0.046	0.001	0.006
MSW1200	1.5	0.14	0.12	1.71	0.55	0.06	0.02	0.002	0.000	-
DP1400	1	0.19	0.55	1.61	0.02	0.05	0.04	0.003	0.000	0.006
DP1000	1.5	0.15	0.57	1.45	0.01	0.03	0.04	0.003	0.000	0.003
DP800	1	0.12	0.24	1.45	0.02	0.04	0.03	0.002	0.000	0.004
TRIP800	1	0.20	1.81	1.48	0.04	0.03	0.04	0.006	0.00	-

Table 2 Chemical composition of ten different UHSS used in Naderi's study [3]

The results showed that only 22MnB5, 27MnCrB5, and 37MnB4 sheets can reach a fully martensitic microstructure when quenched in a water-cooled die. Moreover, when quenched in the nitrogen cooled die, only 22MnB5 and 37MnB4 were able to reach a fully martensitic microstructure. The sheet material that is most commonly used for automotive hot stamping applications is 22MnB5. Boron steel has a pearlitic–ferritic microstructure and has a tensile strength of about 600 MPa in its as-delivered state. After hot stamping, the strength of boron steel can be increased to over 1500 MPa due to the martensitic

transformation. A boron steel blank is typically heated in a furnace up to 930°C for 3-5 minutes to achieve a homogeneous austenitic microstructure. The hot blank is then rapidly transferred to a forming die with a built-in cooling system, and the forming process is therefore completed while the blank is soft. As the part is rapidly quenched, austenite transforms to martensite. If the cooling rate is greater than the critical cooling rate, which is 27°C/s for this 22MnB5 steel, then the austenite will fully transform to martensite and produce a very strong part [2][7](Table 3). If the cooling rate is less than 27°C/s, the resulting microstructure will contain other, more ductile phases such as bainite, ferrite or pearlite [8]. Based on the continuous cooling transformation (CCT) diagram (Figure 3) for 22MnB5 [9], the martensitic transformation takes place between 425°C and 280°C.

Steel	Al	B	C	Cr	Mn	N	Ni	Si	Ti
20MnB5	0,04	0,001	0,16	0,23	1,05	–	0,01	0,40	0,034
22MnB5	0,03	0,002	0,23	0,16	1,18	0,005	0,12	0,22	0,040
8MnCrB3	0,05	0,002	0,07	0,37	0,75	0,006	0,01	0,21	0,048
27MnCrB5	0,03	0,002	0,25	0,34	1,24	0,004	0,01	0,21	0,042
37MnB4	0,03	0,001	0,33	0,19	0,81	0,006	0,02	0,31	0,046

Steel	Martensite start temperature in °C	Critical cooling rate in K/s	Yield stress in MPa		Tensile strength in MPa	
			As delivered	Hot stamped	As delivered	Hot stamped
20MnB5	450	30	505	967	637	1354
22MnB5	410	27	457	1010	608	1478
8MnCrB3	–*	–*	447	751	520	882
27MnCrB5	400	20	478	1097	638	1611
37MnB4	350	14	580	1378	810	2040

Table 3 Chemical composition and mechanical properties of boron steels [1]

AC_1 and AC_3 temperatures are two key points for heating steel. When the temperature of the steel exceeds AC_1, all the phases start to transform into austenite. The material becomes fully austenitized when the temperature exceeds AC_3.

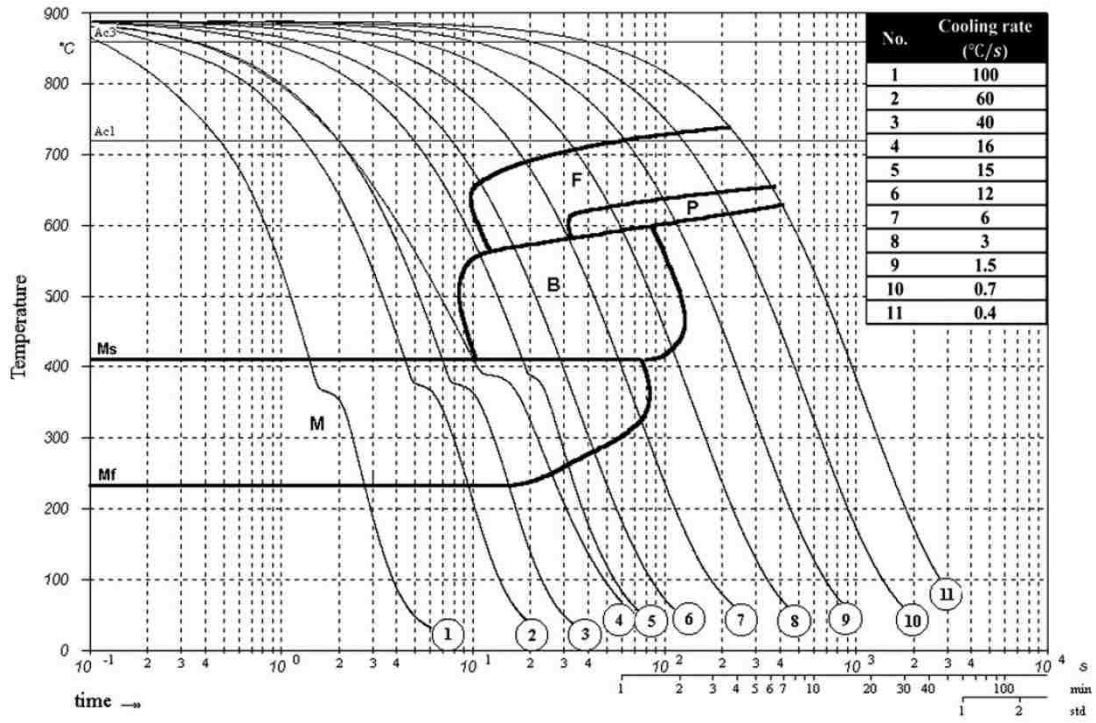

Figure 3 CCT diagram for 22MnB5 steel [2]

Hot stamped parts have very high strength and yet do not exhibit significant springback. Kusumi et al. [10] indicated that such properties not only result from the low flow stress at high temperature but also from the martensitic transformation, which releases the stress imposed in the forming process.

2.2 Cooling Rate

2.2.1 M_s and M_f

The cooling rate that is achieved during the quenching (and forming) processes is very important. In order to develop a fully martensitic microstructure, the cooling rate must be greater than the critical cooling rate (27°C/s for 22MnB5). In addition, the cooling rate also affects the martensite start temperature (M_s), the martensite finish temperature (M_f), and the bainite start temperature (B_s). Nikravesh et al. [11] inserted a 22MnB5 cylindrical specimen into the vacuum chamber of a deformation dilatometer with heating and

quenching process under both deformed and undeformed conditions. M_s, M_f and B_s were also determined from the dilatation versus temperature diagram for each cooling rate [12]. They found that when bainite has been formed before the martensite transformation initiates, the M_s and M_f will increase in both deformed and undeformed conditions as the cooling rate decreases (Table 4 & Table 5). However, if the final state only contains martensite, the M_s and M_f will decrease with the reduction of cooling rate [11]. In addition, according to the data from Table 4 & Table 5, the martensite starts forming from 400°C-460°C while the transformation ends at 200°C-250°C in either the deformed or undeformed condition.

Initial and final transformation temperatures of martensite and bainite in undeformed condition.

Cooling rate (°C/s)	Undeformed condition		
	B_s (°C)	M_s (°C)	M_f (°C)
100		459	267
60		420	253
40		401	249
16	*	359	243
15	*	409	263
12	570	430	282
6	580	444	334
3	580		
1.5	603		

* Omitted data due to the deficiency of volume percent.

Table 4 Influence of cooling rate on B_s, M_s and M_f in undeformed 22MnB5 [11]

Initial and final transformation temperatures of martensite and bainite in deformed condition.

Cooling rate (°C/s)	Deformed condition		
	B_s (°C)	M_s (°C)	M_f (°C)
60	541	405	207
24	622	402	225
12	631	404	240
10	561	426	245
6	*	431	*
3	615	436	*
1.5	617	439	
0.7	617	418	
0.4	611		

* Omitted data due to the deficiency of volume percent.

Table 5 Influence of cooling rate on B_s, M_s and M_f in deformed 22MnB5 [11]

2.2.2 Interfacial Heat Transfer Coefficient

In hot stamping, heat transfer can take place by conduction, radiation and convection. Conduction is the transfer of energy from the more energetic particles of a substance to the adjacent less energetic ones. Heat is also transferred by conduction from the hot sheet to the die that has a lower temperature when quenching takes place. Convection is the mode of energy transfer between a solid surface and the adjacent liquid or gas that is in motion. When a sheet specimen is transferred from the heated furnace to the press, convection takes place from the hot blank to the surrounding air. Radiation is the energy emitted by matter in the form of electromagnetic waves as a result of the changes in the electronic configurations of the atoms or molecules. When a sheet specimen is heated up inside the furnace, radiation takes place from the heating element to the specimen.

The interfacial heat transfer coefficient (IHTC) between the die and the sheet metal has a critical influence on the cooling rate, the temperature distribution, the final microstructure, and consequent mechanical properties. The IHTC is affected by the contact load, the temperature of the blank and the die, the surface roughness of the die, the thickness of the surface oxide, thermal contact resistance, and the thermo-physical properties of the

materials [13].

The heat transfer coefficient between the sheet and the die directly affects the temperature distribution of the specimen throughout the entire forming and quenching process. As the final mechanical properties of the boron steel (22MnB5) strongly depend on the rate of temperature change, the heat transfer coefficient is one of the most important parameters that influence the hot stamping process.

Hung et al. [14] used a die set mounted in an MTS 810 machine to determine the relationship between contact pressure and heat transfer coefficient for boron steel. The inverse method was used to calculate the heat transfer coefficient (Equation 1):

$$h = -\frac{\rho V C_p}{At} \ln\left[\frac{T(t)-T_\infty}{T_0-T_\infty}\right] \quad (1)$$

where A is the area of the contact surface, c_p is the heat capacity, h is the heat transfer coefficient, V is the volume, t is time, T_0 is the initial temperature, T_∞ is the environmental temperature, ρ is the density and $T(t)$ is the temperature of the sheet metal. The authors concluded that the heat transfer coefficient also increases as the contact pressure increases. They also provided a comparison between their results and those from other researchers (Fig. 4). The differences may come from the different sheet materials that were used, the oxide thickness of the blank, the surface roughness of the blank and of the tools, the tool material and the experimental procedures.

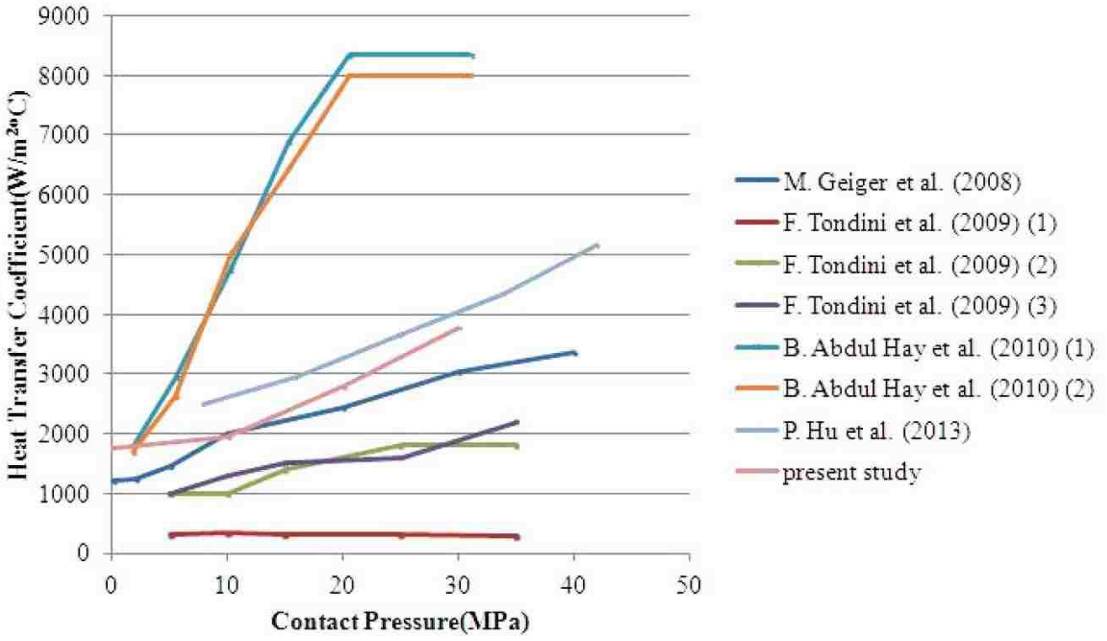

Figure 4 Comparison between Hung et al.'s results and those of other researchers [14]

Abdulhay et al. [15] measured the thermal contact resistance (TCR) under different contact pressures between Usibor1500P steel sheet and tools made of Z160CDV12 steel. By solving a non-linear one-dimensional inverse heat conduction problem, the flux density and surface temperature of both the tool and the steel blank were calculated. It was concluded that the TCR curve had a peak point for each contact pressure and the singularity tended to disappear as the pressure increased. A functional relation was also proposed between TCR and the contact pressure, as shown in Figure 5.

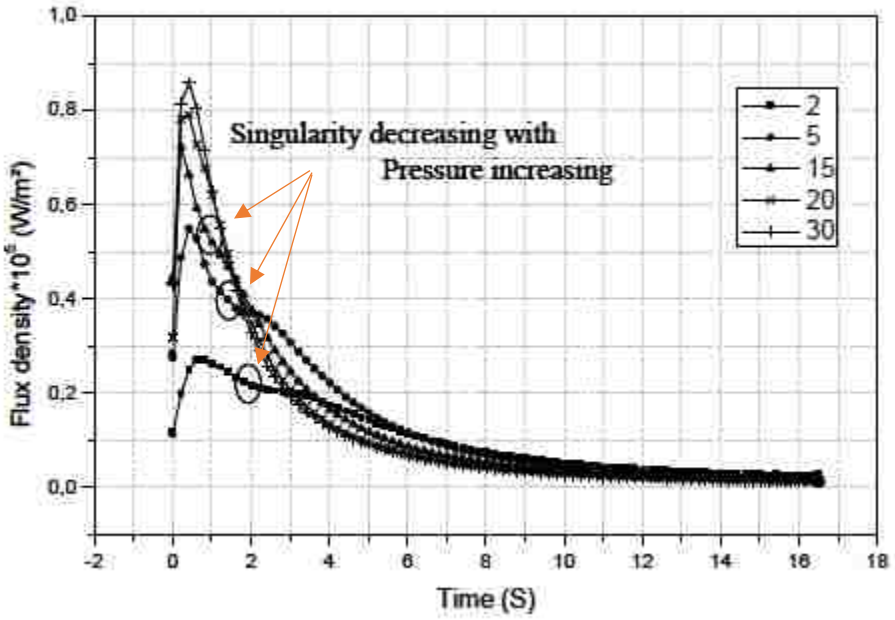

Figure 5 Evolution of flux density with time for Usibor 1500 quenched in Z160CDV12 steel [15]

Hu et al. [16] developed a numerical method to analyze the effects of temperature, pressure and oxide scale thickness during hot stamping. Five different levels of contact pressure were applied from 8 MPa to 42 MPa. To achieve different thickness of the oxide layer from 9 µm and 156 µm, different durations of austenitization from 3 minutes to 60 minutes were held. The experimental setup is shown in Figure 6. It can be concluded that the contact pressure has the most impact on the IHTC. The IHTC decreases when the average temperature between the blank and the die is above 250°C and increases when the latent heat is released. As discussed by the author, when the die temperature was at 250°C, the blank temperature was 380°C. The martensitic transformation just began, and latent heat started to release. The expansion caused by martensitic transformation created more pressure between the blank and the die surface, and therefore the heat conductivity of the oxide scale increased. In addition, the latent heat raised the blank temperature, leading to a greater temperature difference. As a result, the heat transfer coefficient increased.

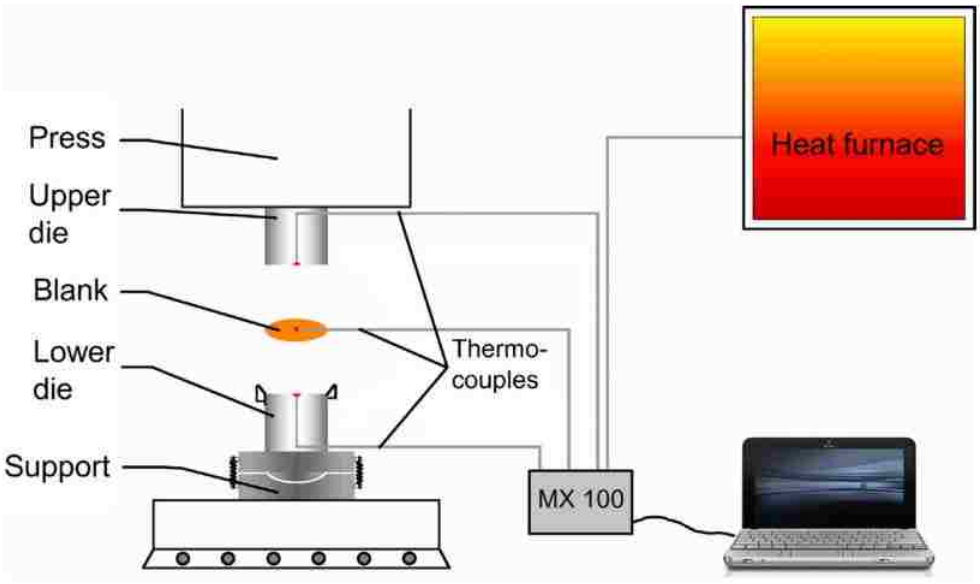

Figure 6 Schematic diagram of heat transfer experimental setup. [16]

2.2.3 Heat Transfer Coefficient vs. Contact Pressure

The topography of the surface of stamping dies and of the sheet metal blank appears rough at the micro-scale. In fact, direct contact between a sheet and the die only occurs at the peaks of the surface, as shown in Figure 7. Between the two surfaces, there are cavities which are filled with air or fluid during the forming process. However, they can be neglected since the cavities are very small and the heat transfer through a fluid is much lower than the conduction between the solid surfaces [17].

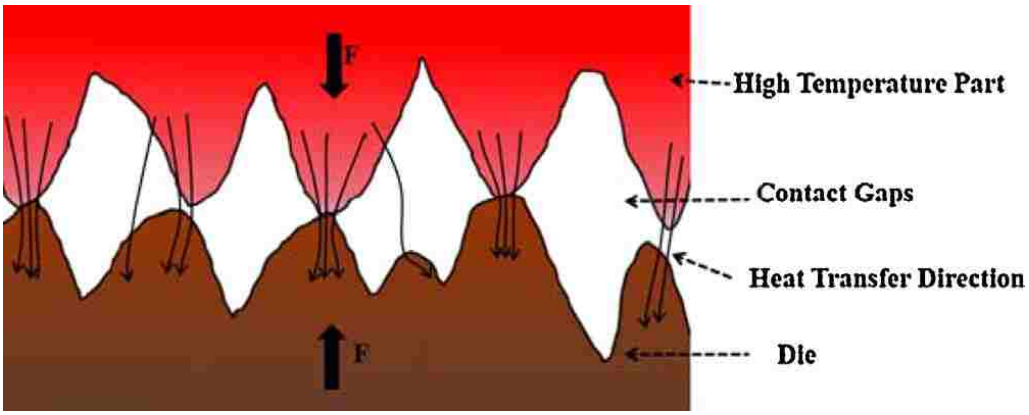

Figure 7 Micro topography at the interface of the blank and die [17].

The contact pressure is the force per unit area that the dies apply on the sheet metal. Merklein et al. [18] built a quenching tool (Figure 8) in a universal mechanical testing machine with a maximum normal force of 400 kN. The die-set contained eight heating cartridges to adjust the temperature of the tool up to 600°C for the determination of heat transfer coefficients. The blanks were heated to 950°C for five minutes to ensure complete austenitization. And the tool temperature was set to 20°C, 100°C, and 300°C in order to determine the heat transfer coefficient in hot stamping tests. It was shown that the heat transfer coefficient increases as the contact pressure between the die and the blank increases (Figure 9). Moreover, the heat transfer coefficient was greatest when the tool temperature was 300°C.

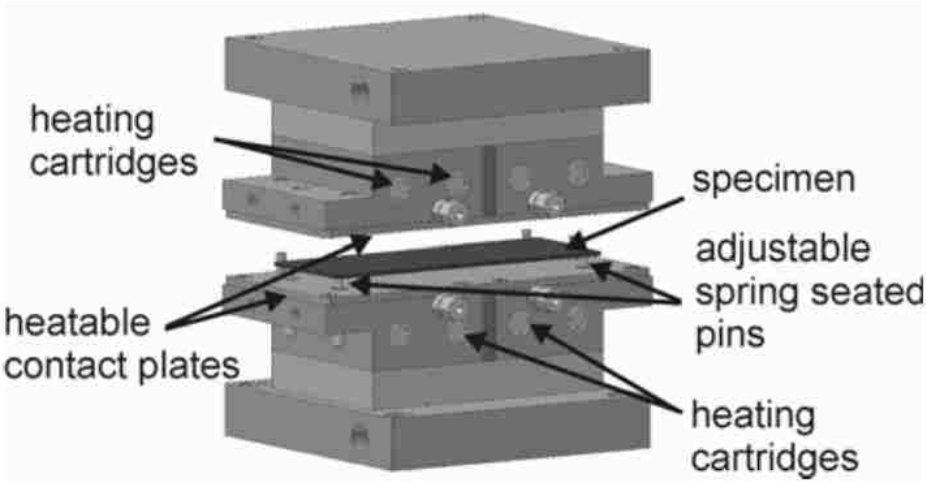

Figure 8 Schematic drawing of the quenching tool with integrated heating cartridges [15]

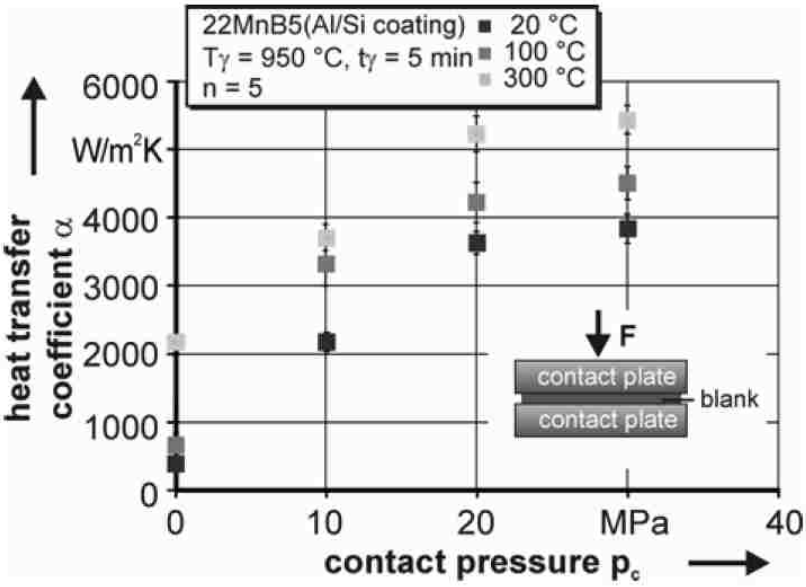

Figure 9 Heat transfer coefficient as a function of the contact pressure for different tool temperatures [15]

At the micro-scale, a larger contact load causes a larger contact area and smaller cavities. Therefore, the heat transfer coefficient increases as a result of the increased contact area. In like manner, the surface roughness also has an influence on the heat transfer coefficient: a smoother surface provides a greater contact area, which decreases the thermal resistance and consequently increases the heat transfer coefficient.

2.2.4 Phase Transformation vs. Heat Transfer Coefficient

When 22MnB5 boron steel is quenched in a die from the austenitic temperature range, it undergoes a martensitic phase transformation around 400°C. In order to clearly determine if the phase transformation affects the heat transfer coefficient, Chang et al. [17] hot stamped two different sheet materials: 22MnB5 (which undergoes a phase transformation during the quenching process) and AISI-304 (which does not exhibit any phase transformation) in the same die to compare the results.

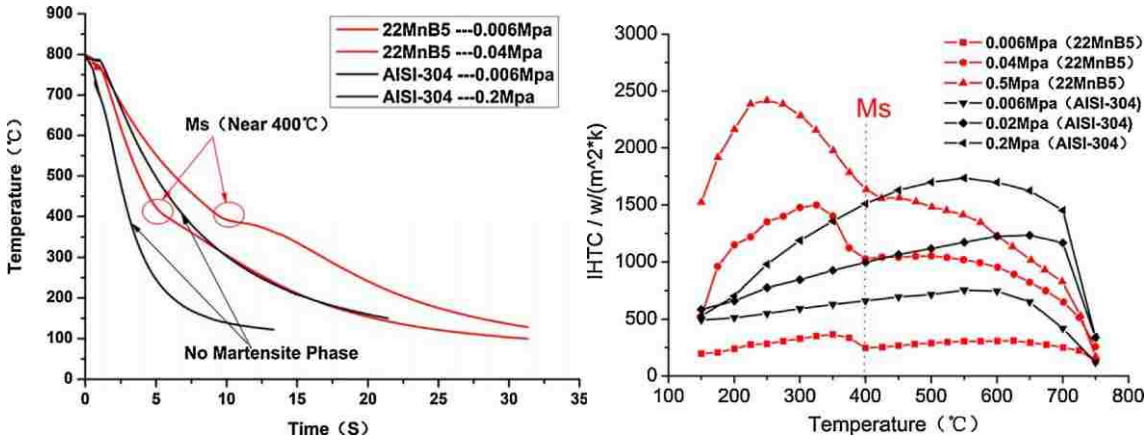

Figure 10 Cooling & heat transfer coefficient curve of 22MnB5 boron steel and AISI-304 stainless steel [14]

Some of their experimental results are shown in Figure 10 [19], where an inflection point can be seen on the cooling curves at about 400°C for 22MnB5 boron steel, when the phase transformation from austenite to martensite begins. In contrast, AISI-304 exhibits smooth cooling curves without any inflection points in both graphs. The inflection points result from the latent heat released during the phase transformation. Chang et al. [17] also concluded that the martensitic transformation has a positive influence on the heat transfer coefficient since it can increase by about 30% after the phase transformation.

2.3 Tailored Properties

The traditional direct or indirect hot stamping process is able to produce sheet metal parts with the desired strength. Nevertheless, some components will perform even better if the as-quenched mechanical properties can be varied from one region of the part to another. For instance, the B-pillar in a vehicle requires a softer zone at its lower end in order to absorb more impact energy in the event of a crash rather than being a fully-martensitic, high-strength structure (Figure 11). However, the rest of the B-pillar still requires high strength in order to prevent intrusion into the passenger compartment. Such tailored mechanical properties can be achieved by decreasing the cooling rate for the soft zone below the critical cooling rate required for martensitic transformation to produce an as-

quenched part with other phases such as bainite, pearlite and ferrite. In order to tailor the strength and ductility for different automotive components, variants of the traditional hot stamping process have been proposed, including partial heating, differential cooling, tailored products and annealing [20].

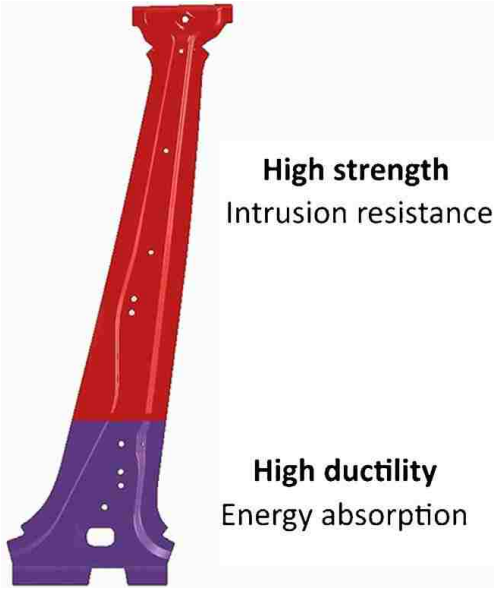

Figure 11 A sample B-Pillar with tailored mechanical properties [20]

2.3.1 Partial Heating

Partial heating consists of heating the same blank to different temperatures in different regions. When the blank is quenched in a die that has a uniform temperature, the cooling rate will vary from one zone to another and therefore, different mechanical properties will be achieved. The zone where a fully martensitic structure is required would be heated to over its AC_3 temperature (>~850°C), whereas the soft region would remain below AC_3 to prevent the transformation to austenite [8]. After the in-die forming and quenching process, the soft zone will have a ferritic-pearlitic structure and a tensile strength that is lower than 1100 MPa [21]. But the region heated above the AC_3 temperature would completely transform to martensite. As a consequence, a transition zone would appear between the two different regions of the part (Figure 12). Due to the temperature gradient between the two

regions, the transition zone is partially austenitized which also leads to a strength gradient from the high-temperature zone to the low-temperature zone (i.e. the fraction of martensite increases from the soft zone to the hard zone). Due to the variation in microstructure across the transition zone, a range of mechanical properties will also develop across the final part. [22]. In order to achieve partial heating on an industrial scale, it is necessary to have one or more furnaces with different heating zones: ceramic brick insulation is required between each heating zone and the temperature in each zone must be controlled independently.

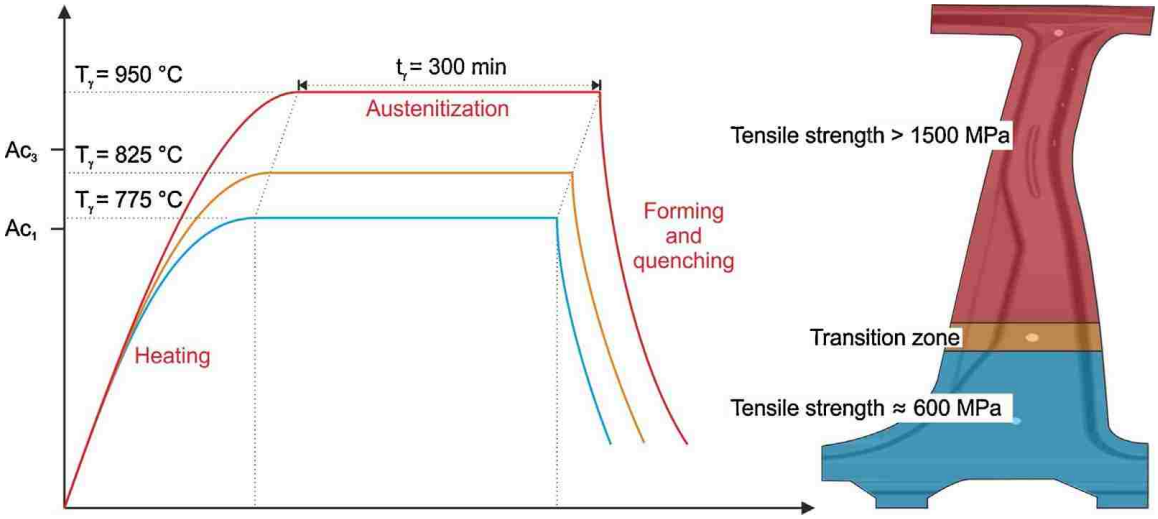

Figure 12 Schematic of the time–temperature-profile for the partial heating process [23]

2.3.2 Differential Cooling

Differential cooling is another method to achieve tailored properties. Instead of heating the blank to different temperatures in different zones, the blank is heated to a uniform temperature and quenched in the die at different cooling rates, which are controlled by adjusting the temperature in different regions of the die (Figure 13). One area of the die is kept sufficiently cold that the cooling rate is above the critical cooling rate (27°C/s for 22MnB5) and this leads to a fully martensitic structure [24]. In another region of the die, the temperature is adjusted higher so that the cooling rate is below the critical cooling rate, which will result in a softer, more ductile material with a microstructure consisting of ferrite, pearlite and bainite. There are three ways to realize differential cooling: heated tool

tailoring, variation of thermal properties in the tool, and the die relief method [20]. Comparing with partial heating, these three methods consist of modifying the cooling process or the die materials. Since the heat transfer behaviour of a blank and die mostly depends on the temperature difference, the heated tool tailoring method separates the die into at least two zones. Each zone has its own independent temperature control system and is cooled by circulating a fluid through built-in channels. Different temperatures across the die result in different cooling rates in the sheet metal and consequently, different as-quenched mechanical properties (Figure 14).

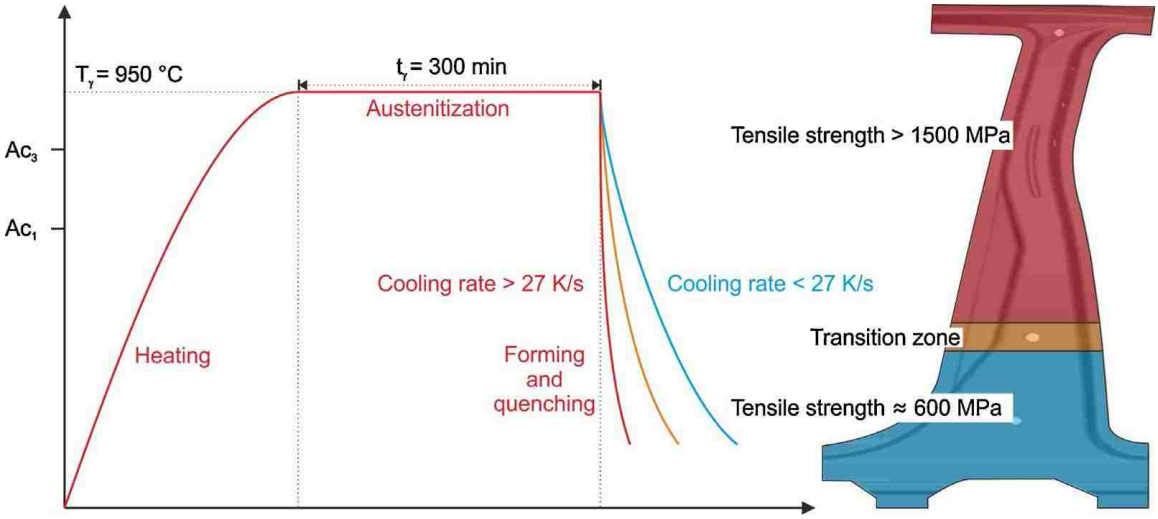

Figure 13 Schematic of the time–temperature-profile for the differential cooling process [18]

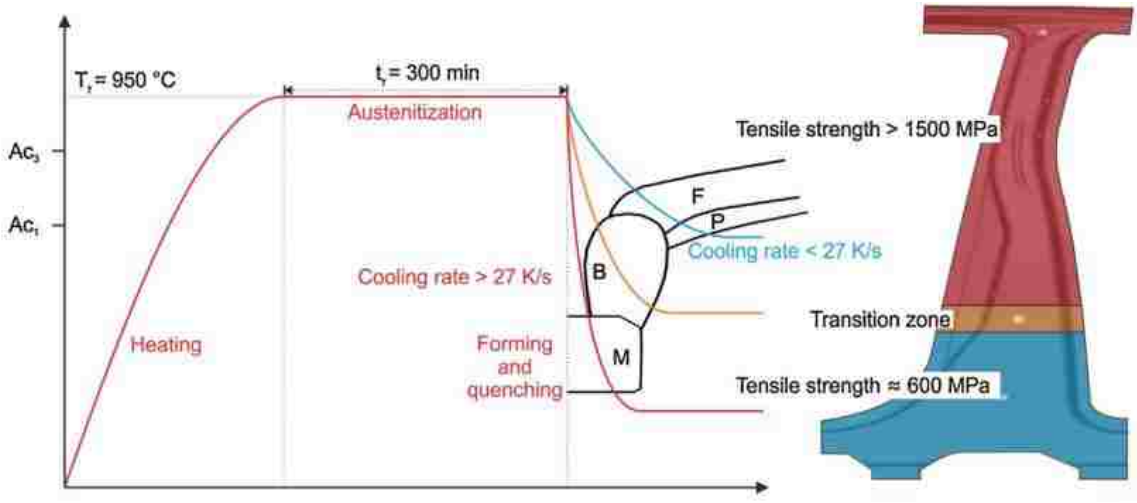

Figure 14 Schematic of the time–temperature-profile for the heated tool tailoring method [19]

Similarly, instead of using different temperatures in the die, the variation of thermal properties of the tool can also separate the die into different zones since different materials have different thermal conductivities (Figure 15). Die inserts that are made of steel with a higher conductivity would allow quenching to a fully martensitic microstructure within 2-4 seconds, while die inserts made of low conductivity material, or insulating material, would remain above the M_s temperature [25].

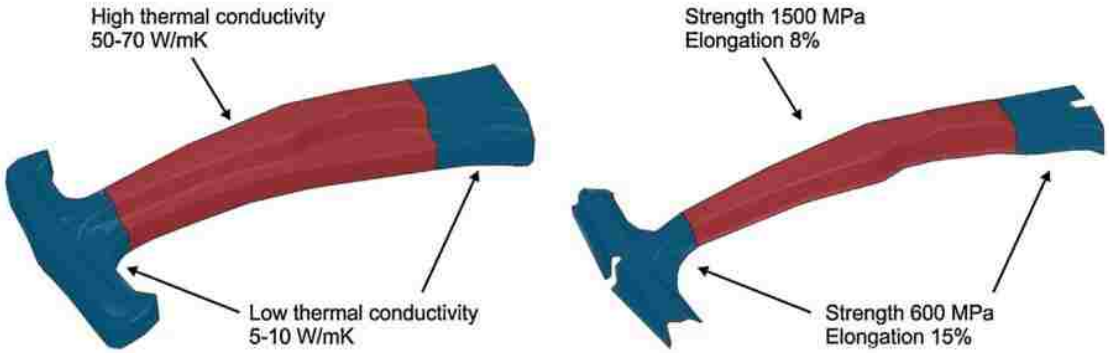

Figure 15 Schematic of components mechanical properties using different thermal properties of tool materials

Similar to the concept of varying the thermal properties in the tool, the die relief method allows the soft zone to cool down with a pocket of air between the blank and the die (Figure 16) [26]. In this case, the blank is only cooled by radiation and inner heat flow across the air pocket. In addition, the gap distance in the relief zone can also be determined during the die design phase. The more shallow the gap is, the greater the strength of the final part in that region [27].

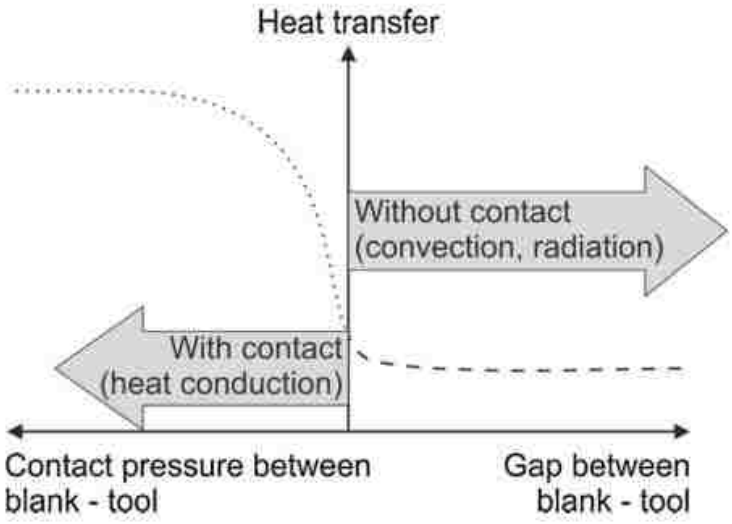

Figure 16 Schematic of heat transfer mechanisms during hot stamping with die relief

2.3.3 Tailored Products

Tailored products can be classified as tailor-welded blanks and tailored rolled blanks. (Figure 17) Tailor-welded blanks are made of different sheet materials that are welded together at their edges before hot stamping to obtain the required mechanical properties. Múnera et al. [28] investigated the possibility of USIBOR 1500P steel being laser-welded to Ductibor 500P steel to achieve tailored properties. These two grades of steel were found to work well together and were able to reduce the mass by 4.1-5.4kg in different applications, such as a light-weight door panel. In addition, the thickness of the two welded blanks could also be different based on the design requirements. Tailor-rolled blanks use the same base sheet material with a flexible rolling process, which can achieve different thicknesses in different regions in order to meet the required mechanical properties. B-pillar reinforcements are examples of parts that are produced using this method. However, the design of the forming die can become complex because of the thickness changes in the transition zones [29].

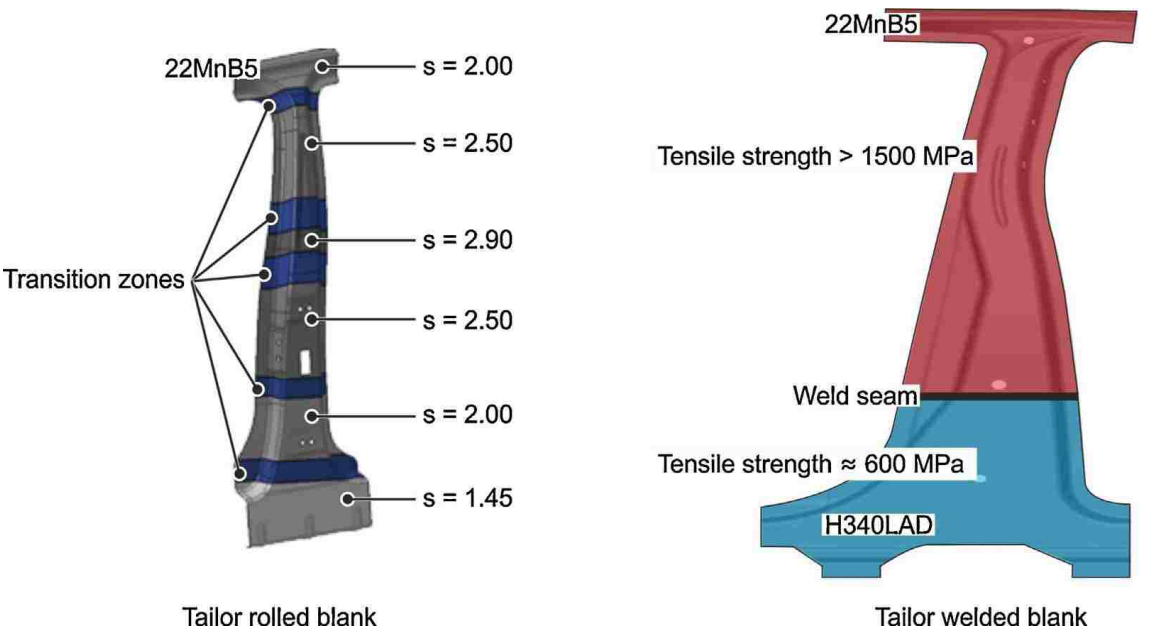

Figure 17 Example of tailored rolled blanks and tailored welded blanks (s is the initial thickness of the sheet in mm) [21]

2.4 Summary of Literature Review

Hot stamping is usually used to produce structural automotive parts with relatively simple geometry. There are two important factors to achieve the martensitic transformation: the start quenching temperature and the cooling rate. The blank needs to be heated up to 930°C, held at this temperature for 3-5 minutes to become fully austenitized and then quenched at a rate of at least 27°C/s.

For some structural components, the crashworthiness of the vehicle could be further improved by creating a local soft zone to absorb the impact energy. Partial heating, differential cooling, and tailored products are three main methods to achieve tailored properties. However, each approach has its own advantages and disadvantages and the specific requirements of each hot stamped part would determine which method is the most appropriate.

Limited research has been done in the area of partial heating to achieve tailored properties because of need for a special furnace to obtain different starting temperatures in the same blank. Ford's customized electrical resistance furnace with three independent heating zones provides the opportunity to investigate how partial heating works and the advantage over some other methods to achieve tailored properties.

3 Experimental Procedures

The experimental work consisted of two types of tests. Mechanical tests were used to characterize the original as-received material (22MnB5) as well as as-quenched blanks. Hot stamping tests were conducted with a custom-made furnace with three independent heating-zones and a hydraulic press that is designed to form sheet metal specimens under various loading conditions, which will be discussed in detail in this chapter.

3.1 Sheet Materials

The sheet material that was used in all the experimental work is Usibor 1500 (Aluminized 22MnB5). Two different thicknesses (0.9 mm and 1.8 mm) of the sheet material were tested. The 22MnB5 sheets were coated with an AlSi coating to avoid oxidation during the heating process. A micrograph of the as-received 22MnB5 was obtained after polishing and etching with 2% Nital and is shown in Figure 18. The as-received 22MnB5 consists of 75% ferrite and 25% pearlite.

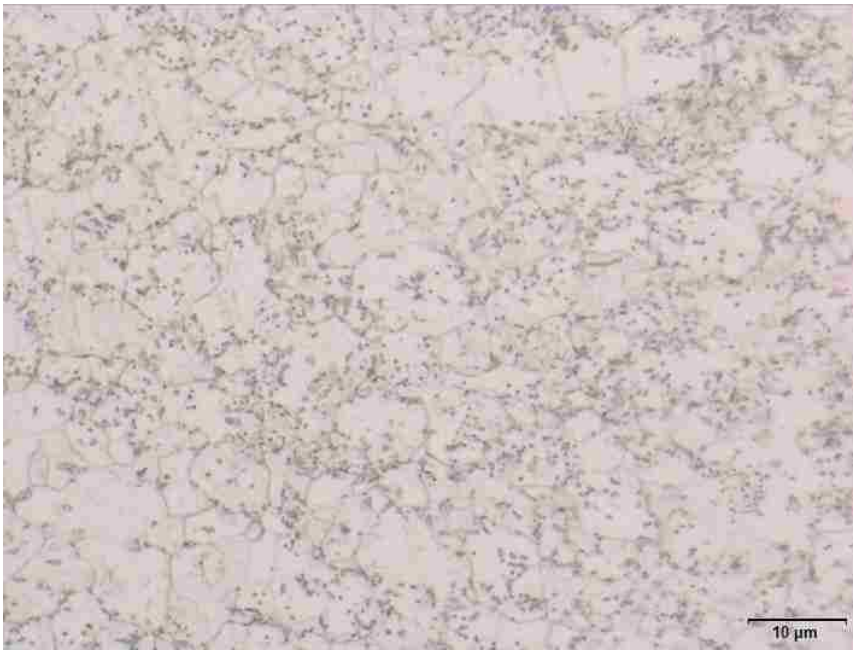

Figure 18 Micrograph of as-received 22MnB5 (2% Nital etchant)

3.2 Uniaxial Tensile Tests with DIC

The purpose of these tensile tests was to obtain the mechanical properties and the work hardening behaviour of as-quenched 22MnB5 sheet specimens. The tensile data were used to correlate the final mechanical properties with starting temperatures and microstructures. ASTM E8 tensile specimens were machined from both as-received and as-quenched sheets using wire electric-discharge machining (EDM). A random speckle pattern was painted on all the tensile specimens in order to use digital image correlation (DIC) technology to determine strains. Every sheet specimen was tested along two different orientations (in the rolling and transverse directions) to characterize the planar anisotropy of the material. Tensile tests were performed on an MTS Model 43 Universal testing machine with a 50-kN loading capacity. A 25-mm gauge mechanical extensometer, a video extensometer and 2D DIC post-processing tools were used to measure strains in the specimen gauge. The results of all these strain measurement methods was compared in order to ensure the accuracy of measurements. All the data from the MTS machine and DIC software were combined and processed by a custom MatLab code to obtain the engineering stress – engineering strain flow curve for each test. All the test conditions were repeated twice. Examples of both undeformed and fractured tensile specimens with random speckle pattern are shown in Figure 19.

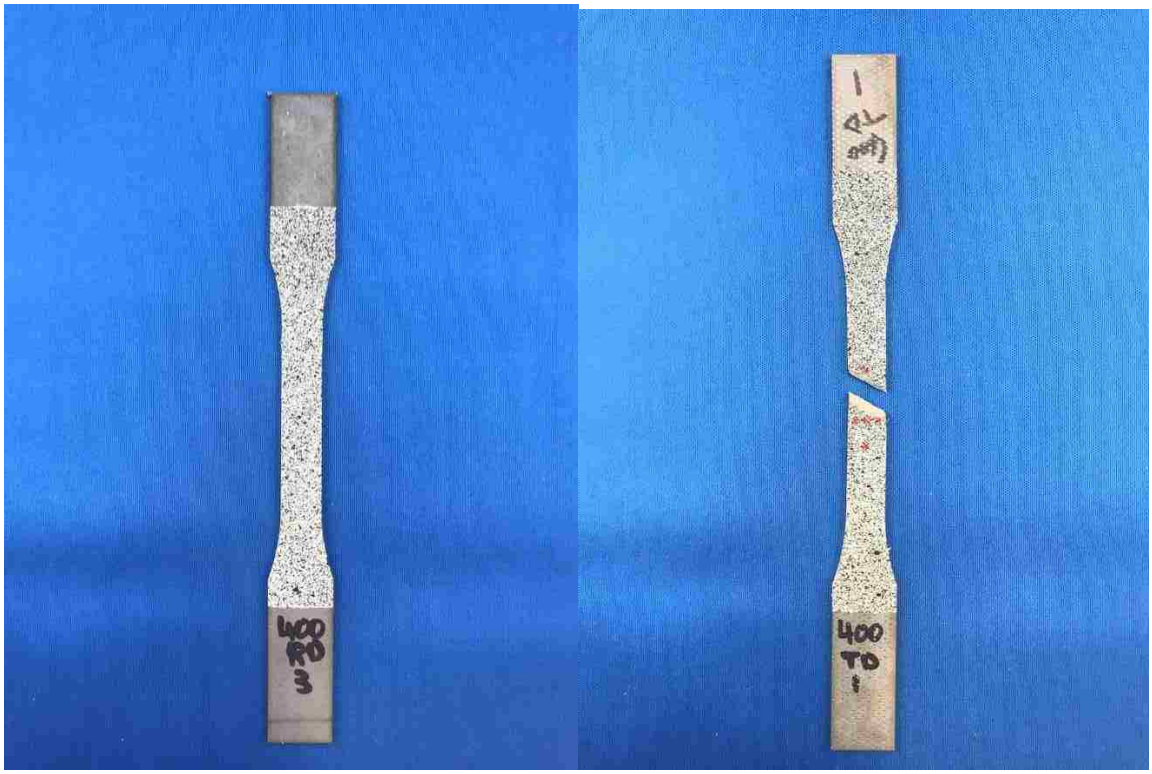

Figure 19 Example of undeformed and fractured tensile specimens with random speckle pattern

3.3 Hot Stamping Tests

Hot stamping tests were performed using Ford's custom-made furnace and the 240-ton hydraulic press. The dies used for the hot stamping trials consisted of two flat plates made of H13 steel and measuring 770 mm × 400 mm × 50 mm (Figure 22). The sheet metal blanks were heated in the furnace, then manually transferred to the dies in the press. The press was then rapidly closed so that the heat in the blank was transferred to the flat dies (initially at room temperature). The blanks were therefore quenched in the dies without any plastic deformation. Although this is not typical of industrial hot stamping, the purpose of this experiment was to investigate the relationships between process parameters such as clamping force, starting temperature, cooling time, and resulting mechanical properties and microstructures. Four different types of hot stamping tests with different test conditions are described in this section.

3.3.1 Designing and Building a Furnace Support

The hydraulic press is surrounded by an elevated platform to enable the operators to easily insert blanks into the dies and remove parts after forming (Figure 20). The control panel is also located on the platform. Since the hot blanks must be transferred as quickly as possible from the furnace to the press, the furnace should also be elevated so that the operator can access the blanks in the furnace when standing on the platform. A support frame was therefore designed and built to hold the furnace at the appropriate level. The dimensions of this furnace are 2.74 m × 2.54 m × 2.24 m (108 in. × 100 in. × 88 in.) and its weight around 5000 kg (detailed drawings of the furnace can be found in Appendix G). The design and analysis of the support frame were performed in CATIA V5 based on the dimensions and the weight of the furnace. The entire frame was built from 63.5 mm (2.5 in.) steel tubing and rests on four leveling pads. Figure 21 shows a CATIA model of the support frame and Figure 20 shows the layout of the testing equipment in the laboratory with the furnace mounted on the support frame. A drawing of the furnace support frame is provided in Appendix F.

Figure 20 Furnace and press setup

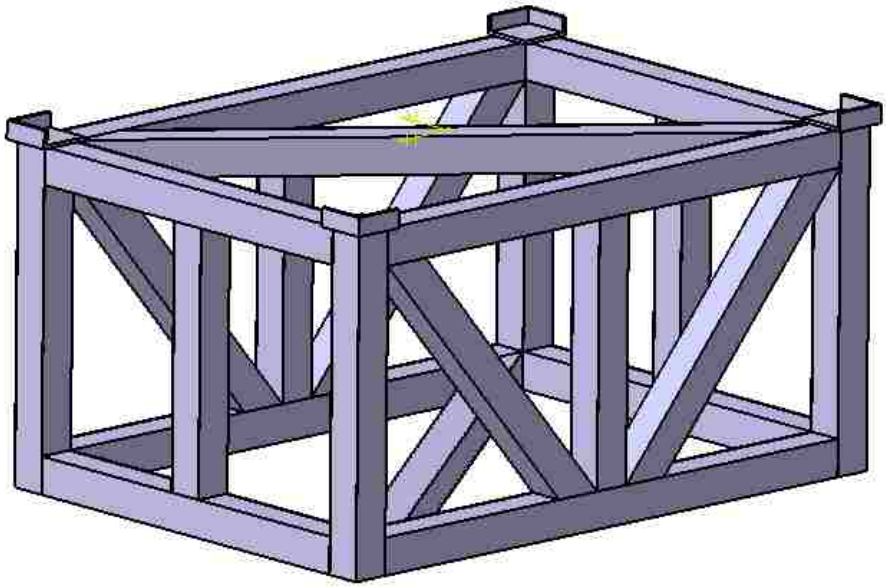

Figure 21 Design of the furnace support frame

Figure 22 Die plates for quenching

3.3.2 Hot Stamping Tests with Different Clamping Forces

A series of heating and quenching tests were conducted using flat dies (i.e. the blank is not deformed during quenching). The main purpose of applying different clamping forces was to investigate the correlation between the cooling time and the clamping force. A secondary purpose of this test was to determine the optimum clamping pressure that will achieve the highest cooling speed. This optimum clamping pressure would be used in all future hot stamping tests. The applied clamping force ranged from 200 KN to 800 KN, and since the size of the sheet specimen was 552 mm by 217 mm, the corresponding pressure ranged from 1.67 MPa to 6.68 MPa. The cooling time and the cooling rate were particularly observed in the range from 500°C to 200°C because the martensitic start temperature and finish temperature are located within this range, which are also affected by the initial

temperature of the blank as it is removed from the furnace. A thermocouple was welded to the edge of each specimen before the test so as to continuously record the temperature change during the heating and quenching process. Two different sheet thicknesses (1.8 mm & 0.9 mm) were also used in the tests. Three operators were needed to perform the test, and the following testing procedures were observed:

1. Preheat the furnace to 930°C. Start the press and PC.
2. Cut the sheet material into blank sizes (552 mm × 217 mm) using the hydraulic shear.
3. Weld a thermocouple on the edge of the blank.
4. Attach the thermocouple to the terminal connected to the PC. A custom LabView code would record the temperature during the test at a rate of 75 Hz.
5. Put on the protective suits and insert the specimen into the furnace using tongs.
6. After 5 min, transfer the red-hot specimen to the press as fast as possible and close the die.
7. Save the recorded temperature profile.

3.3.3 Hot Stamping Tests with Different Starting Temperatures

The purpose of these tests was to establish a relationship between the starting temperature before quenching and the corresponding as-quenched mechanical properties (yield strength, tensile strength, n-value, and uniform elongation.) As indicated in the work of Mairanz-Vatin et al. [8] and Erhardt and Boke [22] and discussed in Section 2.4.1, regions of the blank that are quenched from a temperature above AC_3 will transform to martensite, whereas regions that are quenched from a temperature below AC_3 will not. The different starting temperatures may lead to different microstructures and consequently to different mechanical properties. These tests were conducted in two different ways depending on which furnace door was used to insert and remove the blank. Method 1 consisted of using

the large furnace door (Figure 23). And Method 2 consisted of using only the narrow "visor" located in the center of the main door (Figure 24).

3.3.3.1 Method 1 (separate tests for various starting temperatures)

In this method, each sheet specimen was uniformly heated up to a different starting temperature, which ranged from 400°C to 930°C. The blank size was 552 mm × 217 mm. The clamping pressure during in-die quenching was selected to be 4.17 MPa based on the results of previous tests, because it leads to a relatively higher cooling rate, although the cooling rate did not vary significantly with the clamping pressure from 1.67 MPa to 6.68 MPa. After the quenching process, the sheet specimens were cut into ASTM E8 standard size specimens and tensile tests were carried out according to the procedure described in Section 3.1.

Figure 23 Removing blanks from the furnace using the main door

3.3.3.2 Method 2 (various temperatures on the same specimen)

In this method, each specimen was placed into the furnace through the visor in such a way that a gradient of temperatures developed in the blank from the end that protruded from the

furnace to the end that lay in the hottest part of the furnace (see schematic in Figure 25).

Figure 24 Operating the furnace using the "visor" in the main door

The center of the furnace is hotter than near the entrance and therefore, the closer the specimen is to the entrance, the lower its temperature. Because of this temperature gradient along the length of the specimen, different microstructures and mechanical properties will

be achieved after the specimen is quenched in a die at room temperature. The first step was to create the temperature distribution profile (temperature vs. distance from the entrance) along the length of a blank using five thermocouples welded along its edge, as shown in Figure 25. It can be observed that a gap exists in the temperature distribution due to the thickness of the insulation at the entrance of the furnace.

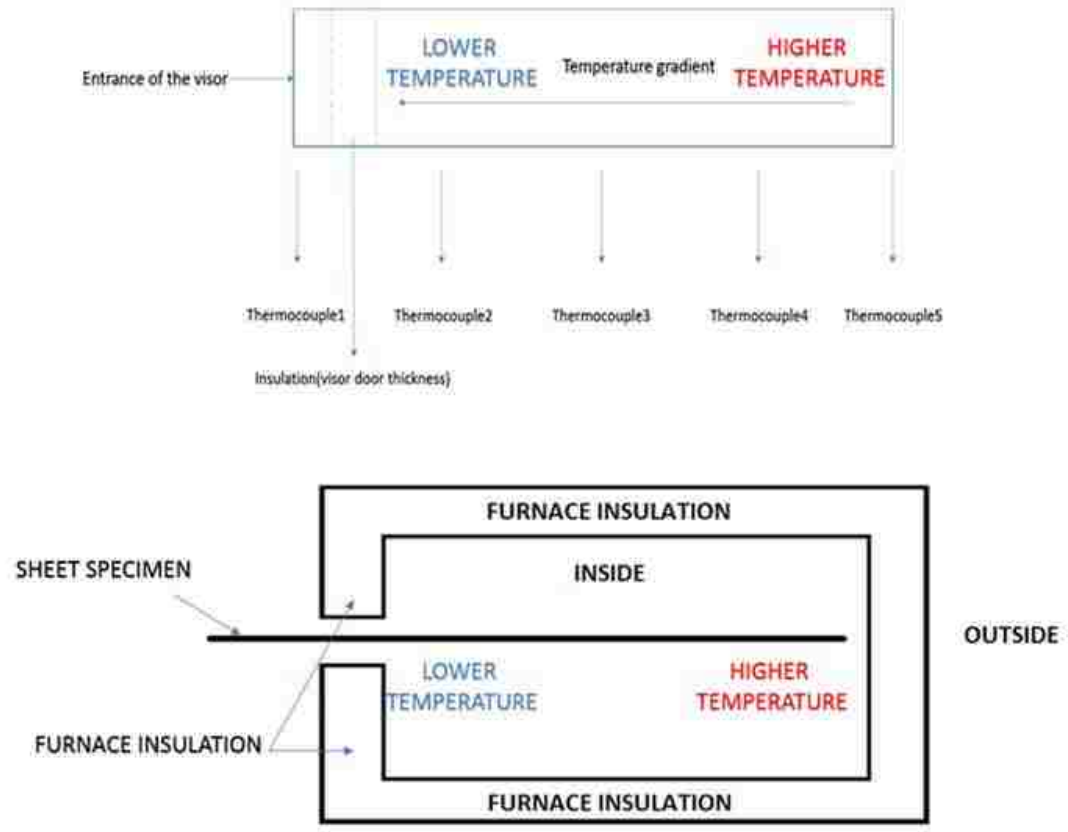

Figure 25 Schematic of the sheet specimen location when inserted through the visor

The time required for the sheet specimen to reach its specified temperature is approximately 5 minutes. When the prescribed temperature is reached, the temperature-distance curve can be easily created from the recorded temperature data. Once the temperature profile was determined, the same test was repeated without any thermocouples. The hot specimen was manually transferred to the press and quenched right away using the optimum clamping pressure (4.17 MPa). The transfer time was approximately 10 seconds.

Based on the temperature-distance curve, tensile specimens were cut in different locations of the blank corresponding to different starting temperatures. Tensile tests were then conducted to determine the mechanical properties of the as-quenched material for different starting temperatures. The following experimental procedure was adopted:

1. Create the temperature distribution profile along the length of the sheet specimen using thermocouples welded at specific locations of the specimen.
2. Do the same test without any thermocouples and quench the specimen in the die.
3. Cut tensile test specimens from each of the identified locations (different starting temperatures) on the quenched sheet.
4. Establish the relationship between mechanical properties and starting temperatures.

3.4 Microstructure Observation

The purpose of microstructure observation and analysis was to establish the microstructure of as-quenched specimens and the final mechanical properties. For metallographic observation of the as-quenched material, specimens were cut and mounted as shown in Figure 26. The surfaces in the normal, rolling and transverse directions were mounted. Mounting was done using Diallyl Phthalate thermosetting powder, cured at 150°C and 20 MPa for 90 s. using a Buehler EcoMet 3. Each specimen was ground using Buehlermet II abrasive paper in grits P60, P120, P280, P400, P600, P800, and P1200. At each grinding stage, water was used as a lubricant for the sample. Polishing was done in two stages. Buehler polishing disk with polycrystalline diamond suspension were used for polishing in sizes 9, 3 and 1 micrometers, respectively. The as-quenched material usually contains martensite, bainite and ferrite. Four different etching methods were attempted, including 2% Nital, 4% Picral acid, LePera, and the two-stage tint method. The two-stage tint etching which was developed for multiphase steel by De et al. [30] resulted in the best micrographs and therefore was used in this project In the first stage, the specimens were gently oscillated in 4% picric acid solution (4 g dry picric acid dissolved in 100 ml ethanol) mixed with 1 ml

concentrated hydrochloric acid for 20 s. After being etched in the picral solution, the specimens were washed in water, then ethanol, and were dried with the compressed air. In the second stage, the specimens were gently oscillated in a 10% aqueous sodium metabisulfite solution. The etching time for the second stage was 10 s. Similarly, the specimens were immediately washed with water, followed by ethanol and then dried with compressed air. With this etching method, the martensite is tinted brown, bainite is tinted black, and the ferrite is tinted as white.

The etched specimens were observed using an Olympus GX51 metallurgical microscope. The Fiji software [31]was used to conduct pixel counting to quantify the area fractions for the different phases (martensite, bainite, ferrite and other phases) present in the microstructure.

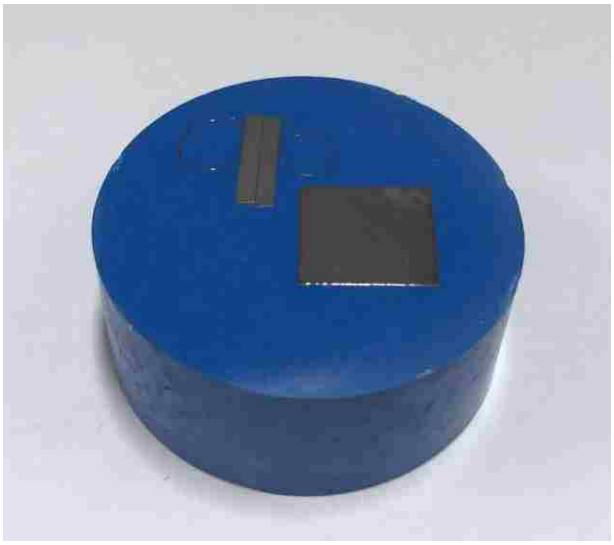

Figure 26 Metallography Specimen prepared for microstructure observation

4 Results and Analysis

In this Chapter, the results from tensile tests, hot stamping tests, and microstructure observations will be discussed. All the sheet specimens that were subject to hot stamping were cut into ASTM E8 tensile specimens and prepared for metallographic observation in order to obtain the corresponding mechanical properties and microstructures.

4.1 Analysis of Hot Stamping with Different Clamping Forces

The temperature-time data was recorded during the heating and quenching process using a Labview DAQ system. 7 in-die quenching tests were conducted with the clamping force ranging from 200 kN to 800 kN. The target starting temperature for these tests was 930°C. The specimen size was 552 mm × 217 mm. The temperature profile for the tests carried out with 200 kN clamping test is shown in Figure 27. The temperature profiles for tests conducted with clamping forces from 300 kN to 800 kN can be found in Appendix A.

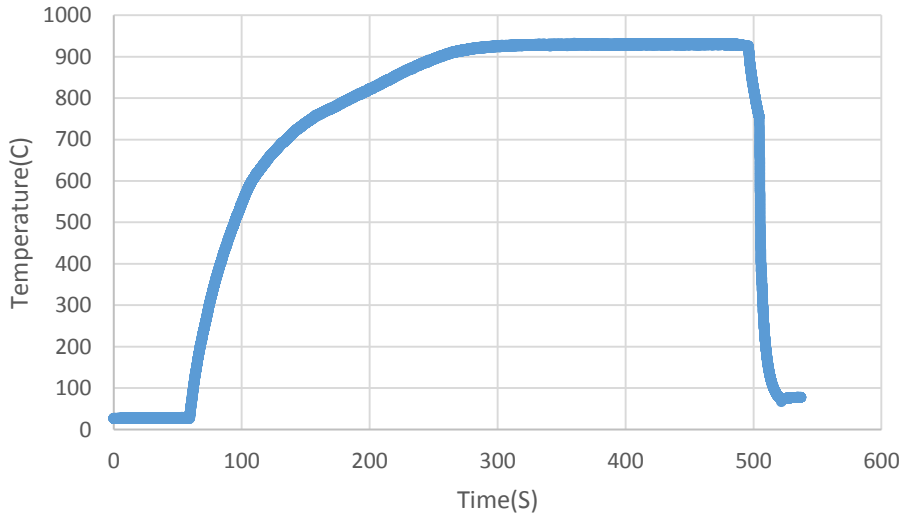

Figure 27 Temperature history for 1.8-mm 22MnB5 steel quenched with a 200-kN clamping force

Since the specimens were manually transferred from the furnace to the press, the actual starting temperature prior to quenching was different for each test. A longer transfer time

resulted in lower starting quenching temperature. In order to correlate the cooling rate with the clamping force (pressure), a datum needs to be selected for each test. The first portion consists of air cooling during the transfer period. The lowest die quenching starting temperature among all the tests was defined to be the start cooling point for multi-test comparisons. The lowest quenching starting temperature was 740°C, which was set to be the starting point for the comparison, as mentioned above. And the first two seconds of the quenching time were taken to be the reference interval during which the cooling rate was determined.

The lowest cooling speed occurred with the 200 kN clamping force, while the highest cooling speed occurred with the 500 kN clamping force. In order to make the results more general and meaningful, all the clamping forces were converted to clamping pressure as shown in Figure 28.

Since it was shown that 500 kN clamping force led to the highest cooling rate, the same quenching tests were investigated with the 0.9-mm (0.035-inch) specimens. As shown in Figure 29 and Appendix A, because of the thinner thickness, the time required to reach the target heating and cooling temperatures was shorter than for the thicker gauge specimens. Similarly, the overall combined die quenching temperature profile was created based on the same start cooling temperature (645°C) as Figure 30. The highest cooling speed occurs with 800 kN while the lowest cooling speed occurs with 500 kN. However, a higher clamping force does not necessarily lead to a higher cooling speed. From 645°C to 200°C, the difference of the cooling time for highest cooling speed and lowest cooling speed is 0.4 second.

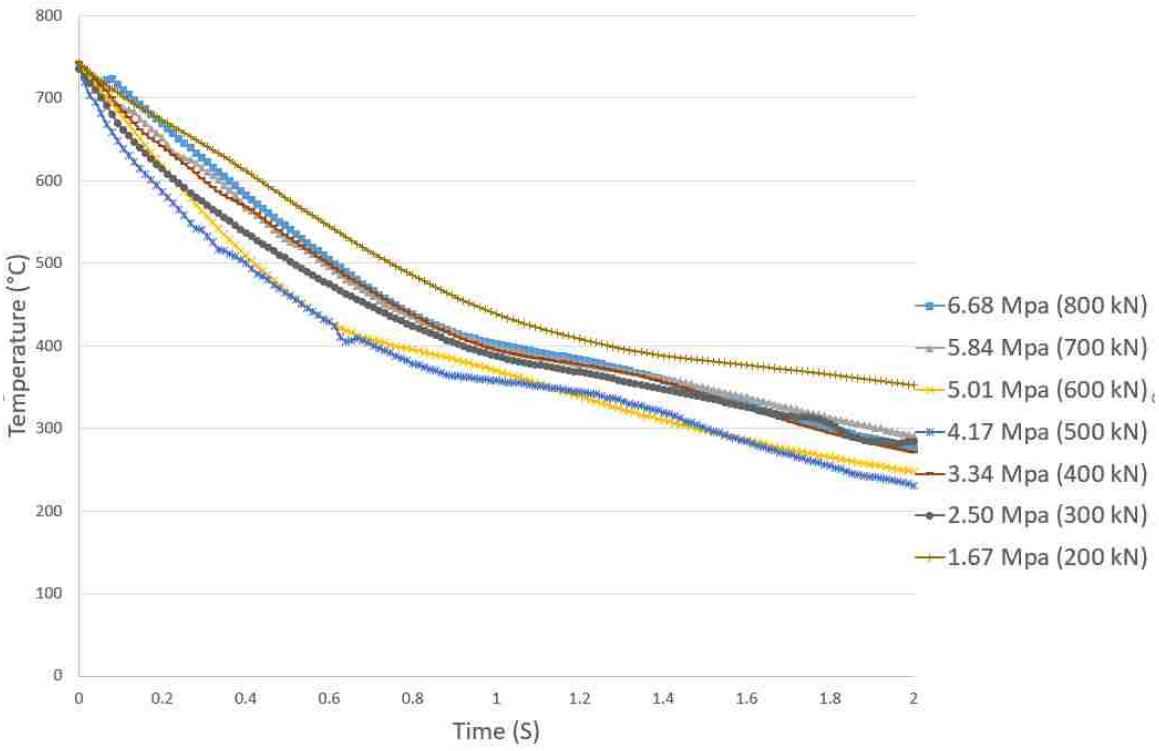

Figure 28 Overall quenching temperature profile for 1.8-mm 22MnB5 steel (different clamping forces)

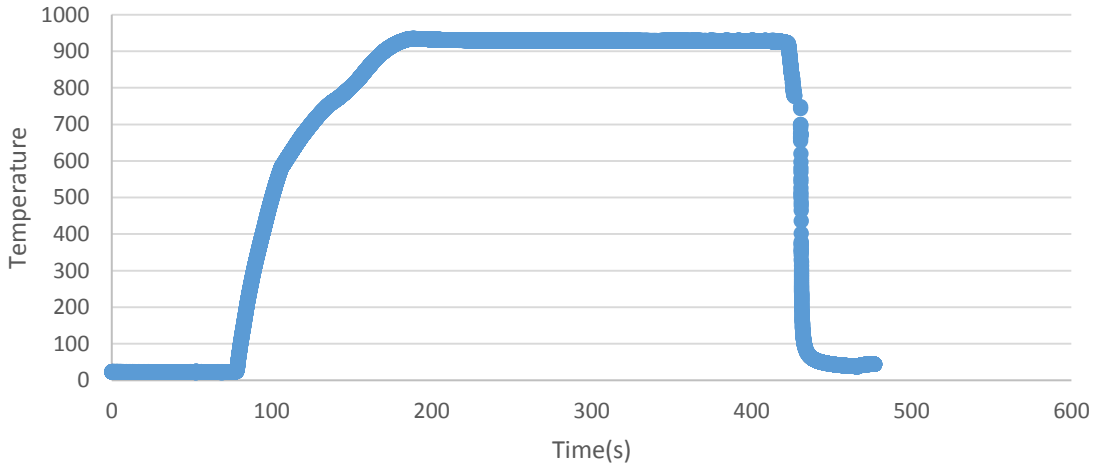

Figure 29 Temperature history for 0.9-mm 22MnB5 steel quenched with a 300-kN clamping force

In order to verify the final as-quenched mechanical properties, tensile tests were also conducted with specimens obtained from the blank quenched with different clamping forces. The tensile tests were only done with the 1.8-mm thickness blank due to the fact

that the thinner blanks have a higher heat transfer rate, and therefore a higher martensite percentage. The engineering stress-strain curve for 1.8-mm 22MnB5 steel quenched with 200 kN and 800 kN clamping force are shown in Figures 31 & 32. The rest of the graphs are in Appendix B. The changes in ultimate tensile stress (UTS) and uniform elongation (UEL) as a function of clamping force are shown in Table 6. The UTS for tests are over 1500 MPa and the UEL are within the range from 4.0% to 5.0%.

Clamping Force (kN)	Clamping Pressure (MPa)	UTS (MPa)	UEL (%)
200	1.67	1535 ± 2	4.0 ± 0.1
300	2.50	1533 ± 1	4.1 ± 0.3
400	3.34	1524 ± 1	4.5 ± 0.2
500	4.17	1532 ± 4	4.9 ± 0.1
600	5.01	1520 ± 4	4.6 ± 0.7
700	5.84	1529 ± 1	4.3 ± 0.1
800	6.68	1523 ± 1	4.6 ± 0.1

Table 6 UTS and UEL of 1.8-mm 22MnB5 steel after being quenched with different clamping forces

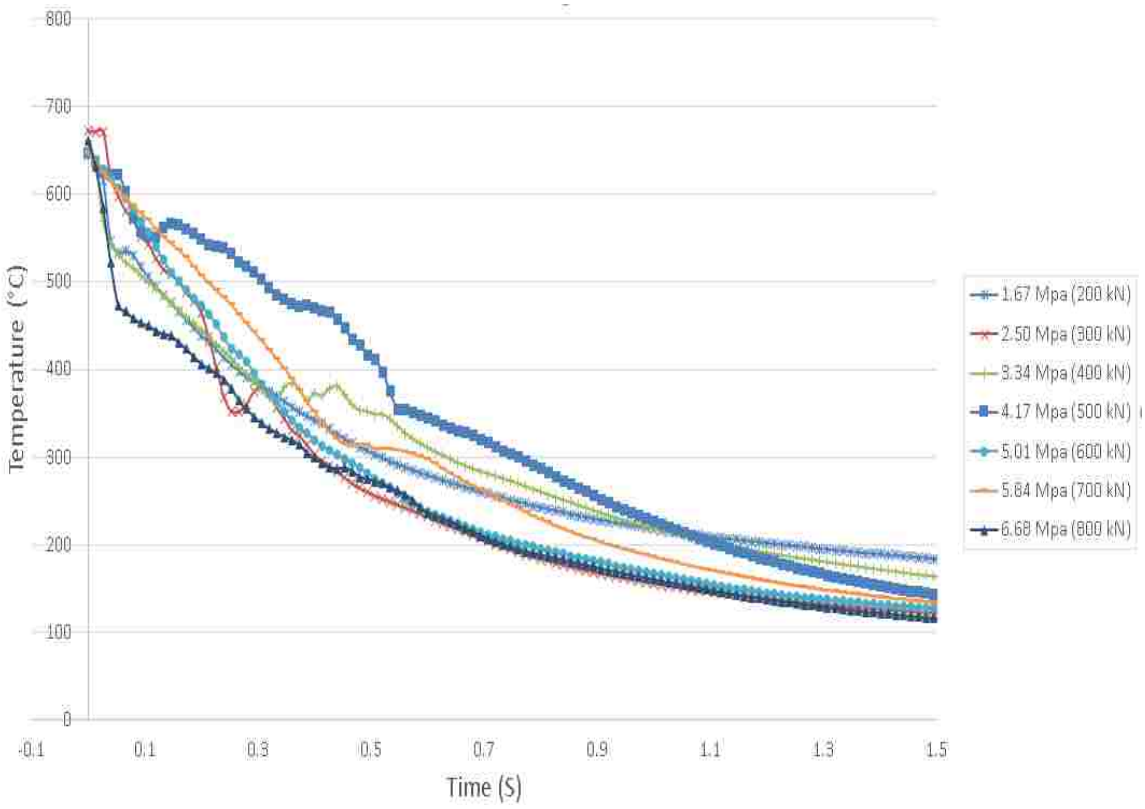

Figure 30 Overall temperature profile for 0.9-mm 22MnB5 steel quenched with different clamping forces

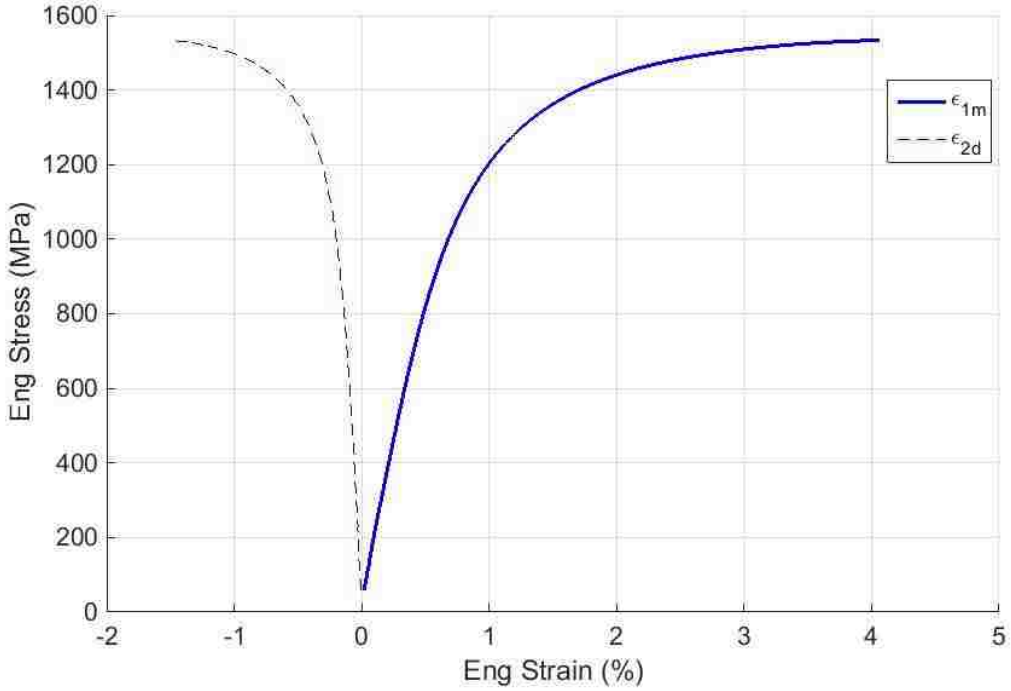

Figure 31 Engineering stress vs. engineering strain of 1.8 mm 22MnB5 steel quenched with 200 kN clamping force

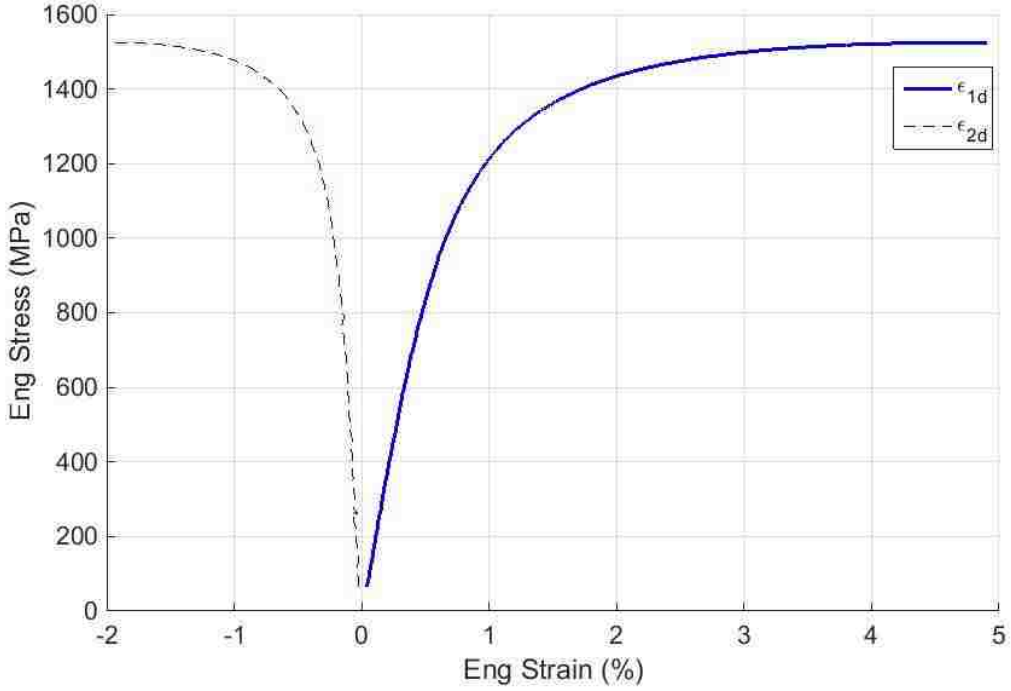

Figure 32 Engineering stress vs. engineering strain of 1.8 mm 22MnB5 steel quenched with 800 kN clamping force

4.2 Analysis of Hot Stamping Tests with Different Starting Temperatures

As mentioned in Section 3.2.3.1 and Section 3.2.3.2, two different types of hot stamping tests were conducted. However, all the research tests reported in this thesis were conducted according to Method 1 due to the fact that Method 2 required longer specimens with multiple thermocouples attached which were difficult to transfer to the press in a reproducible time. Method 1 is to heat the specimen to the specific temperature and quench it right from that temperature. After the hot stamping tests, tensile specimens were taken from the as-quenched specimens in order to determine their mechanical properties. A custom MATLAB code was created to post-process the data from both the MTS tensile machine and the DIC analysis software. In order to ensure the accuracy of the strain measurements, three different major strain measurements, including mechanical, video strain and DIC strain gauge, were compared together. It should be pointed out that the minor strain could only be measured by video extensometer and DIC, because the mechanical extensometer could only measure the strain in the major direction. Pre-load and pre-strain from tightening the grip was also taken into consideration for the starting condition. The experimental data were processed and analyzed in terms of engineering stress and engineering strain.

The specimens were heated to different specific temperatures (490°C, 630°C, 675°C, 720°C, 760°C, 800°C, 845°C and 900°C) for both 1.8 mm (0.07 in) and 0.9 mm (0.035 in) thick sheets and were quenched in the die as soon as they were transferred to the press. The engineering stress vs. engineering strain curves (the solid line represents the major stress vs. major strain and the dashed line is the major stress vs. minor strain) at 490°C, 720°C ,760°C and 900°C for 0.9-mm 22MnB5 steel are shown in Figures 33, 34, 35 and 36, and the rest of the curves are in Appendix C.

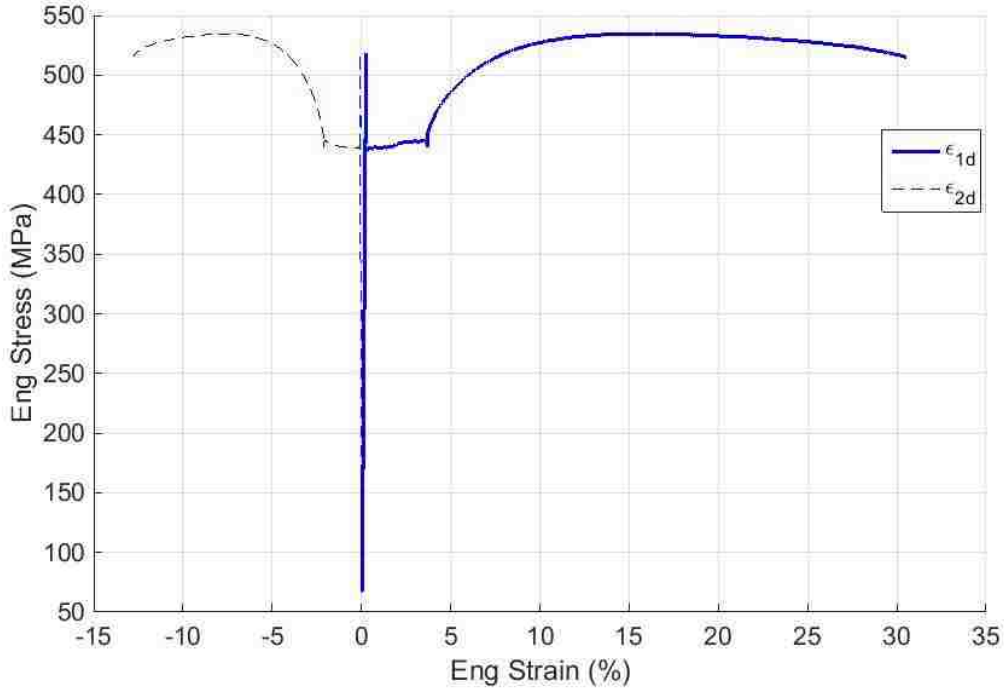

Figure 33 Engineering stress vs. engineering strain of 0.9 mm 22MnB5 steel quenched from 490°C

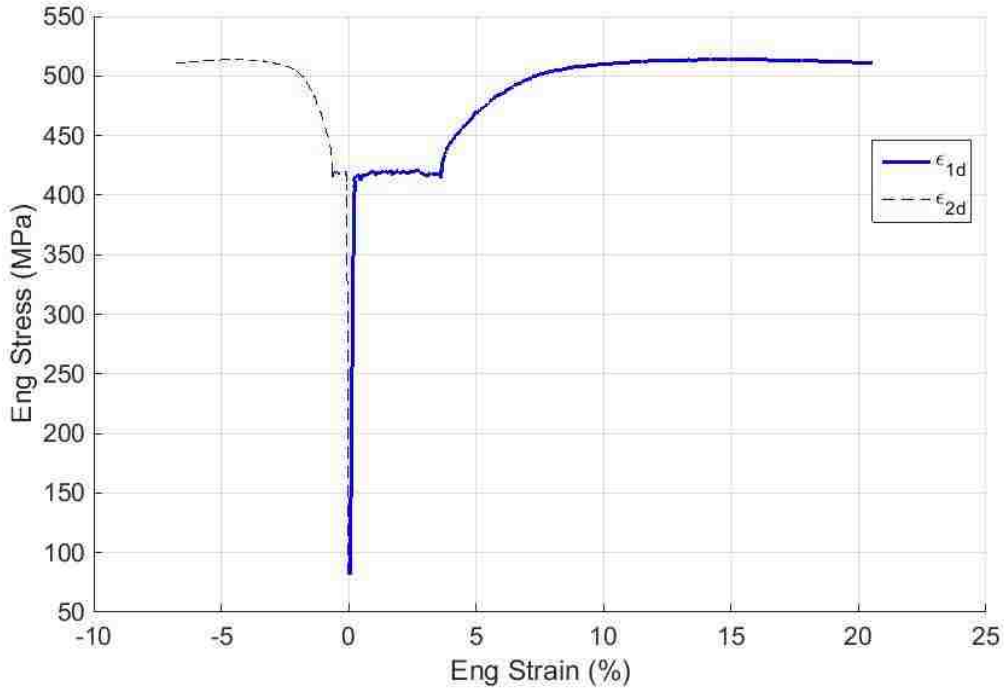

Figure 34 Engineering stress vs. engineering strain of 0.9 mm 22MnB5 steel quenched from 720°C

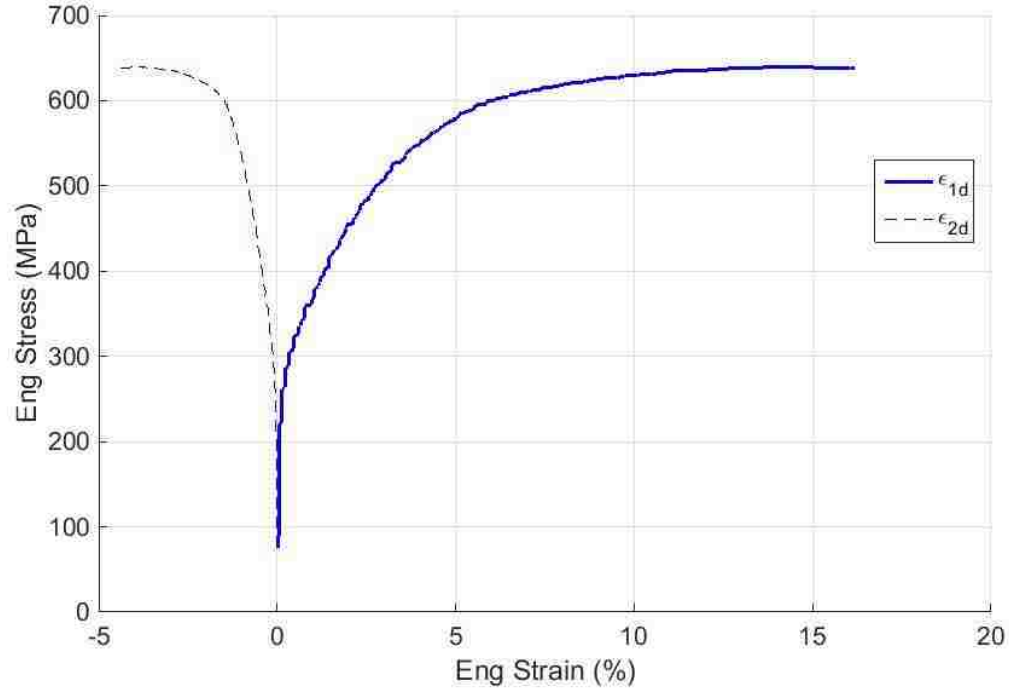

Figure 35 Engineering stress vs. engineering strain of 0.9 mm 22MnB5 steel quenched from 760°C

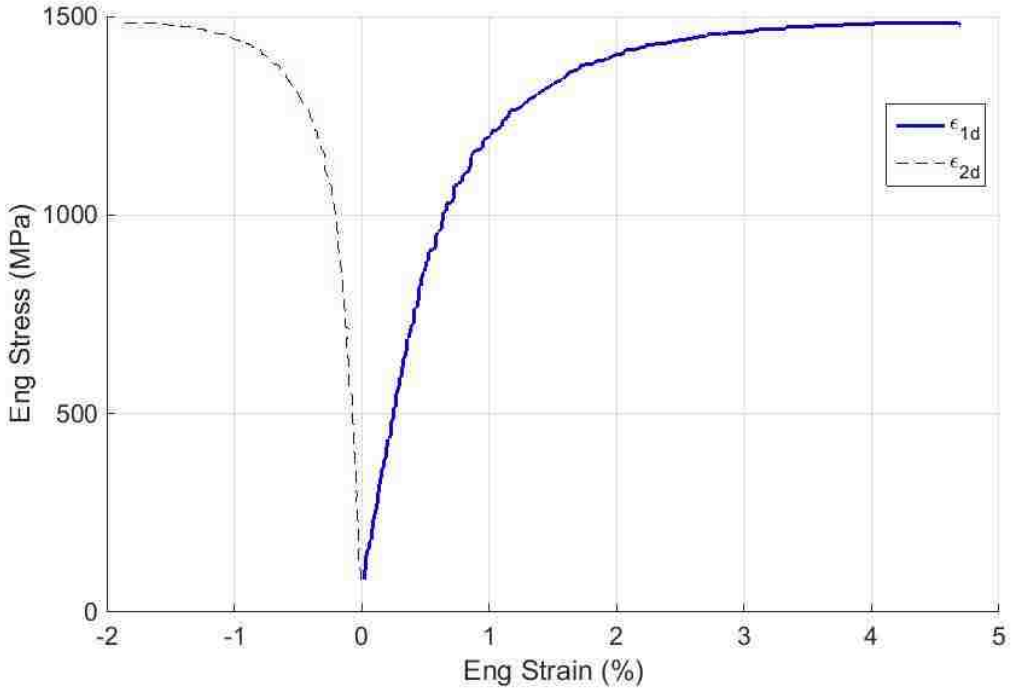

Figure 36 Engineering stress vs. engineering strain of 0.9 mm 22MnB5 steel quenched from 900°C

For specimens with a thickness of 0.9 mm and 1.8 mm, the flow curves are identical for the same starting temperature. When they were heated up to relatively lower temperatures, between 490°C and 720°C, Figure 33 and Figure 34 show evidence of Lüders bands and yield point elongation before work hardening begins, in both major and minor directions. This undesirable, non-uniform plastic deformation is due to the pinning of dislocations by small B and C atoms and their sudden release. The length of the non-uniform plastic deformation and its corresponding starting temperature for 1.8-mm and 0.9-mm thickness are shown in Tables 7 & 8 and in Figures 37 & 38.

Starting Temperature (°C)	Yield Point Elongation (%)
490	3.4
630	3.7
675	3.3
720	3.4
760	0
800	0
845	0
900	0

Table 7 Yield point elongation vs. starting temperature for 1.8-mm 22MnB5 steel sheet

Starting Temperature (°C)	Yield Point Elongation (%)
490	2.0
630	3.9
675	3.4
720	3.6
760	0
800	0
845	0
900	0

Table 8 Yield point elongation vs. starting temperature for 0.9 -mm 22MnB5 steel sheet

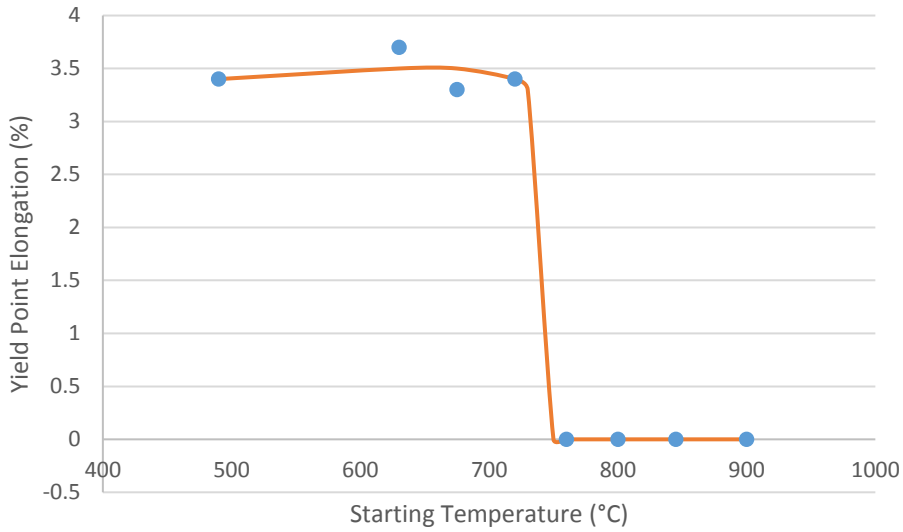

Figure 37 Yield point elongation vs. starting temperature for 1.8-mm 22MnB5 steel sheet

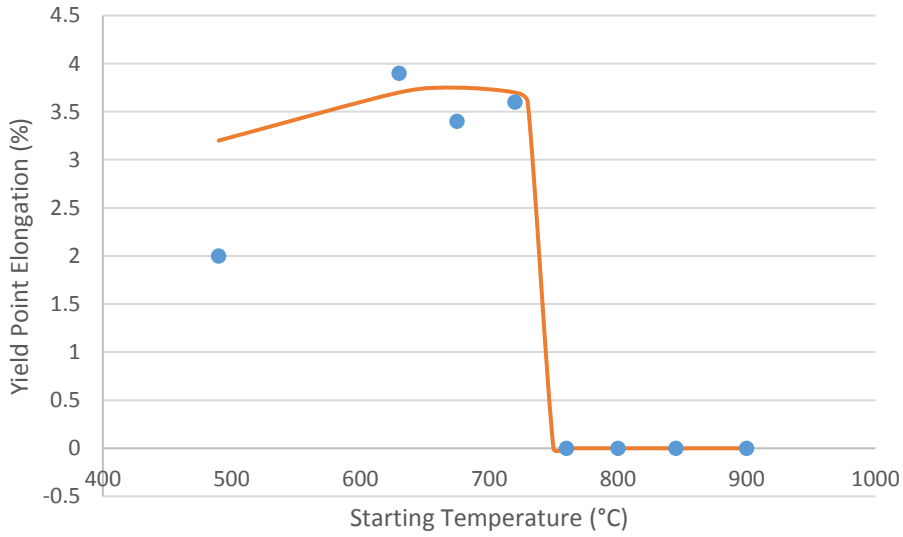

Figure 38 Yield Point Elongation vs. starting temperature for 0.9-mm 22MnB5 steel sheet

The ultimate tensile strength of specimens heated to temperatures in the range from 490°C and 720°C are all approximately over 500 MPa but lower than 600 MPa. However, as the starting temperature increases to 760°C and above, the yield point elongation disappears, the yield stress first decreases somewhat then increases again, and the tensile strength increases up to almost 1000 MPa. When the starting temperature is greater than 800°C, the yield stress increases very significantly and the tensile strength reaches appoximately

1400 MPa and 1500 MPa for starting temperatures of 845°C and 900°C, respectively, Figures 39 and 41 show the tensile stress vs. the starting temperature and Figures 40 and 42 show the uniform elongation vs. starting temperature of the 0.9-mm and 1.8-mm specimens, respectively. The detailed mechanical properties of all the tested specimens are shown in Table 9 & Table 10.

Starting T(°C)	E (GPa)	Yield Stress(MPa)	UTS (MPa)	UEL (%)
490	201	450	535 ±1	15.7 ±0.4
630	196	455	535 ±3	13.4 ±0.2
675	219	425	517 ±1	14.5 ±0.3
720	224	416	515 ±2	14.7 ±0.5
760	184	300	639 ±1	13.9 ±1.2
800	180	439	951 ±3	6.8 ±1.1
845	170	1011	1402 ±29	4.6 ±0.4
900	175	1047	1487 ±7	5.0 ±0.2

Table 9 Mechanical properties of 0.9-mm 22MnB5 steel after quenching from different temperatures

Starting T(°C)	E (GPa)	Yield Stress (MPa)	UTS (MPa)	UEL (%)
490	179	384	563 ±4	16.7 ±0.1
630	195	498	569 ±1	15.9 ±0.1
675	202	486	552 ±3	14.4 ±0.3
720	189	435	530 ±1	16.6 ±0.1
760	185	332	760 ±2	14.3 ±0.2
800	190	459	992 ±1	10.8 ±1.7
845	193	808	1365 ±6	5.0 ±1.7
900	199	1089	1545 ±5	4.6 ±0.1

Table 10 Mechanical properties of 1.8-mm 22MnB5 steel after quenching from different temperatures

The as-quenched mechanical properties of the 22MnB5 steel are very similar for both sheet thicknesses, although the tensile strength of the 1.8-mm specimens is slightly greater than that of the 0.9-mm specimens for the same starting temperature. And likewise, the uniform elongation of the 0.9-mm specimens is slightly greater than that of the 1.8-mm specimens at the same starting temperature.

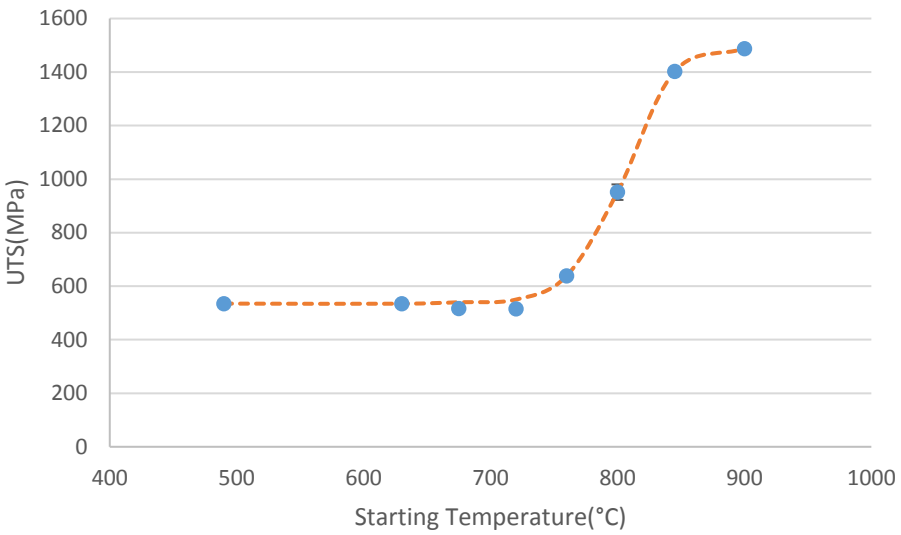

Figure 39 Ultimate tensile Stress vs. starting temperature for 0.9-mm 22MnB5 steel

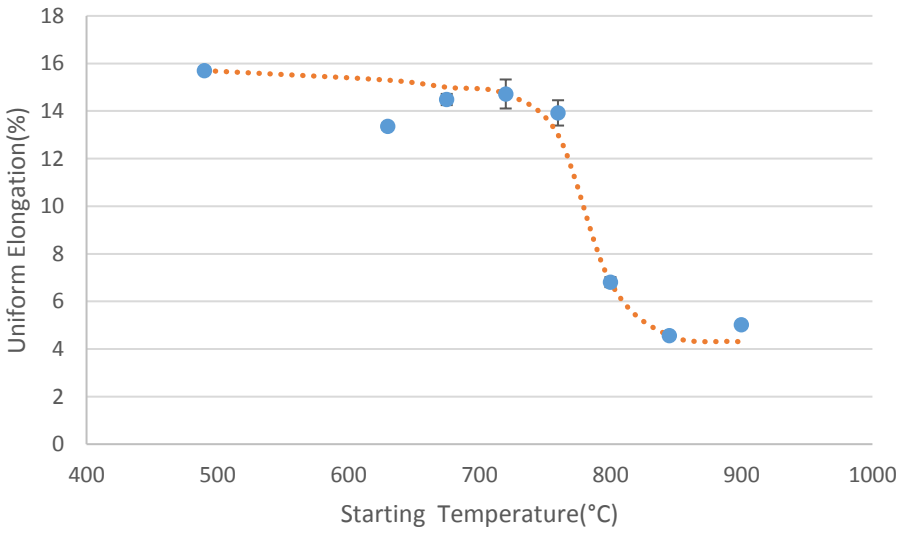

Figure 40 Uniform elongation vs. starting temperature for 0.9-mm 22MnB5 steel

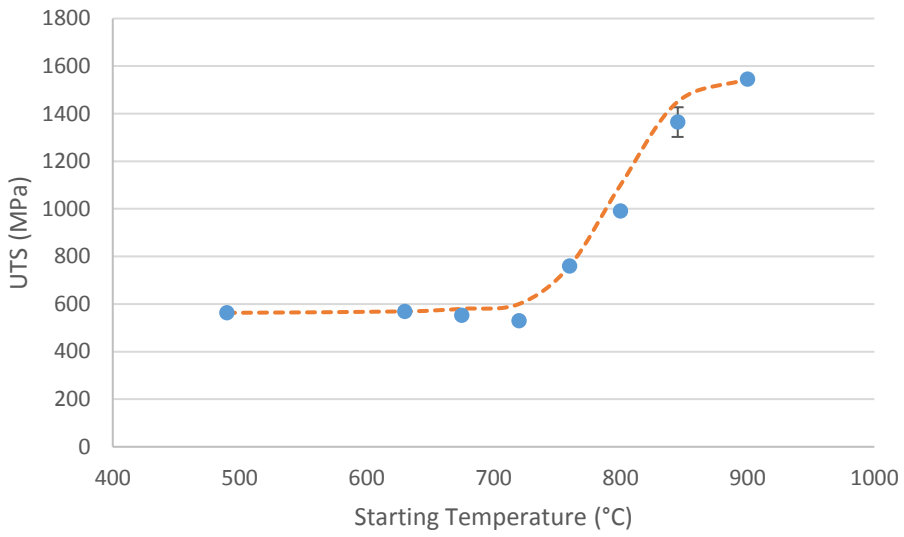

Figure 41 Ultimate tensile Stress vs. starting temperature for1.8-mm 22MnB5 steel

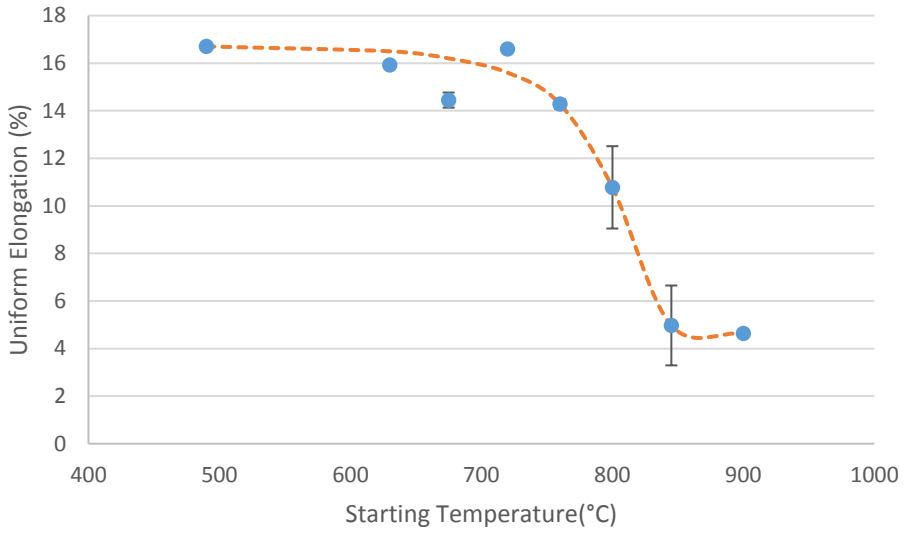

Figure 42 Uniform elongation vs. starting temperature for1.8-mm 22MnB5 steel

Young's modulus for all specimens ranged from 180 GPa to 210 GPa, which is reasonable for steel. For some of the specimens quenched from 490°C to 800°C, it was difficult to define the slope of the linear elastic portion of the curve. The yield stress remains in the range of ~400 MPa to ~500 MPa when the start temperature is 800°C or less. However, when the starting temperature is above 845°C, the yield stress increases dramatically to

nearly 1000 MPa. In contrast, as the starting temperature increases from 490°C to 720°C, the ultimate tensile strength (UTS) stays within the range of 500 MPa to 600 MPa. But when the starting temperature exceeds 720°C, the UTS begins to increase rapidly. From 760°C to 800°C (only a 40°C temperature difference), the UTS increases from 639 MPa to 951 MPa and from 760 MPa to 991 MPa for 0.9-mm-thick and 1.8-mm-thick 22MnB5 steel, respectively. The UTS increases to over 1300 MPa when the temperature reaches 845°C (Figures 39 & 41). As the temperature increases from 845°C to 900°C, the UTS further increases from about 1300 MPa to 1500 MPa. As expected, the uniform elongation for both thickness decreases continuously with increasing UTS (Figures 40 & 42).

4.3 Microstructure Observation and Analysis

The purpose of the microstructure analysis was to relate the microstructure content with the as-quenched mechanical properties of 22MnB5 steel sheets. From the result of mechanical properties of Section 4.2, the UTS and uniform elongation of the specimens whose starting temperature were below 760°C were within a narrow range. The primary reason is the starting temperature did not reach the AC_1 temperature and therefore the mechanical properties remained similar to those of as-received 22MnB5 steel. Therefore, only the specimens whose starting temperature was above 760°C were polished, etched and observed under the microscope. A specimen cut from the middle of the as-quenched specimen was used for metallographic analysis of each quenching condition. The micrographs (88 μm×66.6 μm) show the through-thickness microstructure of the as-quenched specimens and were used to quantify the area fraction of as-quenched phases. Figures 43-46 show the optical micrographs for 0.9-mm specimens quenched from 760°C, 800°C, 845°C and 900°C, respectively. The colour-tint etching caused the martensite to become brown, as shown in Figure 45 (quenched from 900°C), the bainite microstructure to become black, and the ferrite or retained austenite to be white. The fraction of different

phases is indicated in both the micrographs and in Tables 11 & 12. Finally, the micrographs for as-quenched 1.8-mm 22MnB5 specimens are in Appendix E.

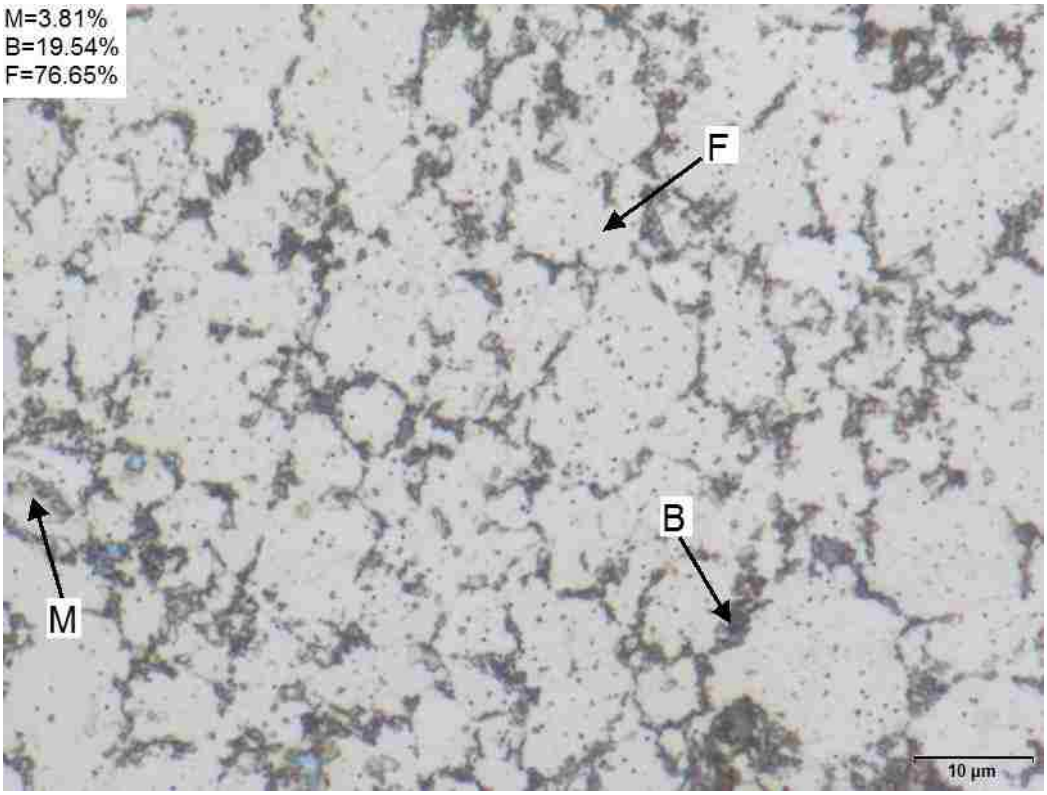

Figure 43 Colour-tint etched optical micrograph for 0.9-mm 22MnB5 steel sheet quenched from 760°C

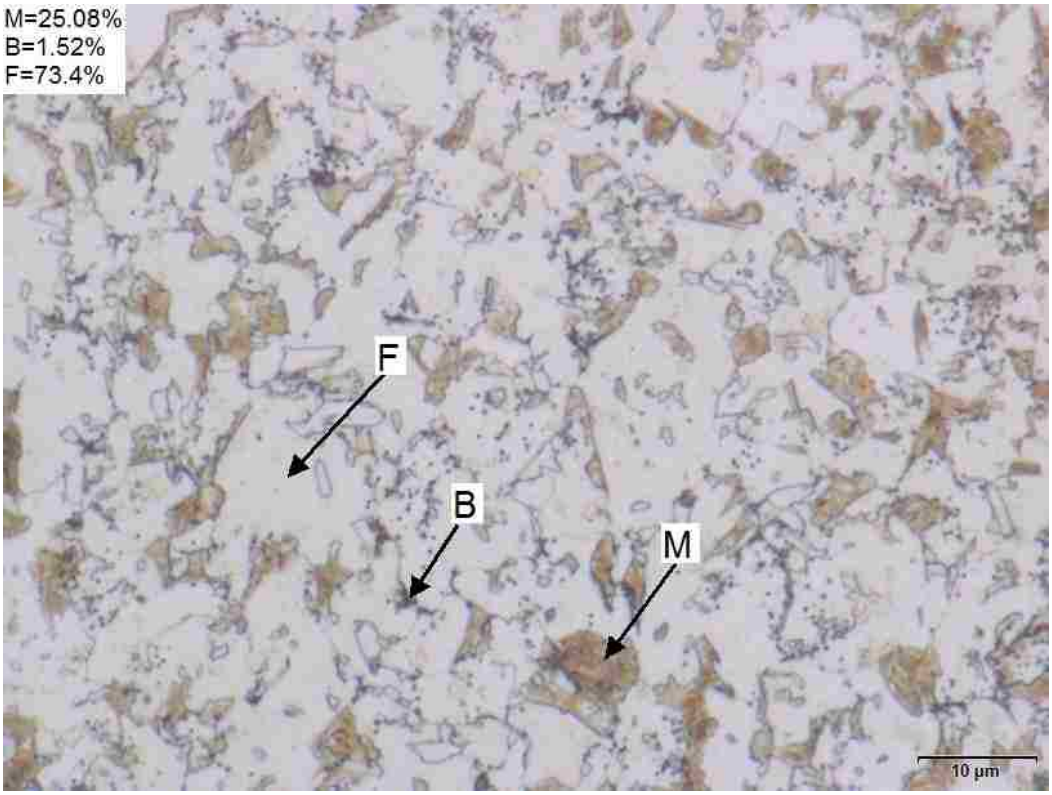

Figure 44 Colour-tint etched optical micrograph for 0.9-mm 22MnB5 steel sheet quenched from 800°C

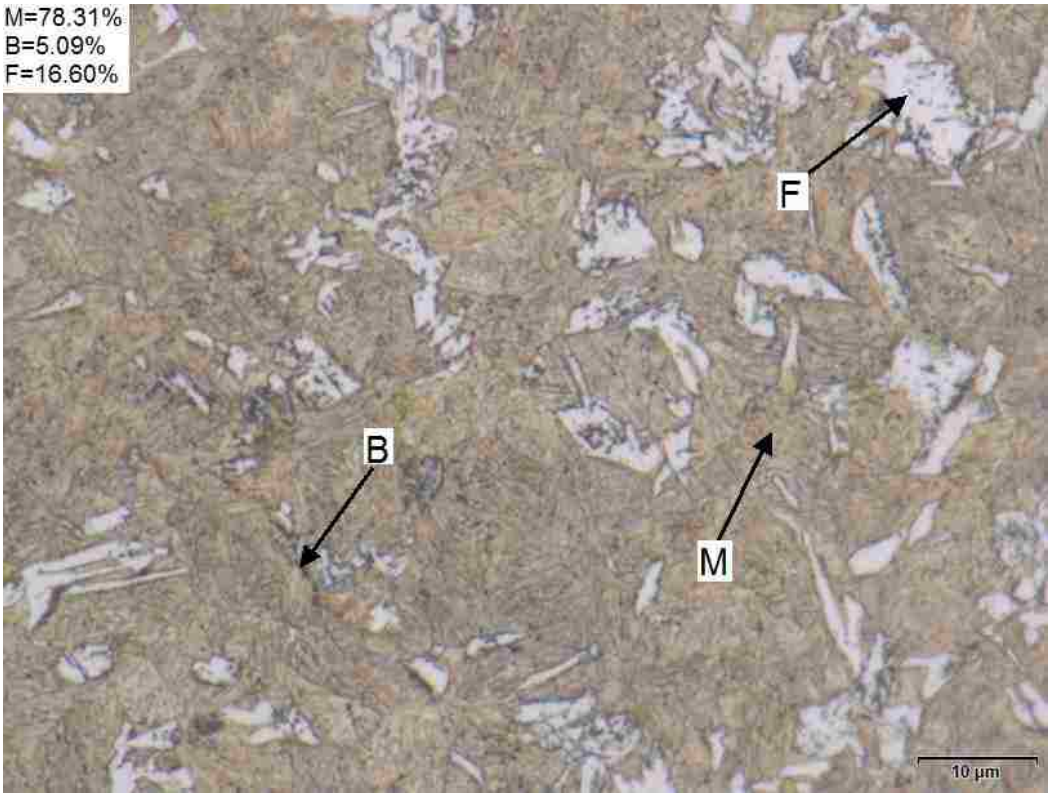

Figure 45 Colour-tint etched optical micrograph for 0.9-mm 22MnB5 steel sheet quenched from 845°C

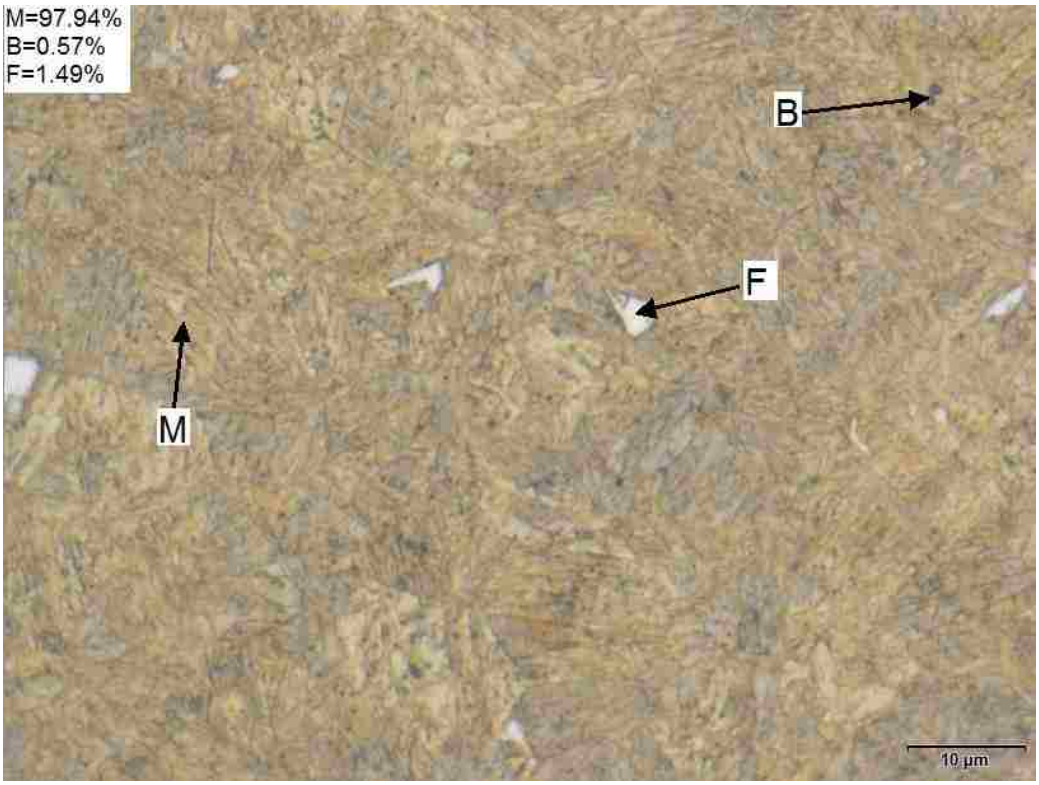

Figure 46 Colour-tint etched optical micrograph for 0.9-mm 22MnB5 steel sheet quenched from 900°C

Starting temperature (°C)	Martensite (%)	Bainite (%)	Ferrite (%)
760	3.81±1.07	19.54±3.67	76.65±2.6
800	25.08±0.2	1.52±0.12	73.4±0.32
845	78.31±1.65	5.09±0.42	16.6±1.23
900	97.94±0.32	0.57±0.11	1.49±0.21

Table 11 Phase fraction for 0.9-mm 22MnB5 steel sheet quenched from different temperatures

Starting temperature (°C)	Martensite (%)	Bainite (%)	Ferrite (%)
760	37±1.61	1.53±0.3	61.47±1.31
800	49.19±2.33	0.24±0.07	50.57±2.26
845	43.3±0.44	11.57±0.7	45.13±1.14
900	95.02±0.89	1.3±0.11	3.68±0.78

Table 12 Phase fraction for 1.8-mm 22MnB5 steel sheet quenched from different temperatures

5 Discussion

5.1 Optimum clamping pressure

The martensite starting and finishing temperatures are about 450°C and 200°C, respectively for 22MnB5 steel. The average cooling rates from 500°C to 200°C with different clamping force (pressure) were calculated and are given in Tables 13 & 14 for both 1.8-mm and 0.9-mm thick specimens. Figures 47 and 48 show the relation between clamping pressure and average cooling rate.

Clamping Force (kN)	Clamping Pressure (MPa)	Cooling rate from 500°C to 200°C (°C/s)
200	1.67	71.4
300	2.50	57.7
400	3.34	115.4
500	4.17	150.0
600	5.01	125.0
700	5.84	103.4
800	6.68	130.4

Table 13 Cooling rate from 500°C to 200°C with different clamping force for 1.8-mm 22MnB5 steel sheet

Clamping Force (kN)	Clamping Pressure (MPa)	Cooling rate from 500°C to 200°C (°C/s)
200	1.67	272.7
300	2.50	576.9
400	3.34	300.0
500	4.17	370.4
600	5.01	491.8
700	5.84	416.7
800	6.68	441.2

Table 14 Cooling rate from 500°C to 200°C with different clamping force for 0.9-mm 22MnB5 steel sheet

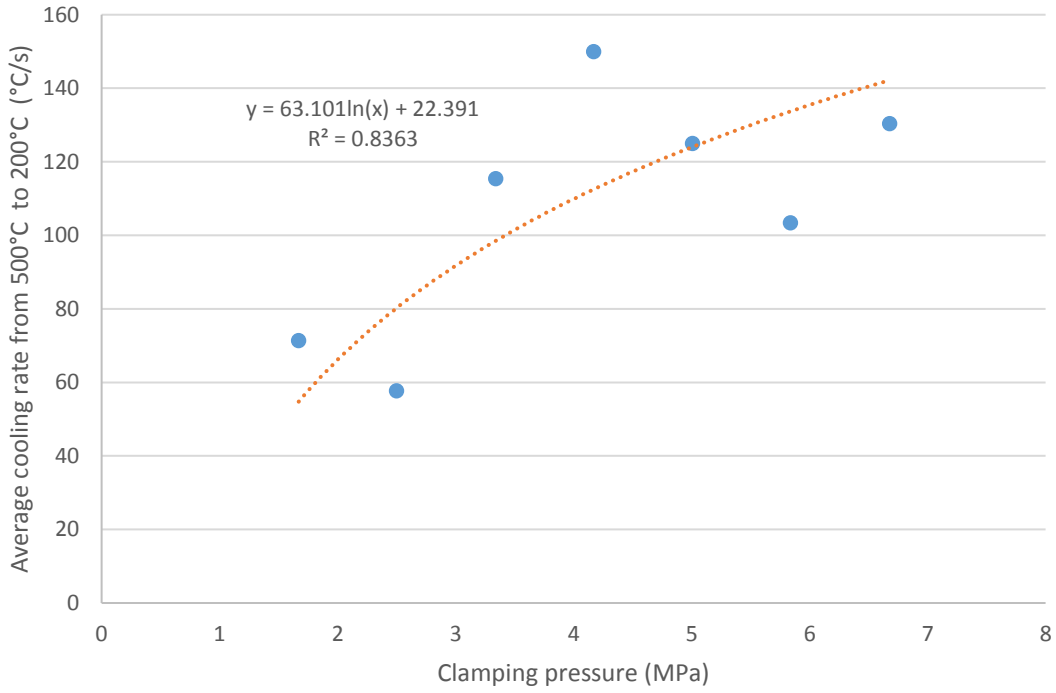

Figure 47 Average cooling rate from 500°C to 200°C vs. clamping pressure for 1.8-mm 22MnB5 steel sheet

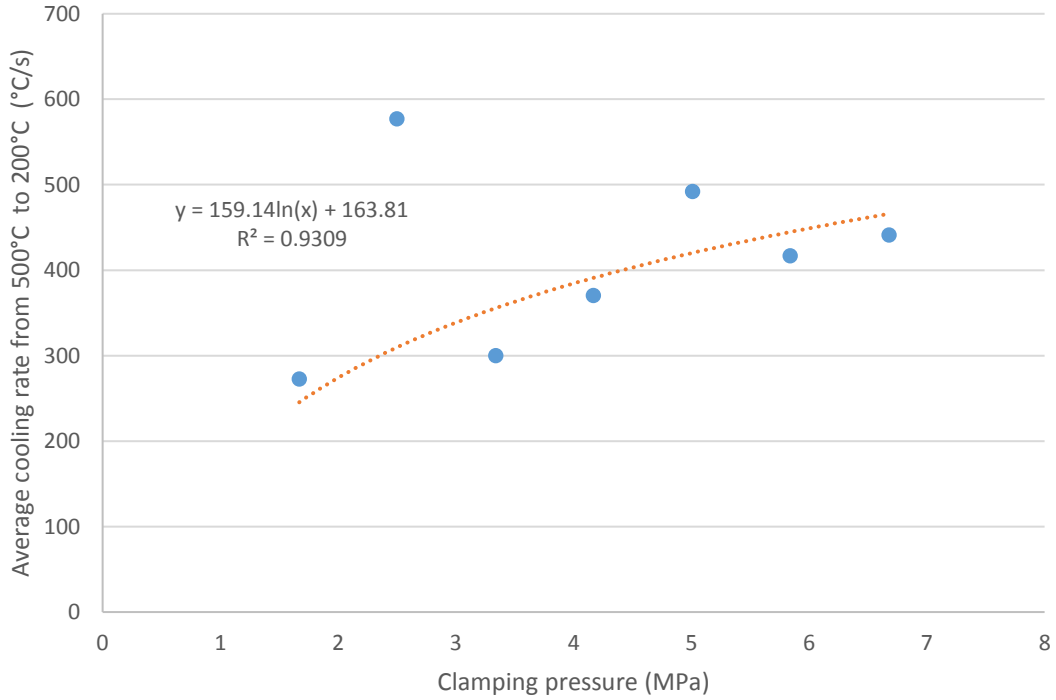

Figure 48 Average cooling rate from 500°C to 200°C vs. clamping pressure for 0.9-mm 22MnB5 steel sheet

Although the average cooling rate vs. clamping pressure exhibits some fluctuations for

both thicknesses of 22MnB5 steel sheet, the trend lines approximately show the relationship between average cooling rate and clamping pressure. The equation of the trend line for the 1.8-mm sheet thicknesses is $y = 63.1\ln(x)+22.4$ and the equation for the 0.9-mm sheet is $y = 159.14\ln(x)+163.8$. The fluctuations may be due to differences resulting from manually transferring the blanks from the furnace to the die, the slightly different die starting temperatures etc.

It is also evident from Figures 47 and 48 that the average cooling rate of the 0.9-mm thick specimens (up to approximately 500°C/s) was much greater than that of the 1.8-mm thick specimens (around 100°C/s). The thinner specimens have a half of the mass of the thicker specimens with the same starting temperature, which results in an increased cooling rate in both air- and die-cooling. However, the very high cooling rate (over 300°C/s) for the 0.9-mm specimen might cause some issues for the coating in industrial hot stamping practice, even though they all reached a fully martensitic microstructure after quenching.

Referring to Table 6 in Section 4.1, the UTS of all the specimens ranges from 1520 MPa to 1535 MPa and the UEL ranges from 4.0% to 4.9%. The consistent mechanical properties (UTS, UEL) of all the tested specimens shows that almost 100% martensitic transformation took place regardless of the clamping pressure. A slight decrease in UTS and an increase in UEL with increasing pressure is shown in Figures 49 and 50. However, since all the as-quenched specimens were almost fully martensitic, and the range of the tensile stress is only 15 MPa (less than 1% of the average value), the variability in the data can be neglected.

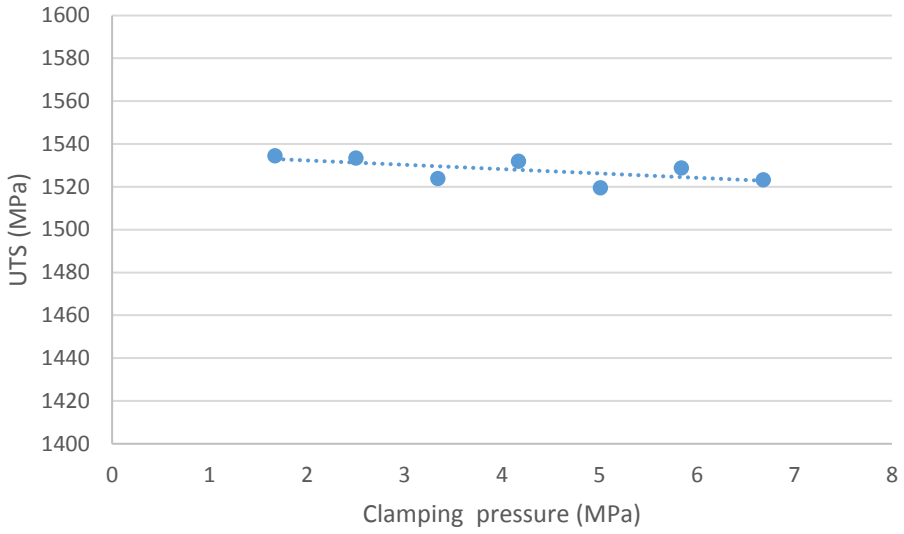

Figure 49 UTS vs. clamping pressure for 1.8-mm 22MnB5 steel

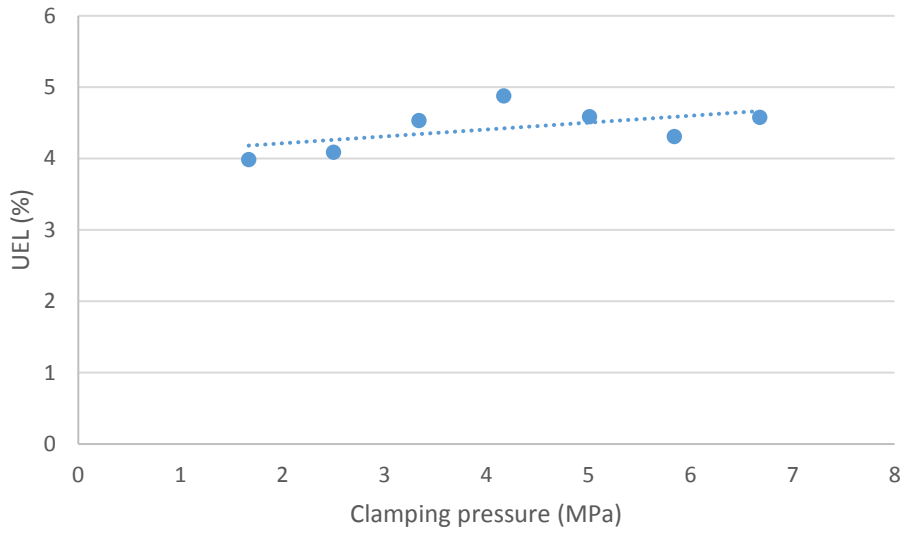

Figure 50 UEL vs. clamping pressure for 1.8-mm 22MnB5 steel

Based on the as-quenched mechanical properties and average cooling rate of the specimens for both sheet thicknesses, it can be concluded that when 22MnB5 steel sheets are quenched from 930°C with a clamping pressure ranging from 1.67 MPa to 6.68 MPa, a fully martensitic microstructure is achieved. In addition, for both 0.9-mm and 1.8mm blanks, when they were quenched from 700°C to 200°C, with different clamping pressures (1.67 MPa to 6.68 MPa), the difference of the cooling time between the highest and lowest

cooling rate was within 0.5 seconds. The clamping pressure in this range does not have a significant influence on the cooling rate or on the as-quenched mechanical properties.

The optimum clamping pressure was chosen to be 4.17 MPa for all the remaining experimental work, due to the fact that the greatest cooling rate took place with this clamping pressure on 1.8-mm 22MnB5 specimens.

5.2 Relationship Among Microstructure, Mechanical Properties and Starting Temperature.

When the starting temperature prior to quenching was between 490°C and 720°C, the corresponding UTS and uniform elongation remained relatively constant. However, when the starting temperature exceeded 760°C, the UTS started to significantly increase while the uniform elongation began to decrease (refer to Figures 39-42 in Section 4.2). In addition, for starting temperatures within the 490°C to 720°C range the mechanical properties are also very close to the as-received mechanical properties. Therefore, the AC_1 temperature of this batch of 22MnB5 steel is between 720°C and 760°C, which is also in accordance with the CCT diagram in Figure 3 (Section 2.1). When the starting temperature is above the AC_1 temperature, the specimen begins to transform to austenite. Tables 15 and 16 show the phase volume fractions and mechanical properties for different starting temperatures. As the starting temperature increases, the martensite volume fraction also increases, which also leads to an increase of UTS and a corresponding decrease of UEL. Figures 51 and 52 show the trend of the evolution of each phase fraction as a function of the starting temperature. The martensite volume fraction influences the UTS the most; for example, for the specimens that were quenched from 760°C, the 1.8-mm specimen has a greater martensite content and a greater UTS than the 0.9-mm specimen. A possible reason for the existence of a high percentage of bainite could be the low cooling rate during the manual transfer of the blank from the furnace to the die.

Starting temperature (°C)	Martensite (%)	Bainite (%)	Ferrite (%)	UTS (MPa)	UEL (%)
760	3.81±1.07	19.54±3.67	76.65±2.6	639 ±1	13.9 ±1.2
800	25.08±0.2	1.52±0.12	73.4±0.32	951 ±3	6.8 ±1.1
845	78.31±1.65	5.09±0.42	16.6±1.23	1402 ±29	4.6 ±0.4
900	97.94±0.32	0.57±0.11	1.49±0.21	1487 ±7	5.0 ±0.2

Table 15 Mechanical properties and phase volume fraction for 0.9 mm 22MnB5 steel sheet quenched from different temperatures

Starting temperature (°C)	Martensite (%)	Bainite (%)	Ferrite (%)	UTS (MPa)	UEL (%)
760	37±1.61	1.53±0.3	61.47±1.31	760 ±2	14.3 ±0.2
800	49.19±2.33	0.24±0.07	50.57±2.26	992 ±1	10.8 ±1.7
845	43.3±0.44	11.57±0.7	45.13±1.14	1365 ±6	5.0 ±1.7
900	95.02±0.89	1.3±0.11	3.68±0.78	1545 ±5	4.6 ±0.1

Table 16 Mechanical properties and phase volume fraction for 1.8 mm 22MnB5 steel sheet quenched from different temperatures

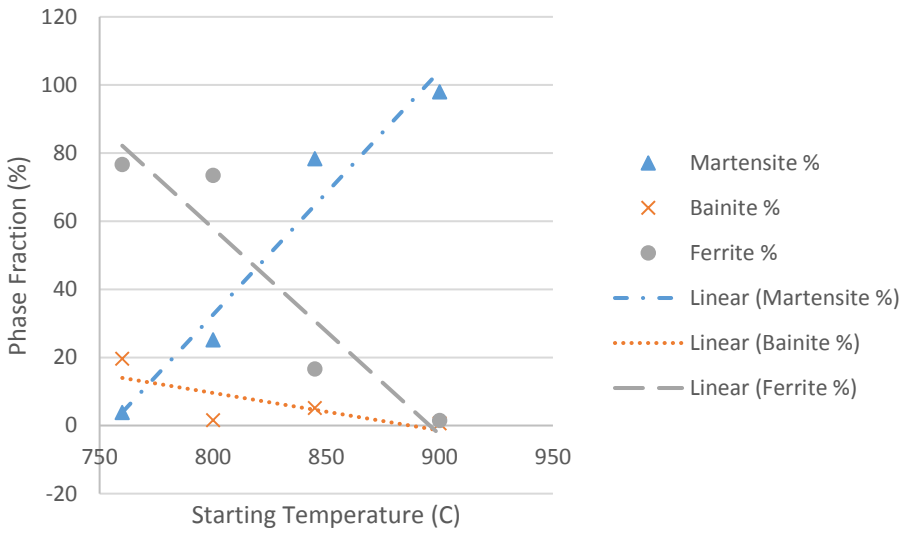

Figure 51 Phase fraction vs. Starting temperature for 0.9-mm 22MnB5 steel sheet

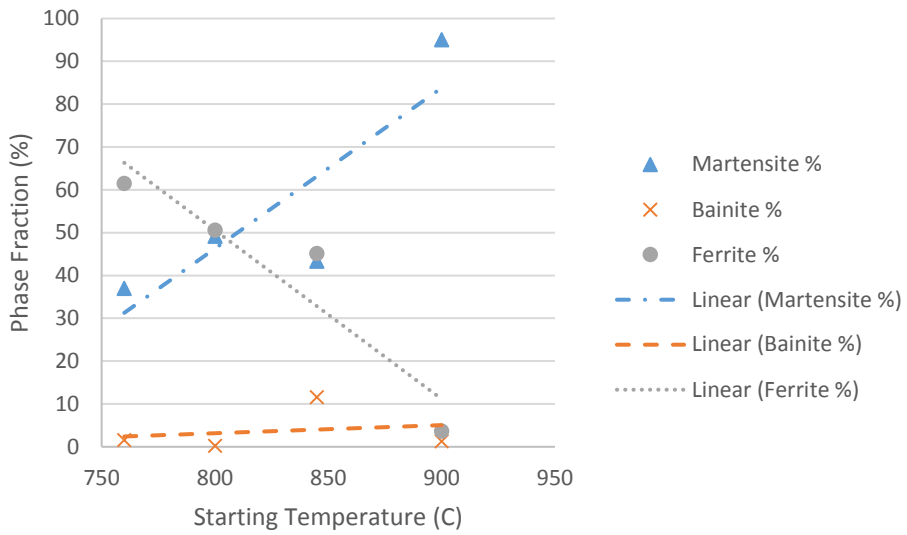

Figure 52 Phase fraction vs. Starting temperature for 0.9-mm 22MnB5 steel sheet

5.3 Recommendations and Future Work

5.3.1 Die Temperature Measurement and Die Cooling

Although the cooling curves were obtained from the DAQ system, the heat transfer coefficient calculation would require the measurement of the die temperature. Due to the big size of the die plate, several thermocouples located in different regions of the die would be needed. Since there might be a temperature gradient along the die plate thickness, the thermocouple should be welded as close to the die contact surface as possible. Holes could be drilled from the bottom of the die plate for thermocouple welding. The thermocouples welded on the die would allow the real-time monitoring on the die temperature. If a series of hot stamping tests are required to be done in a row, tracking the die temperature would be an easier and more efficient way to shorten the cooling waiting period between the tests.

Die cooling can also be improved in different ways. Currently, the cooling of the die between tests consisted of air cooling with a fan which is time-consuming if several tests

will be conducted in a row. Liquid cooling channels could be built in the die plates. There are several reasons for using cooling channels in the die. Firstly, cooling channels can increase the cooling rate of the die which will also improve the efficiency of the tests. Secondly, controlling the liquid cooling circulation speed will allow to control the quenching speed of blanks. With a good control system, a constant cooling rate may also be achieved.

5.3.2 Transfer Method and Time

Transferring steel blanks from the furnace to the die is also one of the main issues in this experimental setup. It is impossible to precisely control the transfer time if the blanks are manually transferred. Especially for tests with slightly different starting temperatures (for example, after two blanks are heated to 800°C and 825°C, respectively, in the furnace and manually transferred to the press) the resulting actual start quenching temperature could both be the same (e.g. 730°C) due to the different transfer times. If a robot was used to do the transfer, then the transfer times would be very repeatable. It could also avoid the heat exposure for a human operator.

5.3.3 Future Work

In this project, all the hot stamping operations were carried out without any deformation of the steel specimens. The focus was on the quenching process. However, in the next research stage, the forming process would also be included, which is consistent with industrial hot stamping practice. It also would involve more problems, including coating, tribology, microstructure, spring-back, die design etc. The maximum clamping pressure in this project was 6.68 MPa. Additional experiments could be done with higher clamping pressures (up to 100 MPa) to more extensively investigate how the clamping pressure

affects the as-quenched material. However, both the specimen and the die set might need to be designed into smaller sizes. From the results of tests with different starting temperatures, the stress-strain curve changed significantly as the temperature increased. The influence of different soaking times for each starting temperature could also be investigated.

6 Conclusions

The following conclusions can be drawn from this research:

1) Quenching 22MnB5 steel sheets from the austenitic temperature range in a room-temperature die with a clamping pressure ranging from 1.67 MPa to 6.68 MPa leads to a fully martensitic microstructure. Under these conditions, the clamping pressure does not have a significant effect on the quenching process for clamping pressures ranging from 1.67 MPa to 6.68 MPa.

2) The partial heating method can be used to obtain tailored properties in hot stamped parts. Since the AC_1 temperature of 22MnB5 steel lies between 720°C and 760°C, a wide range of as-quenched mechanical properties can be achieved for quenching start temperatures above 720°C.
   i) For quenching start temperatures below 720°C, 22MnB5 steel remains quite formable (YS < 500 MPa, UTS < 570 MPa and UEL > 13.5%)
   ii) For quenching start temperatures above 900°C, 22MnB5 steel reaches very high strength with relatively low formability (YS > 1050 MPa, UTS > 1490 MPa and UEL < 5%).
   iii) For quenching start temperatures in the transition range between 720°C and 900°C, 22MnB5 steel will exhibit a wide range of mechanical properties. And Tables 9 & 10 in Section 4.2 can be used to adjust the start temperature prior to quenching so as to obtain the desired mechanical properties in particular locations of the part.

3) The martensite content in the microstructure of 22MnB5 steel sheets has the most significant influence on the mechanical properties (yield stress, UTS and uniform elongation). When the quenching start temperature is in the range of 760°C to 900°C and the quenching is performed in a die that is initially at room-temperature,

the final as-quenched mechanical properties are similar to those of dual-phase steels (i.e. ferrite + martensite, or ferrite + martensite + bainite), with the UTS and the martensite content increasing with the starting temperature.

4) Two thicknesses (0.9 mm and 1.8 mm) of 22MnB5 steel sheets were tested. The two sheet materials responded in a very similar manner to the quenching start temperature, although the thinner gauge specimens exhibited faster cooling rates and lower cooling time for both air- and die-cooling.

References

[1] "2017-2025 Model Year Light-Duty Vehicle GHG Emissions and CAFE Standards: Supplemental Notice of Intent - ProQuest."

[2] H. Karbasian and A. E. Tekkaya, "A review on hot stamping," *J. Mater. Process. Technol.*, vol. 210, no. 15, pp. 2103–2118, 2010.

[3] M. Merklein and J. Lechler, "Determination of Material and Process Characteristics for Hot Stamping Processes of Quenchenable Ultra High Strength Steels with Respect to a FE-based Process Design," *SAE Int. J. Mater. Manf.*, vol. 1, pp. 411–426, 2008.

[4] M. Nikravesh, M. Naderi, G. H. Akbari, and W. Bleck, "Phase transformations in a simulated hot stamping process of the boron bearing steel," *Mater. Des.*, vol. 84, pp. 18–24, 2015.

[5] M. Merklein, J. Lechler, and T. Stoehr, "Characterization of tribological and thermal properties of metallic coatings for hot stamping boron-manganese steels," 2008.

[6] L. G. Aranda, Y. Chastel, J. F. Pascual, and T. D. Negro, *Experiments and Simulation of Hot Stamping of Quenchable Steels*. JSTP, 2002.

[7] M. Naderi, "Hot Stamping of Ultra High Strength Steels," 2007.

[8] M. Maikranz-Valentin, U. Weidig, U. Schoof, H.-H. Becker, and K. Steinhoff, "Components with Optimised Properties due to Advanced Thermo-mechanical Process Strategies in Hot Sheet Metal Forming," *steel Res. Int.*, vol. 79, no. 2, pp. 92–97, Feb. 2008.

[9] S. Salari, M. Naderi, and W. Bleck, "Constitutive Modeling During Simultaneous Forming and Quenching of a Boron Bearing Steel at High Temperatures," *J. Mater. Eng. Perform.*, vol. 24, no. 2, pp. 808–815, 2014.

[10] K. Kusumi, S. Yamamoto, T. Takeshita, and M. Abe, "The effect of martensite transformation on shape fixability in the hot stamping process," *Steel Res. Int*, 2008.

[11] M. Nikravesh, M. Naderi, and G. H. Akbari, “Influence of hot plastic deformation and cooling rate on martensite and bainite start temperatures in 22MnB5 steel,” *Mater. Sci. Eng. A*, vol. 540, pp. 24–29, 2012.

[12] M. C. Somani, L. P. Karjalainen, M. Eriksson, and M. Oldenburg, “Dimensional Changes and Microstructural Evolution in a B-bearing Steel in the Simulated Forming and Quenching Process.,” *ISIJ Int.*, vol. 41, no. 4, pp. 361–367, Apr. 2001.

[13] K. Ikeuchi and J. Yanagimoto, “Valuation method for effects of hot stamping process parameters on product properties using hot forming simulator,” *J. Mater. Process. Technol.*, vol. 211, no. 8, pp. 1441–1447, 2011.

[14] T.-H. Hung, P.-W. Tsai, F.-K. Chen, T.-B. Huang, and W.-L. Liu, “Measurement of Heat Transfer Coefficient of Boron Steel in Hot Stamping,” *Procedia Eng.*, vol. 81, pp. 1750–1755, 2014.

[15] B. Abdulhay, B. Bourouga, and C. Dessain, “Experimental and theoretical study of thermal aspects of the hot stamping process,” *Appl. Therm. Eng.*, vol. 31, no. 5, pp. 674–685, 2010.

[16] P. Hu, L. Ying, Y. Li, and Z. Liao, “Effect of oxide scale on temperature-dependent interfacial heat transfer in hot stamping process,” *J. Mater. Process. Technol.*, vol. 213, no. 9, pp. 1475–1483, 2013.

[17] Y. Chang, X. Tang, K. Zhao, P. Hu, and Y. Wu, “Investigation of the factors influencing the interfacial heat transfer coefficient in hot stamping,” *J. Mater. Process. Technol.*, vol. 228, pp. 25–33, 2016.

[18] M. Merklein, J. Lechler, and T. Stoehr, “Investigations on the thermal behavior of ultra high strength boron manganese steels within hot stamping,” *Int. J. Mater. Form.*, vol. 2, no. SUPPL. 1, pp. 259–262, 2009.

[19] S. Sjöström, *The calculation of quench stresses in steel*. Division of solid mechanics and strength of materials, Department of mechanical engineering [Inst. för konstruktions-och produktionsteknik], Univ., 1982.

[20] M. Merklein, M. Wieland, M. Lechner, S. Bruschi, and A. Ghiotti, “Hot stamping of boron steel sheets with tailored properties: A review,” *J. Mater. Process. Technol.*, vol. 228, pp. 11–24, 2016.

[21] T. Stöhr, J. Lechler, and M. Merklein, “Investigations on different strategies for influencing the microstructural properties with respect to partial hot stamping,” in *2nd International Conference on Hot Sheet Metal Forming of High Performance Steels, Luleå, Sweden, June*, 2009, pp. 15–17.

[22] J. Erhardt, R., Boke, “Industrial application of hot forming process simulation,” *1st Int. Conf. Hot Sheet Met. Form. High-Performance Steel*, p. Pages 83-88, 2003.

[23] M. Merklein and T. Svec, “Hot stamping: Manufacturing functional optimized components,” *Prod. Eng.*, vol. 7, no. 2–3, pp. 141–151, 2013.

[24] S. Lenze, F.J., Banik, J., Sikora, “Applications of hot formed parts for body in white,” in *International Deep Drawing Research Group IDDRG*, 2008, pp. 511–519.

[25] B. Casas, D. Latre, N. Rodriguez, and I. Valls, “Tailor made tool materials for the present and upcoming tooling solutions in hot sheet metal forming,” in *1st International Conference on Hot Sheet Metal Forming of High Performance Steels, Luleå, Sweden, October*, 2008, pp. 22–24.

[26] C. Hoff, *Untersuchung der Prozesseinflussgrößen beim Presshärten des höchstfesten Vergütungsstahls 22MnB5*. Meisenbach, 2007.

[27] K. Mori and Y. Okuda, “Tailor die quenching in hot stamping for producing ultra-high strength steel formed parts having strength distribution,” *CIRP Ann. - Manuf. Technol.*, vol. 59, no. 1, pp. 291–294, 2010.

[28] D. D. Múnera, A. Pic, D. Abou-khalil, and F. Shmit, “Innovative Press Hardened Steel Based Laser Welded Blanks Solutions for Weight Savings and Crash Safety Improvements,” *SAE Int. J. Mater. Manuf.*, vol. 1, no. 1, pp. 472–479, 2008.

[29] B. Brecht, J., Goeddeke, “Warmgeformte tailor rolled products, Funktionsoptimaler Leichtbau für die Fahrzeugkarosseries,” *Proc. 8th Erlanger Work.*

Warmblechumformung, pp. 85–94.

[30] A. K. De, J. G. Speer, and D. K. Matlock, “Color tint-etching for multiphase steels,” *Adv. Mater. Process.*, vol. 161, no. 2, pp. 27–30, 2003.

[31] J. Schindelin *et al.*, “Fiji: An open-source platform for biological-image analysis,” *Nat. Methods*, vol. 9, no. 7, pp. 676–682, 2012.

Appendices

Appendix A: Temperature Profile for 22MnB5 steel sheet quenched with different clamping force.

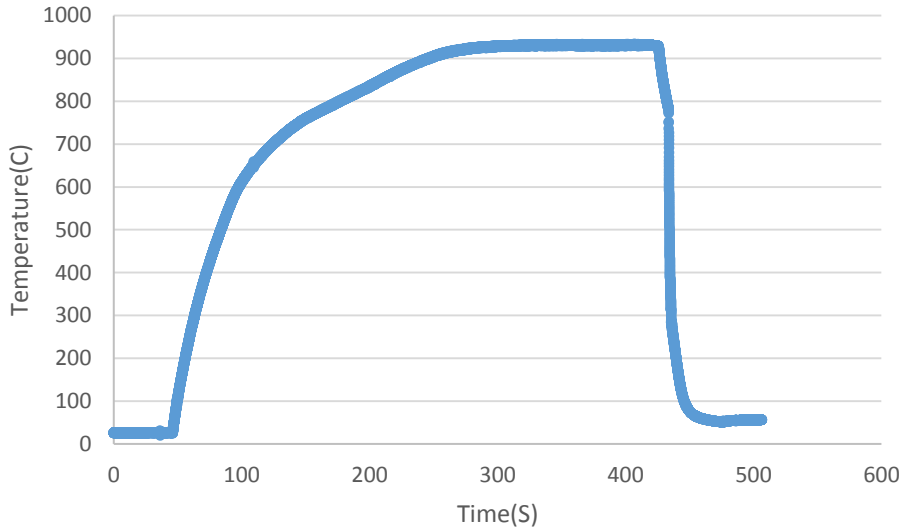

Figure 53 Temperature history for 1.8-mm 22MnB5 steel quenched with a 300-kN clamping force

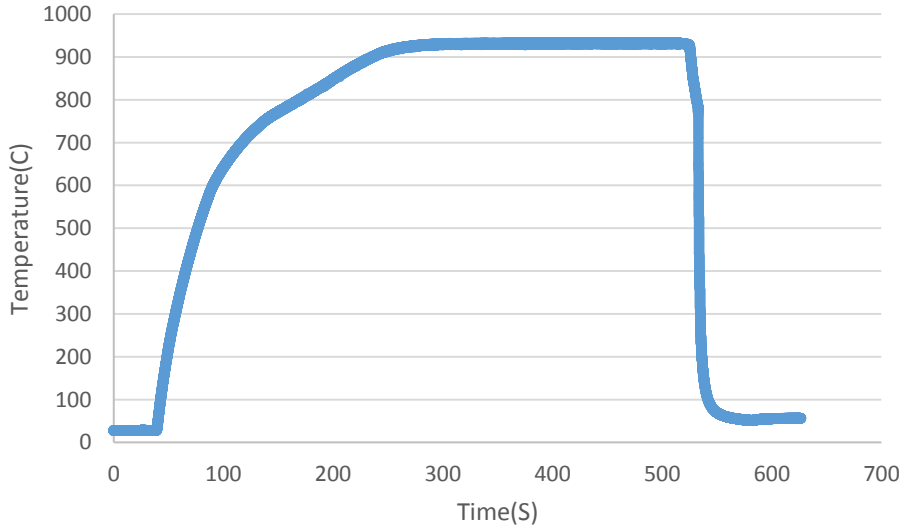

Figure 54 Temperature history for 1.8-mm 22MnB5 steel quenched with a 400-kN clamping force

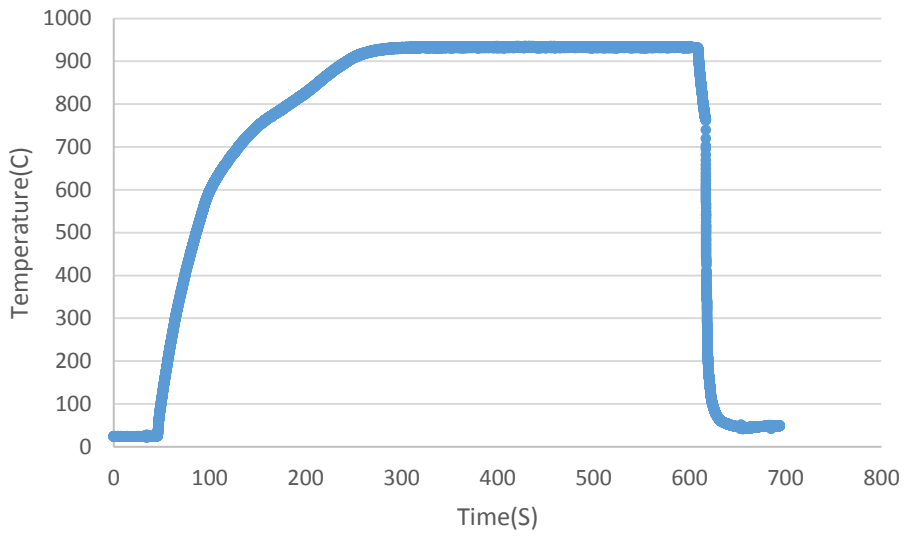

Figure 55 Temperature history for 1.8-mm 22MnB5 steel quenched with a 500-kN clamping force

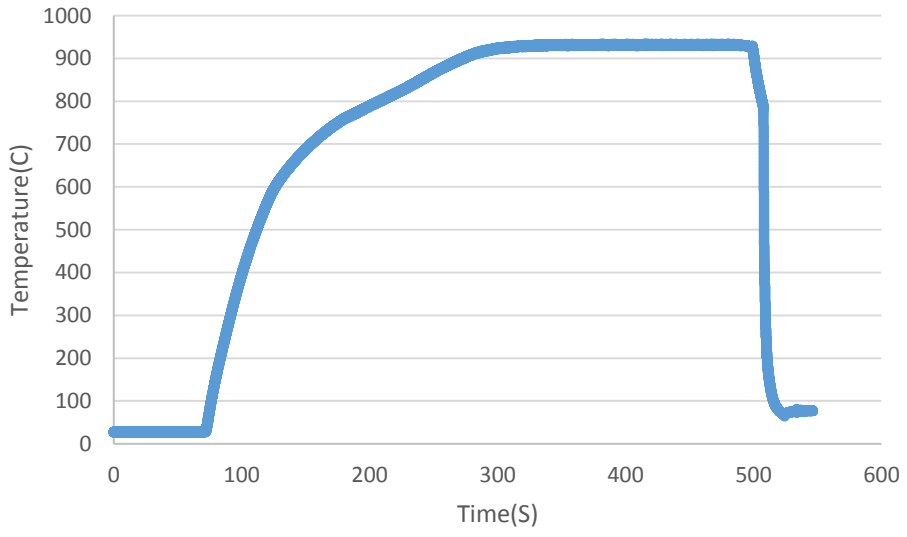

Figure 56 Temperature history for 1.8-mm 22MnB5 steel quenched with a 600-kN clamping force

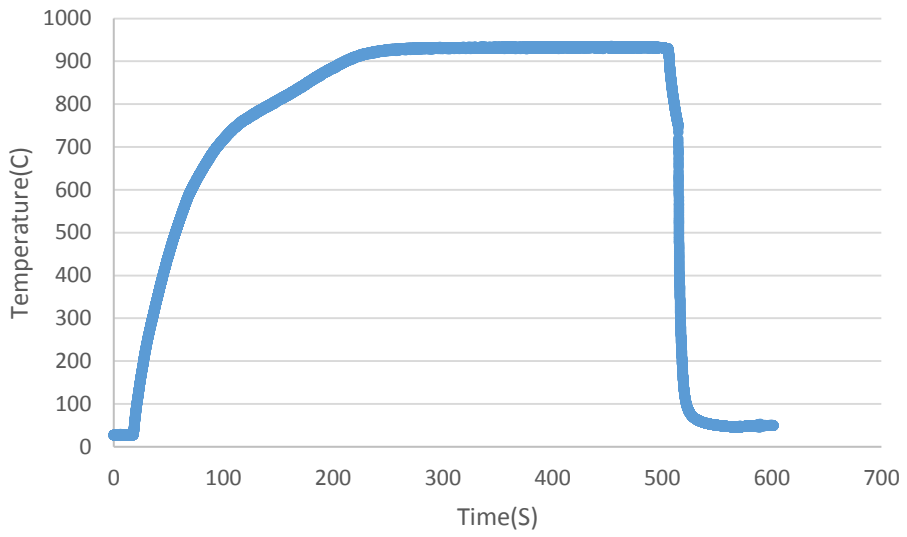

Figure 57 Temperature history for 1.8-mm 22MnB5 steel quenched with a 700-kN clamping force

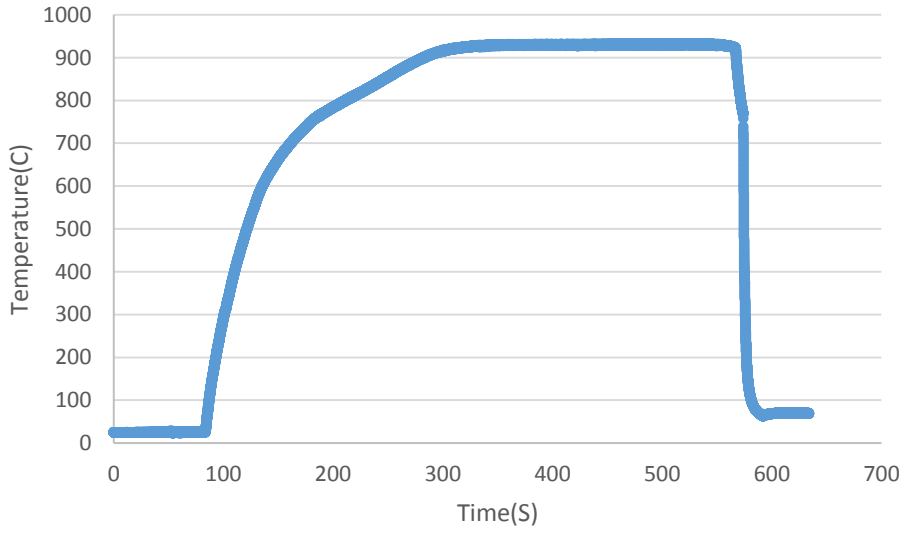

Figure 58 Temperature history for 1.8-mm 22MnB5 steel quenched with a 800-kN clamping force

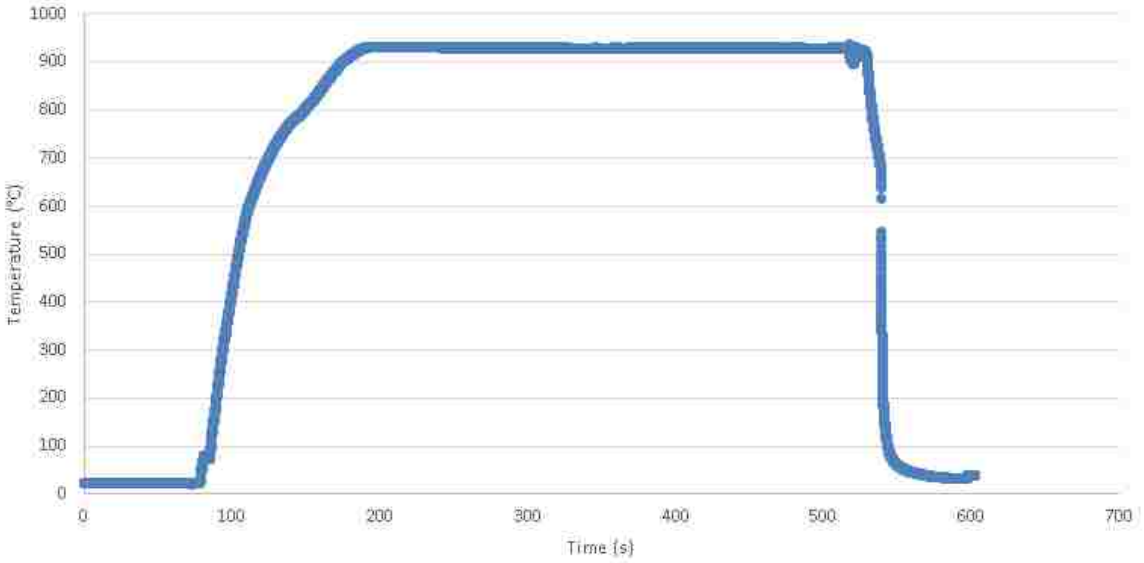

Figure 59 Temperature history for 0.9-mm 22MnB5 steel quenched with a 200-kN clamping force

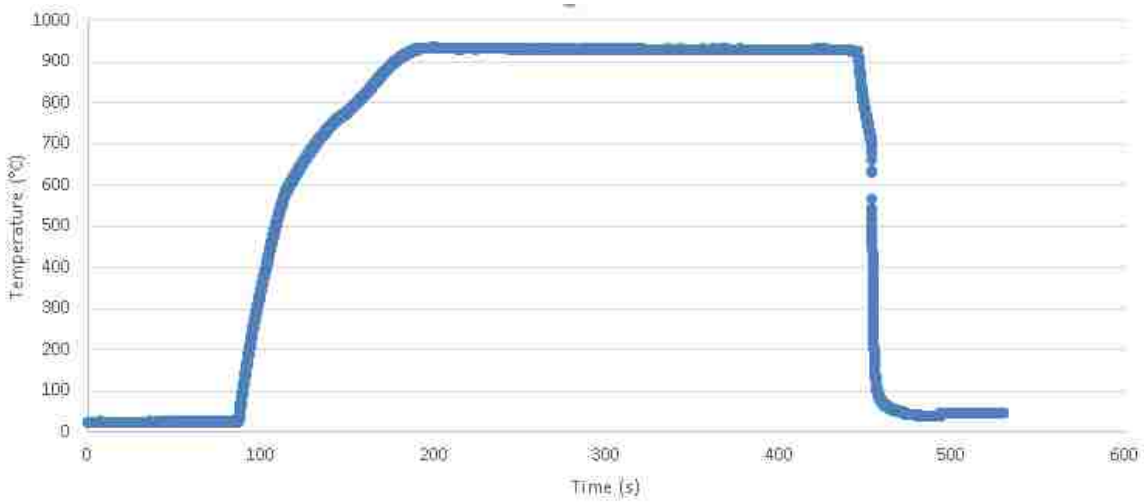

Figure 60 Temperature history for 0.9-mm 22MnB5 steel quenched with a 400-kN clamping force

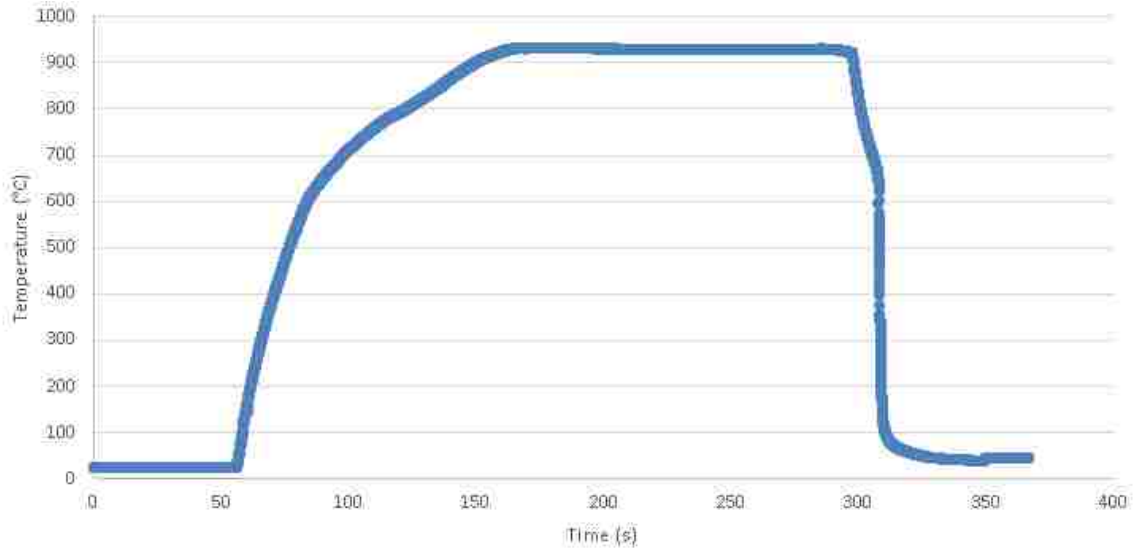

Figure 61 Temperature history for 0.9-mm 22MnB5 steel quenched with a 500-kN clamping force

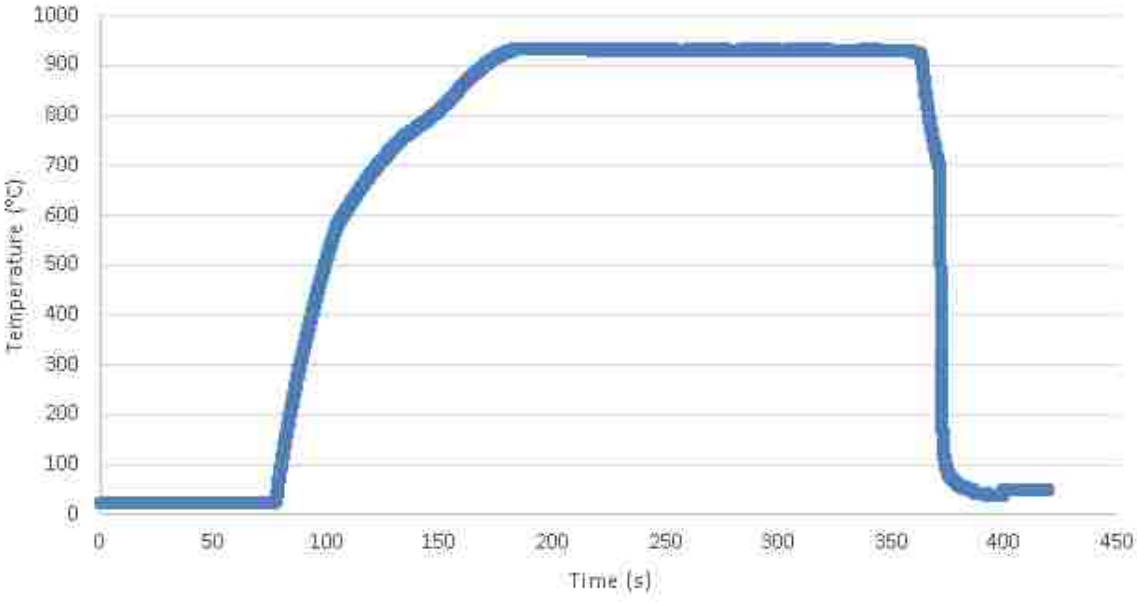

Figure 62 Temperature history for 0.9-mm 22MnB5 steel quenched with a 600-kN clamping force

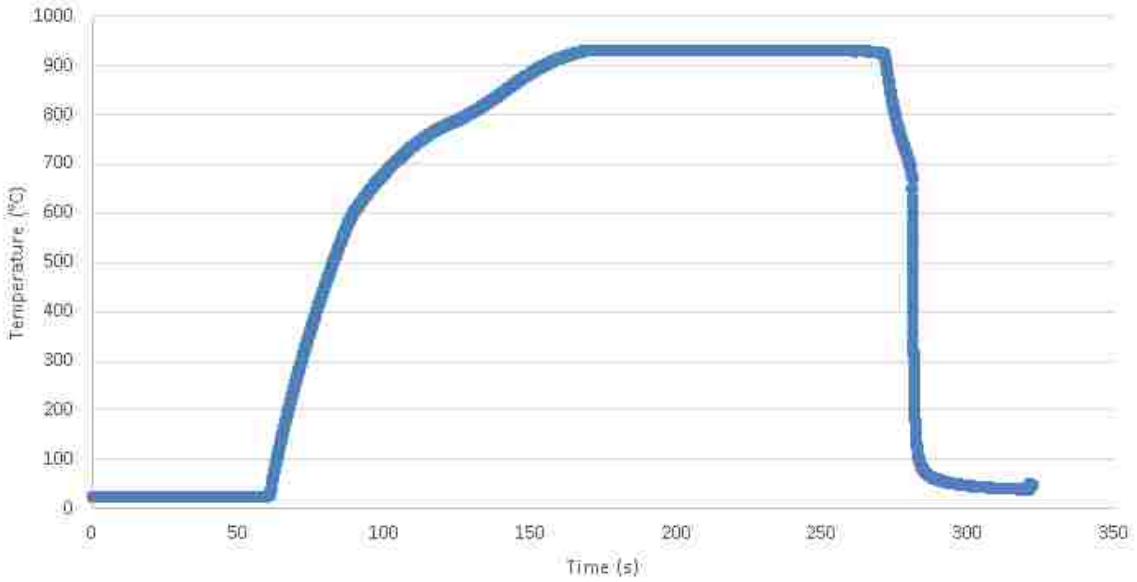

Figure 63 Temperature history for 0.9-mm 22MnB5 steel quenched with a 700-kN clamping force

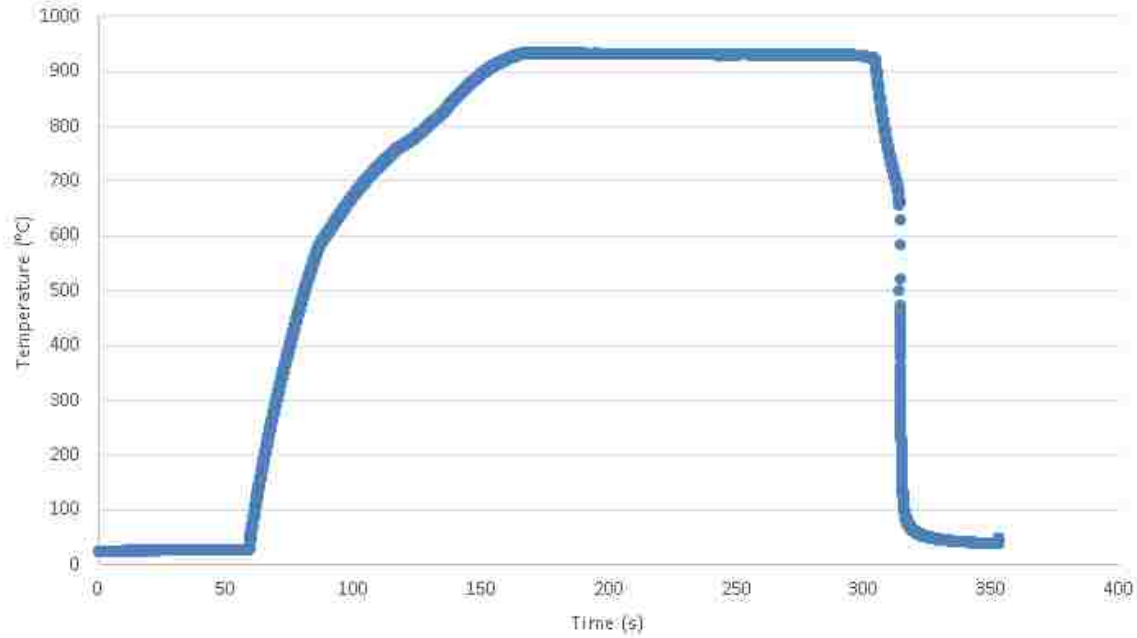

Figure 64 Temperature history for 0.9-mm 22MnB5 steel quenched with a 800-kN clamping force

Appendix B: Engineering stress vs. Engineering stress Curve for 1.8-mm 22MnB5 steel with different clamping forces.

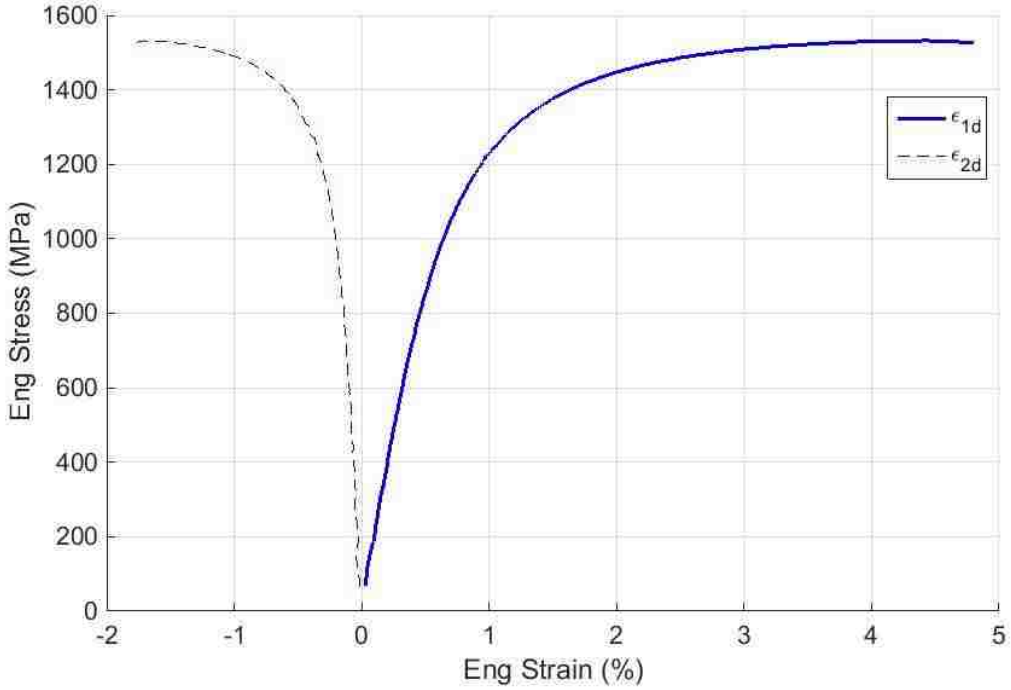

Figure 65 Engineering stress vs. engineering strain of 1.8 mm 22MnB5 steel quenched with 300 kN clamping force

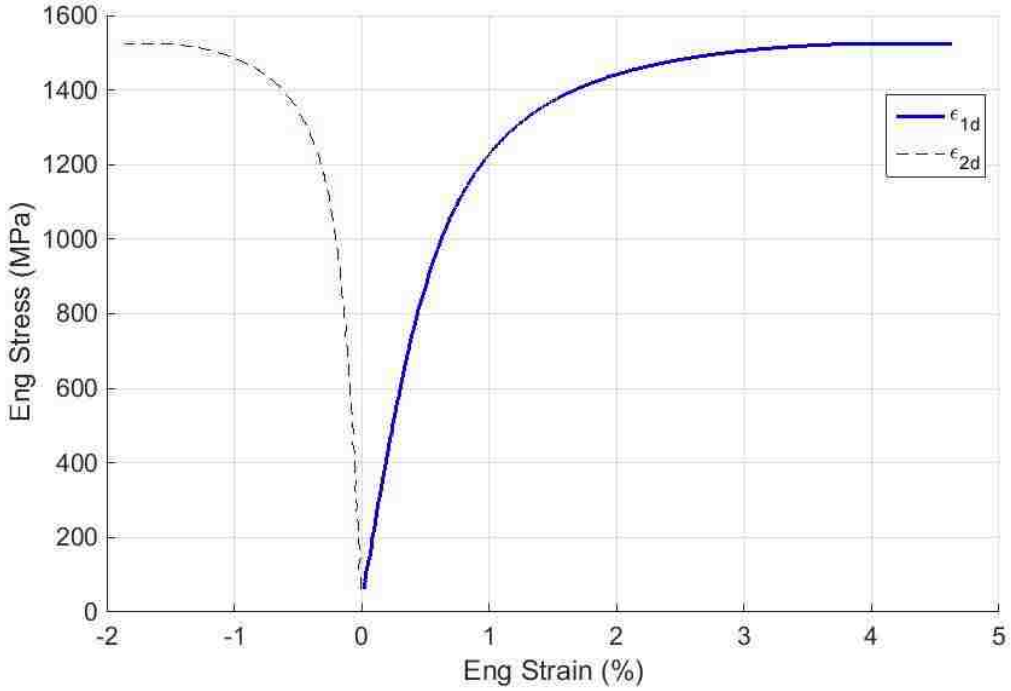

Figure 66 Engineering stress vs. engineering strain of 1.8 mm 22MnB5 steel quenched with 400 kN clamping force

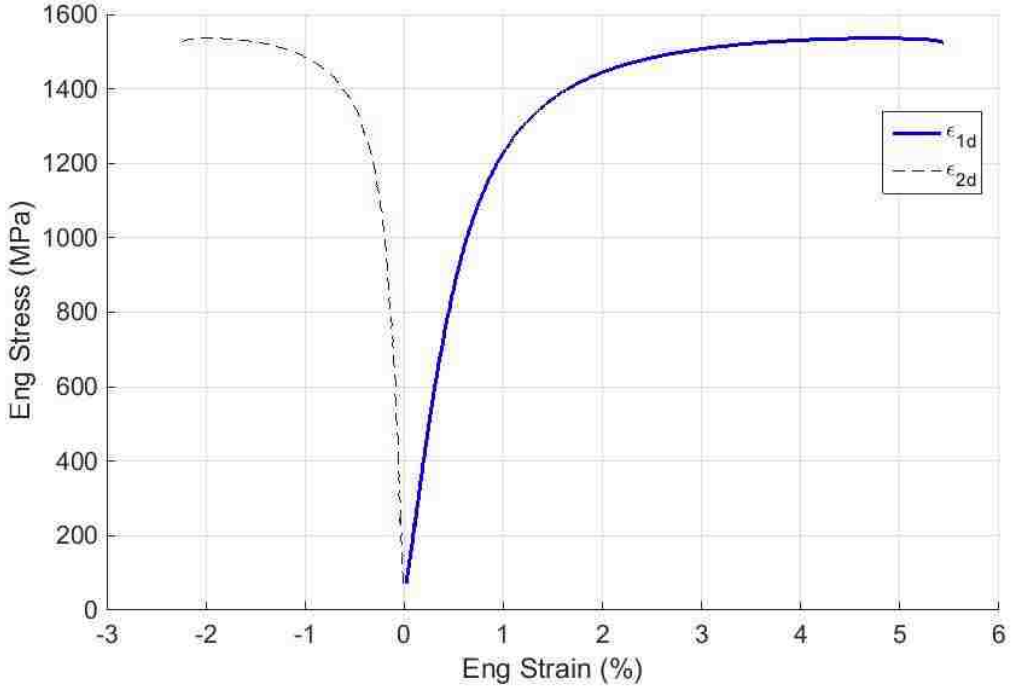

Figure 67 Engineering stress vs. engineering strain of 1.8 mm 22MnB5 steel quenched with 500 kN clamping force

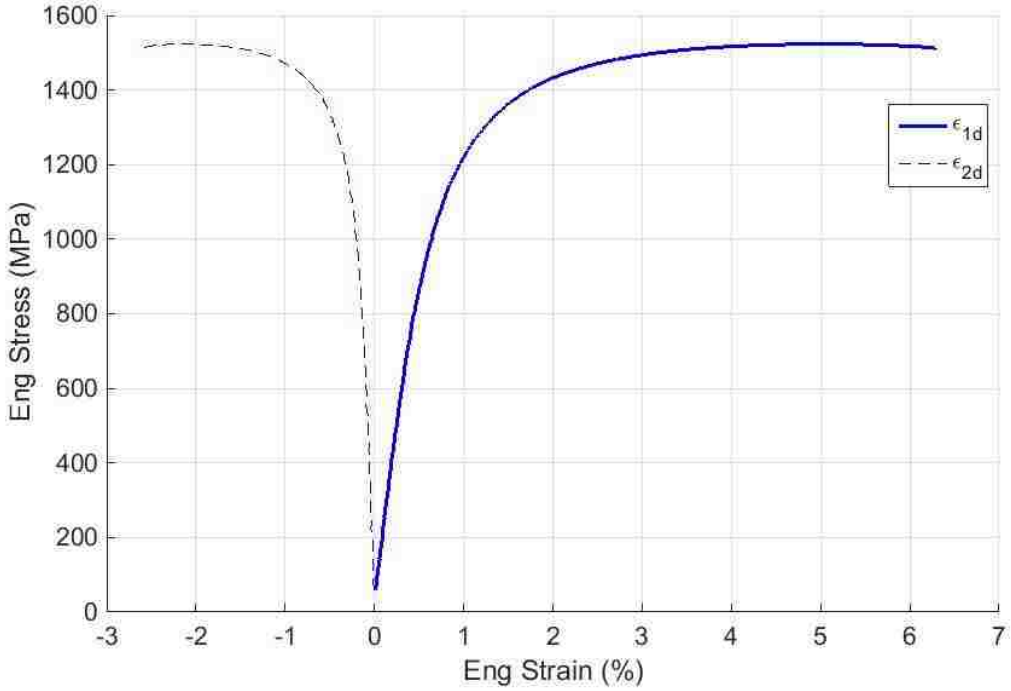

Figure 68 Engineering stress vs. engineering strain of 1.8 mm 22MnB5 steel quenched with 600 kN clamping force

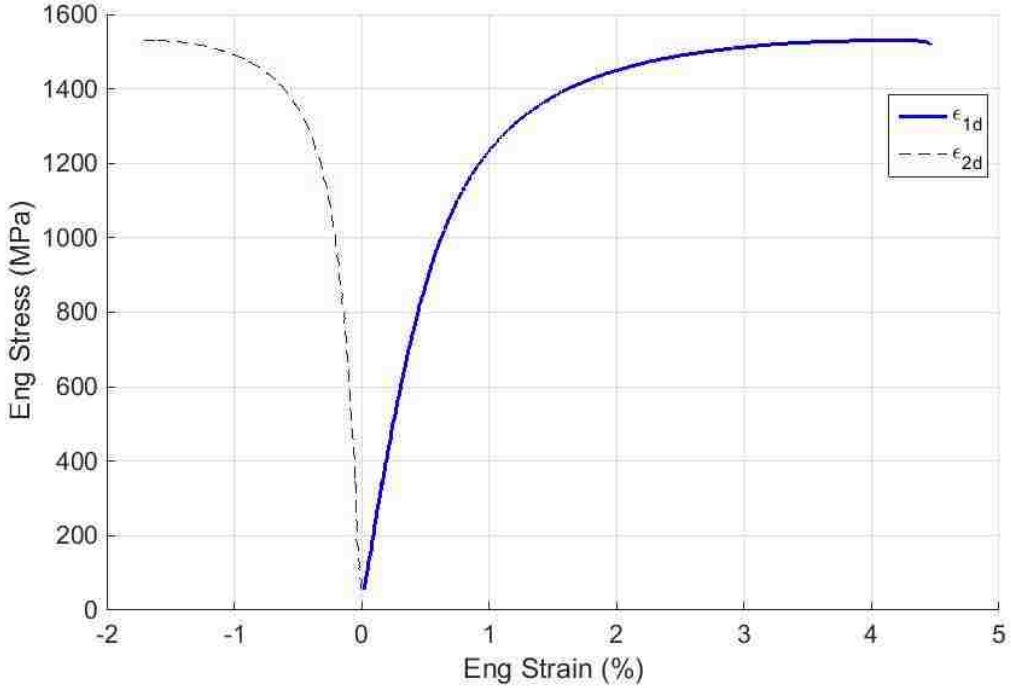

Figure 69 Engineering stress vs. engineering strain of 1.8 mm 22MnB5 steel quenched with 700 kN clamping force

Appendix C: Engineering stress vs. Engineering stress Curve for 0.9 mm 22MnB5 steel quenched from different starting temperatures.

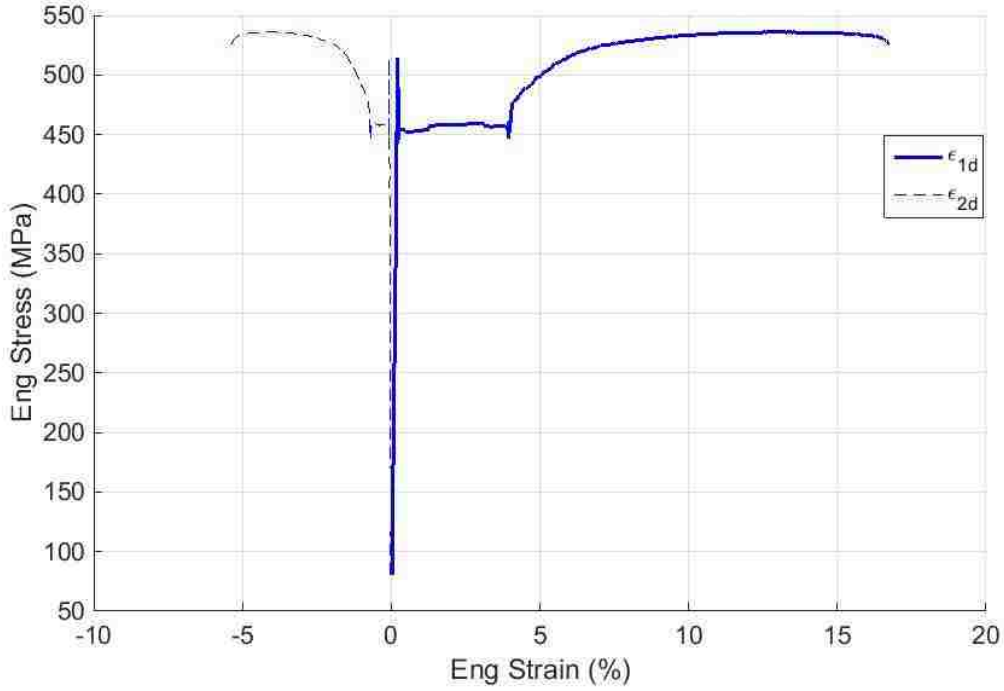

Figure 70 Engineering stress vs. engineering strain of 0.9 mm 22MnB5 steel quenched from 630°C

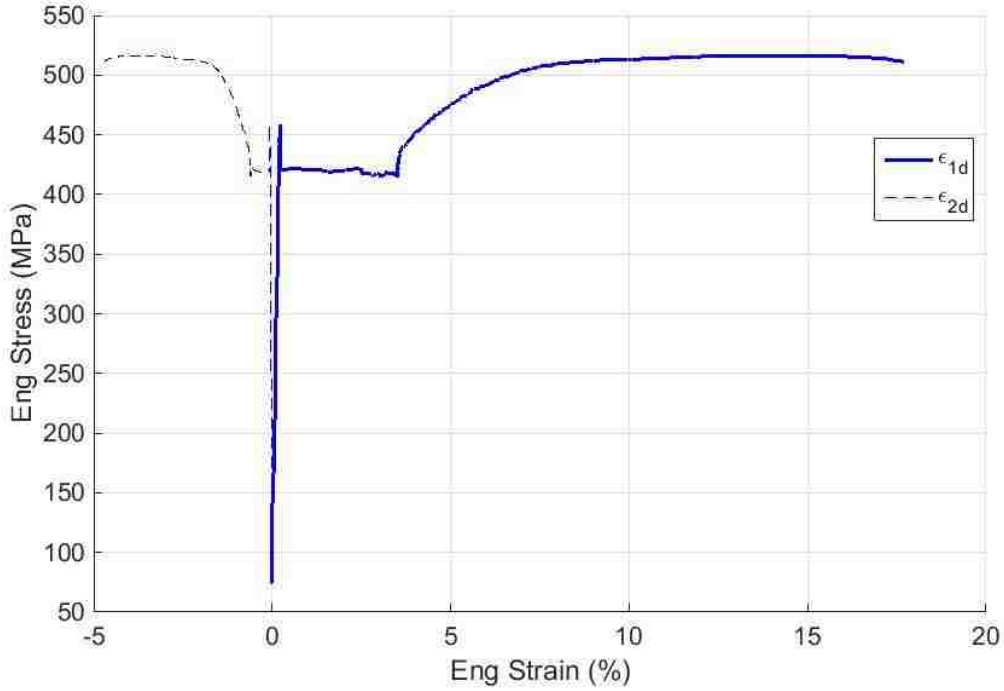

Figure 71 Engineering stress vs. engineering strain of 0.9 mm 22MnB5 steel quenched from 675°C

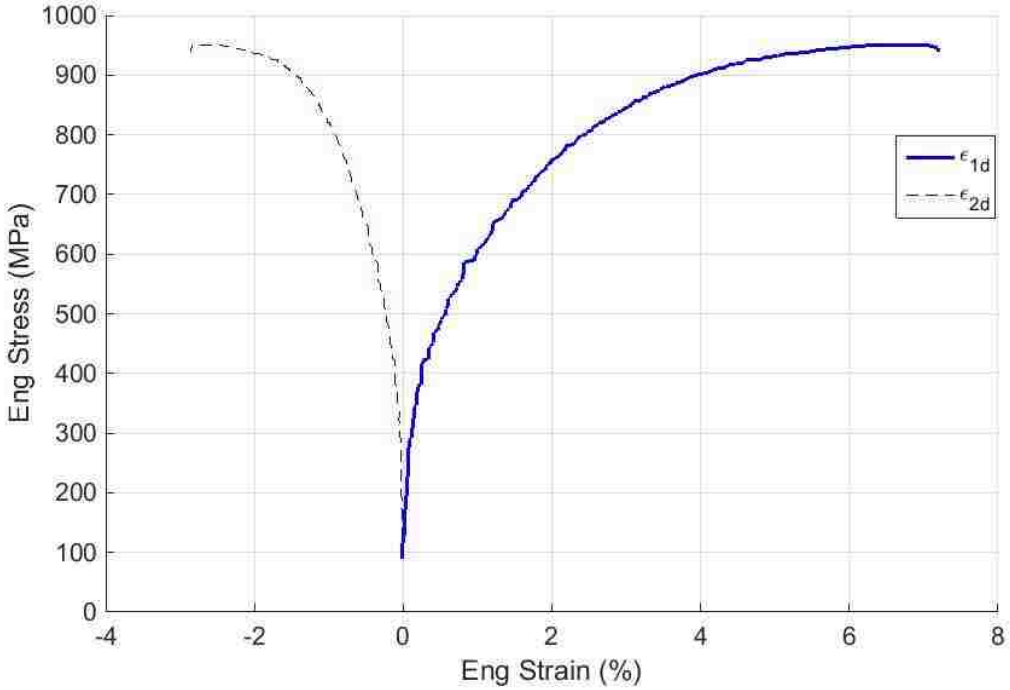

Figure 72 Engineering stress vs. engineering strain of 0.9 mm 22MnB5 steel quenched from 800°C

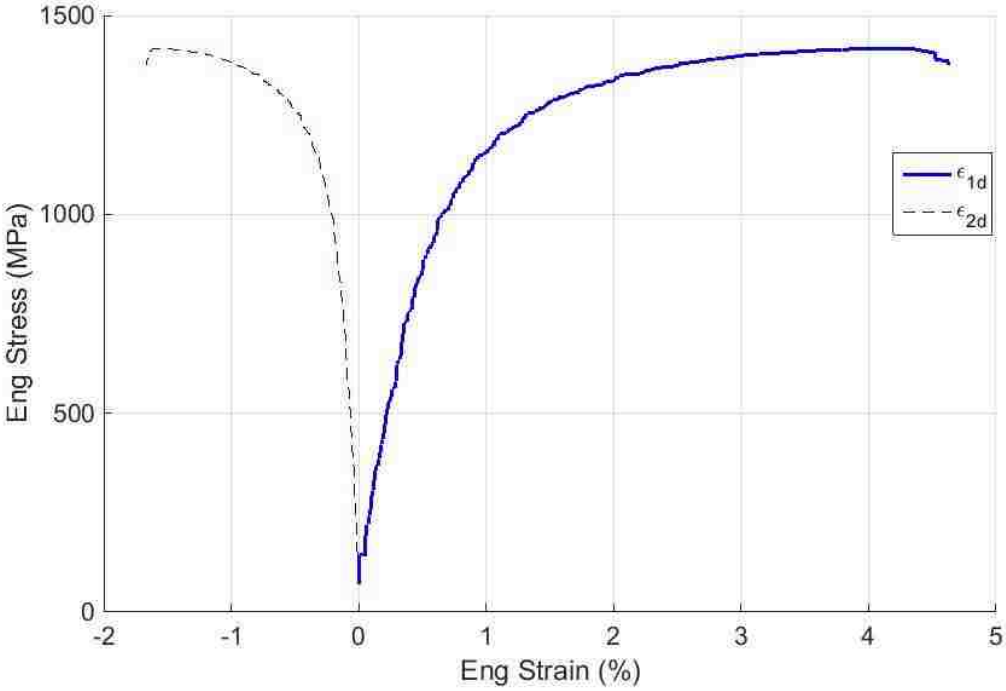

Figure 73 Engineering stress vs. engineering strain of 0.9 mm 22MnB5 steel quenched from 845°C

Appendix D: Temperature Profile for 22MnB5 steel sheet quenched from different temperatures.

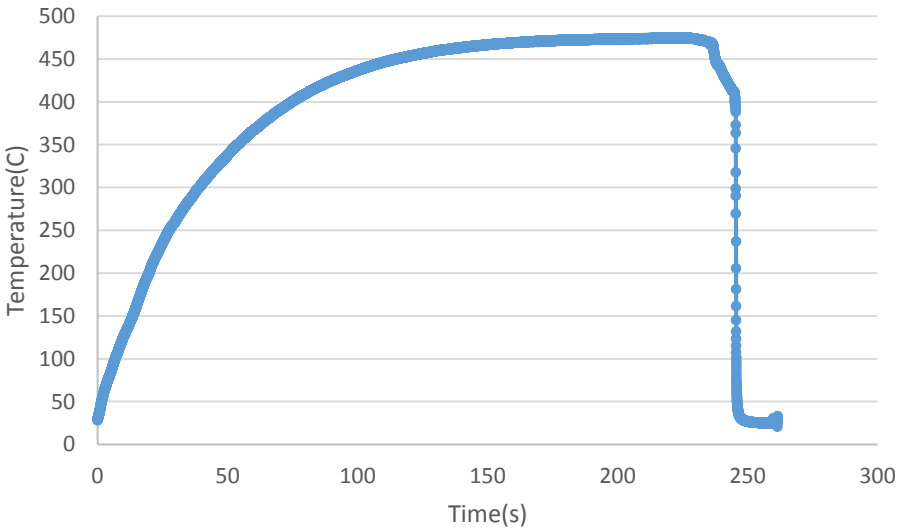

Figure 74 Temperature history for 0.9-mm 22MnB5 steel quenched from 490°C

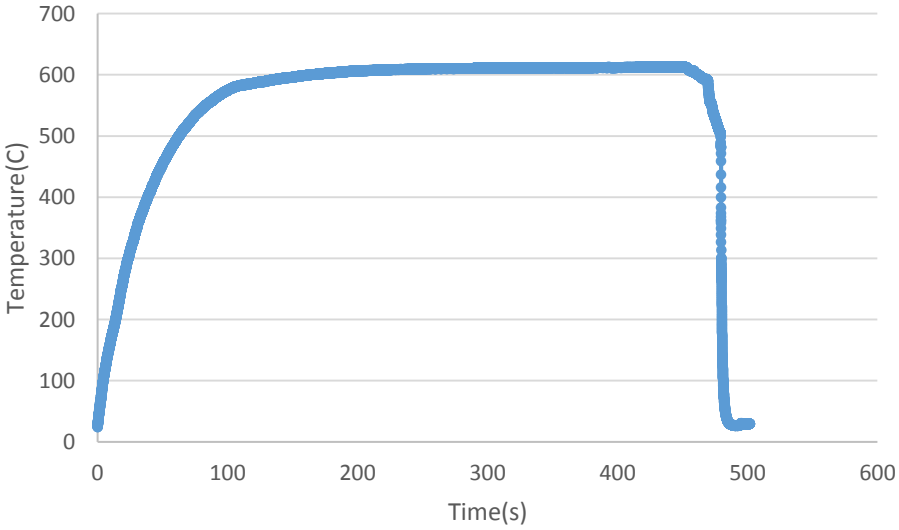

Figure 75 Temperature history for 0.9-mm 22MnB5 steel quenched from 630°C

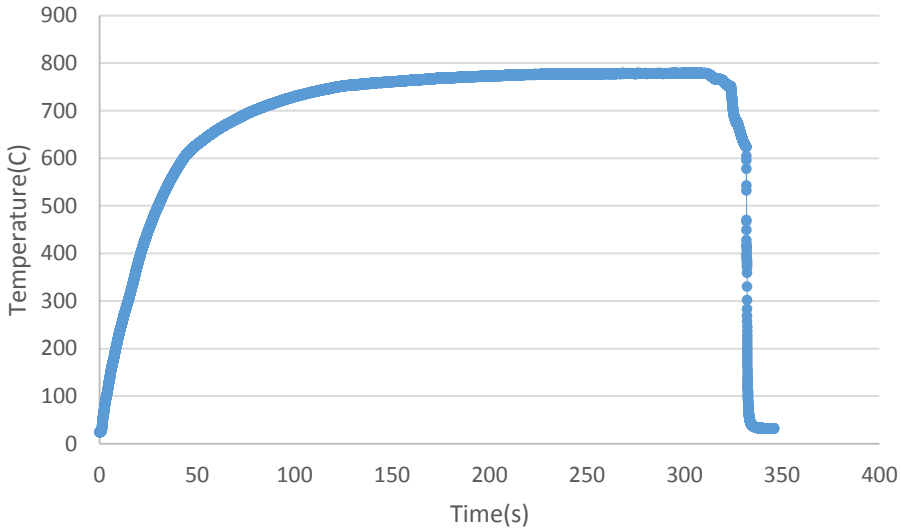

Figure 76 Temperature history for 0.9-mm 22MnB5 steel quenched from 800°C

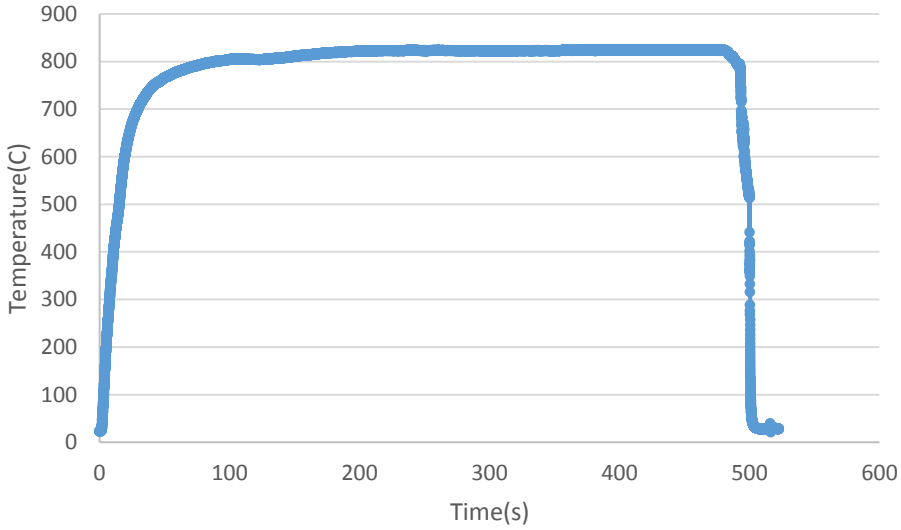

Figure 77 Temperature history for 0.9-mm 22MnB5 steel quenched from 845°C

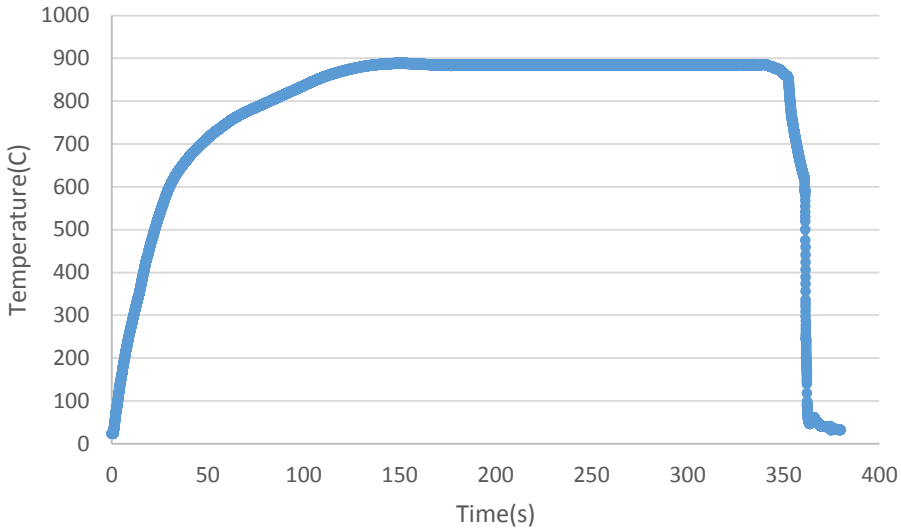

Figure 78 Temperature history for 0.9-mm 22MnB5 steel quenched from 900°C

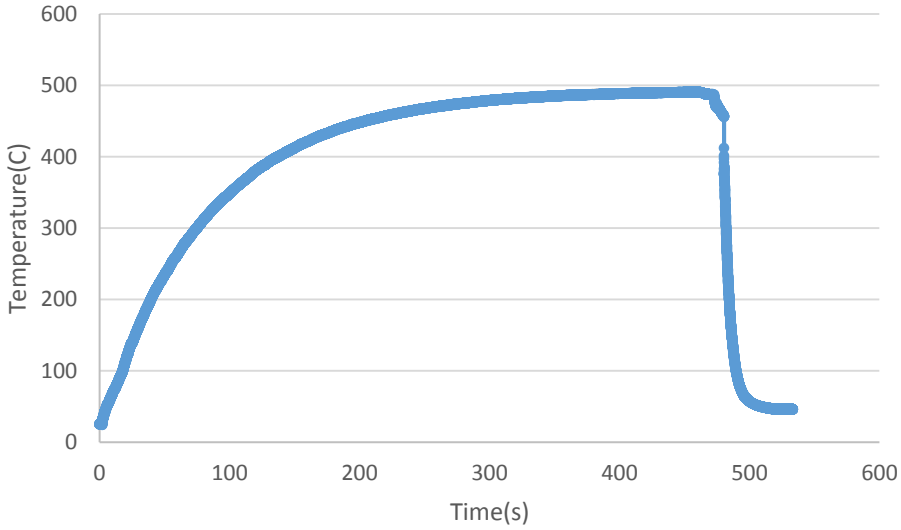

Figure 79 Temperature history for 1.8-mm 22MnB5 steel quenched from 490°C

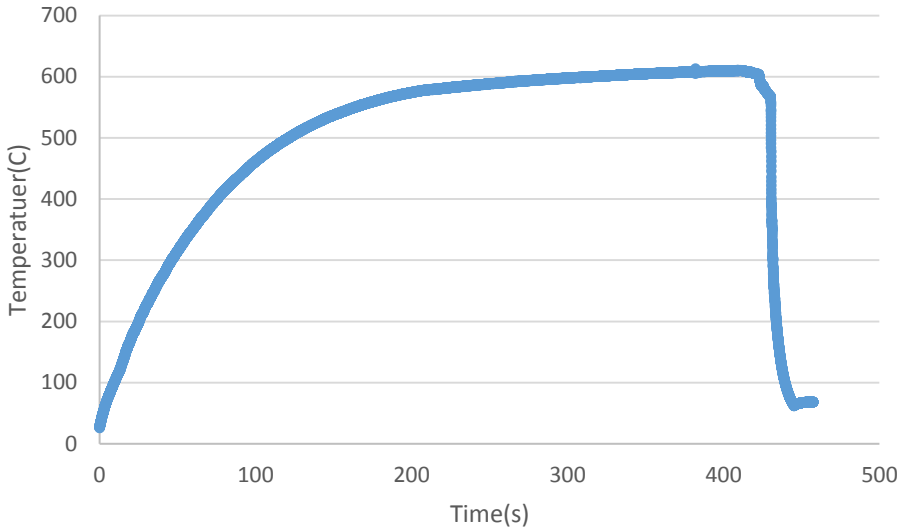

Figure 80 Temperature history for 1.8-mm 22MnB5 steel quenched from 630°C

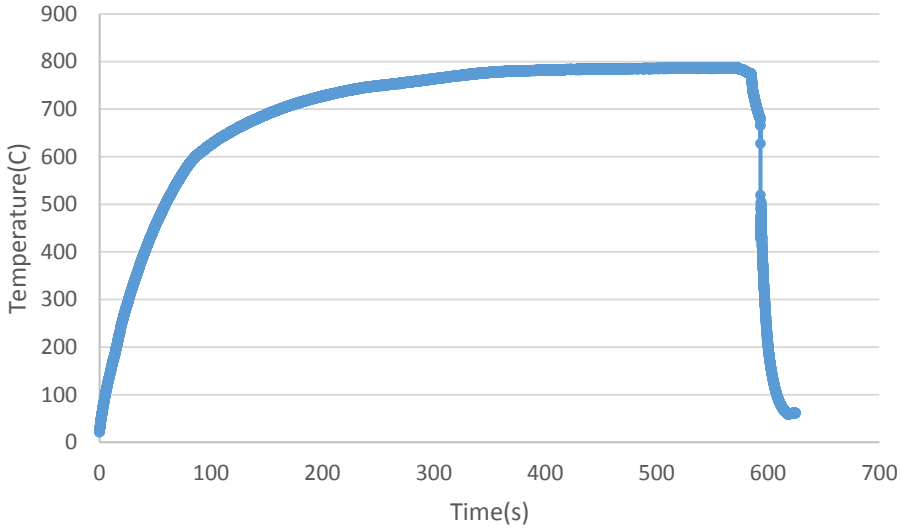

Figure 81 Temperature history for 1.8-mm 22MnB5 steel quenched from 800°C

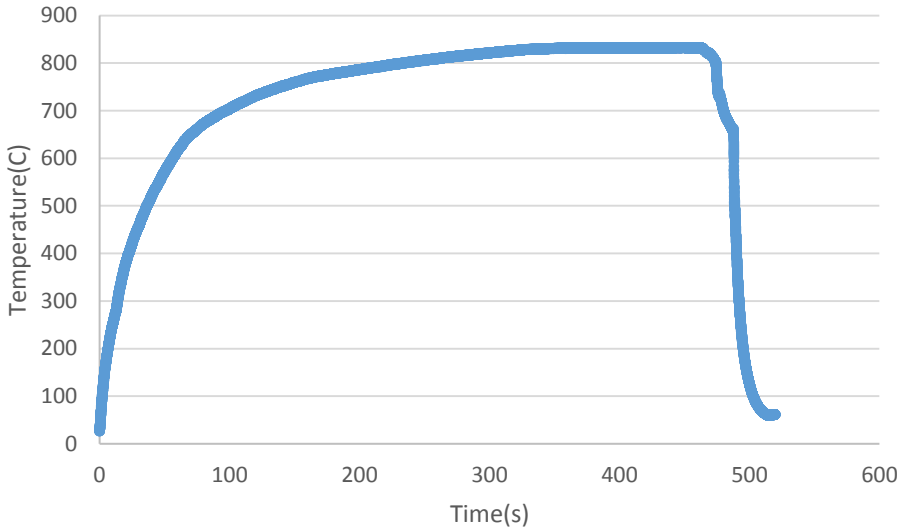

Figure 82 Temperature history for 1.8-mm 22MnB5 steel quenched from 845°C

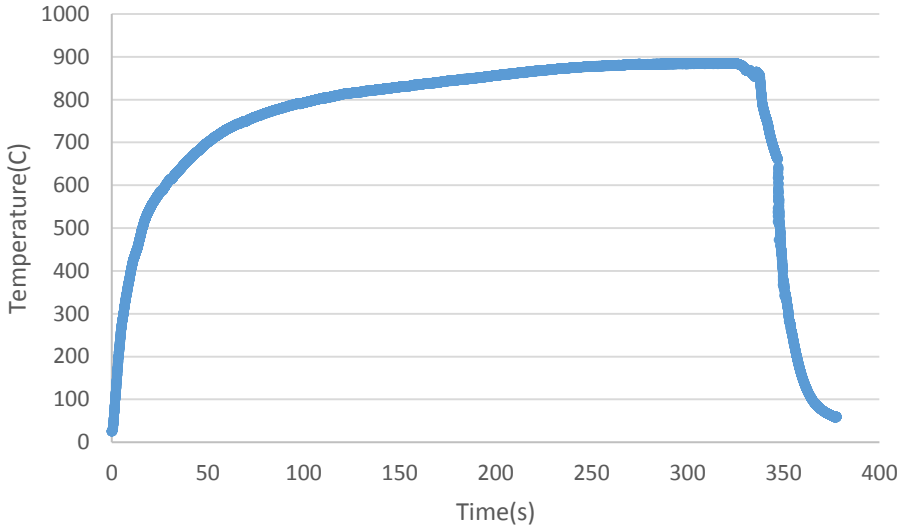

Figure 83 Temperature history for 1.8-mm 22MnB5 steel quenched from 900°C

Appendix E: Micrographs for 1.8-mm 22MnB5 steel sheets quenched from different temperatures.

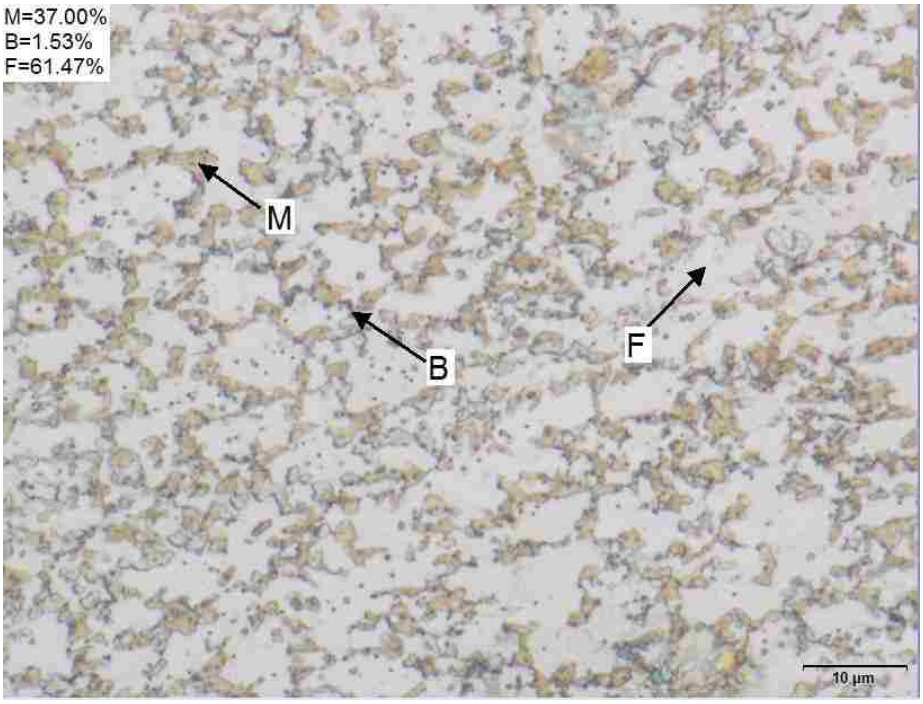

Figure 84 Colour-tint etched optical micrograph for 1.8-mm 22MnB5 steel sheet quenched from 760°C

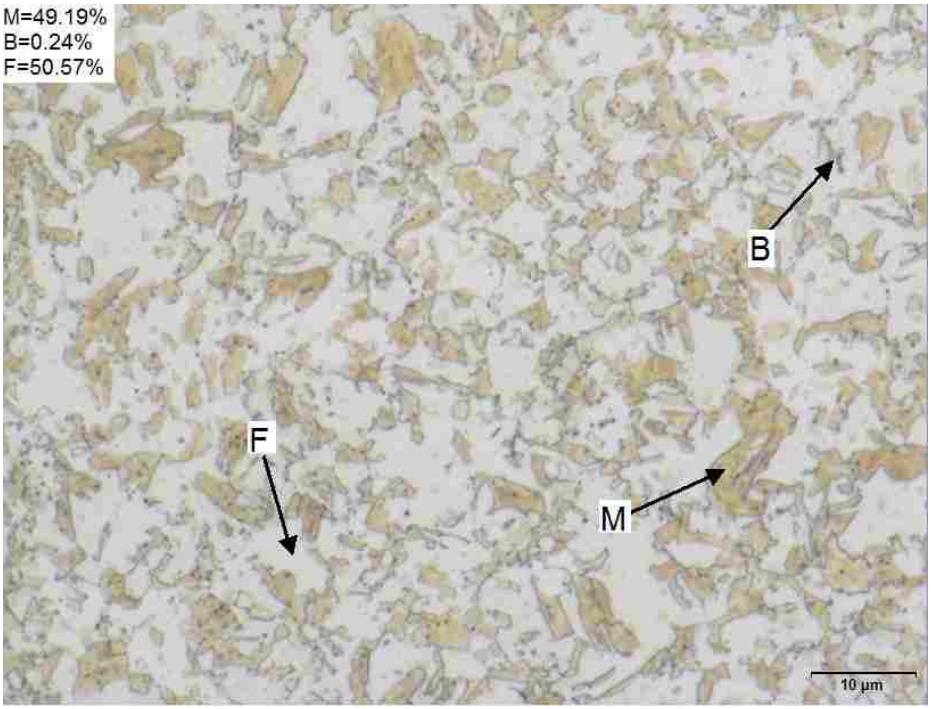

Figure 85 Colour-tint etched optical micrograph for 1.8-mm 22MnB5 steel sheet quenched from 800°C

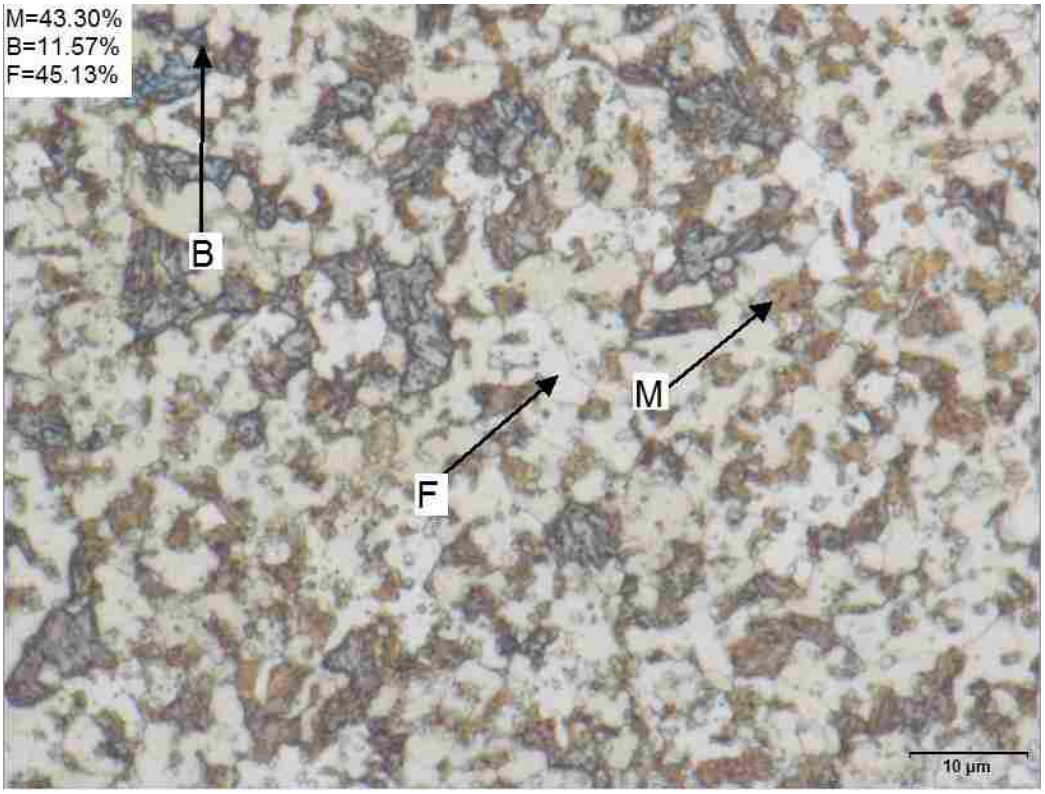

Figure 86 Colour-tint etched optical micrograph for 1.8-mm 22MnB5 steel sheet quenched from 845°C

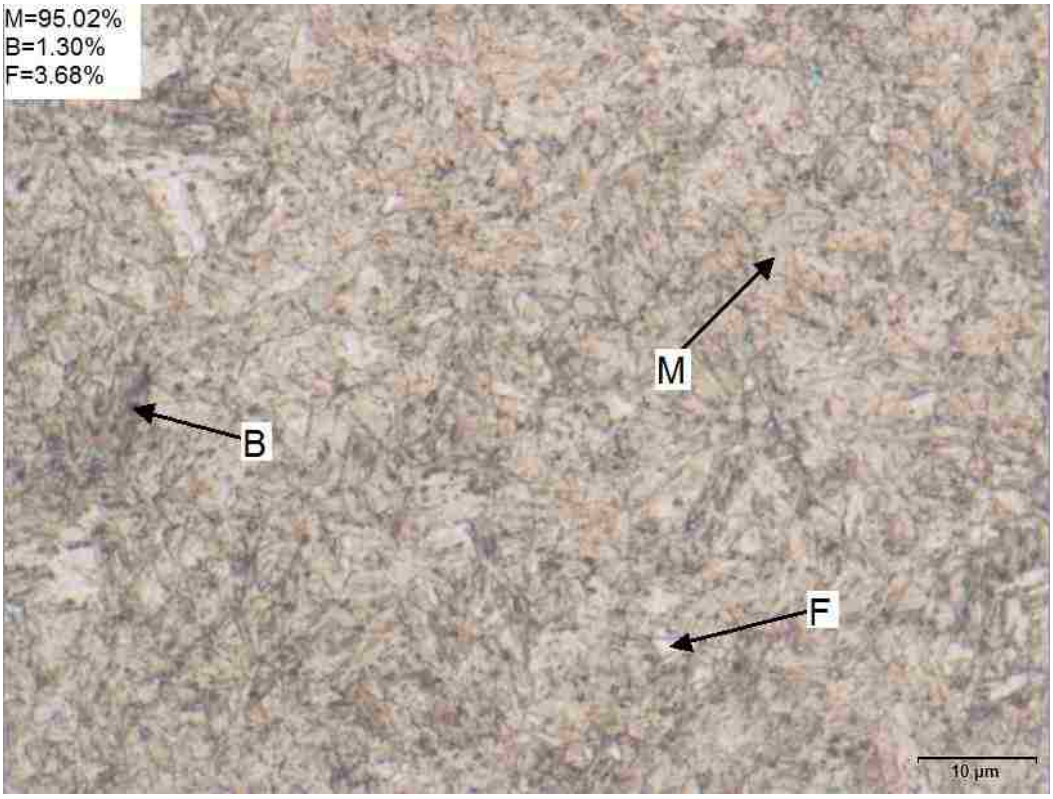

Figure 87 Colour-tint etched optical micrograph for 1.8-mm 22MnB5 steel sheet quenched from 900°C

Appendix F: Drawing of the Furnace Support Frame

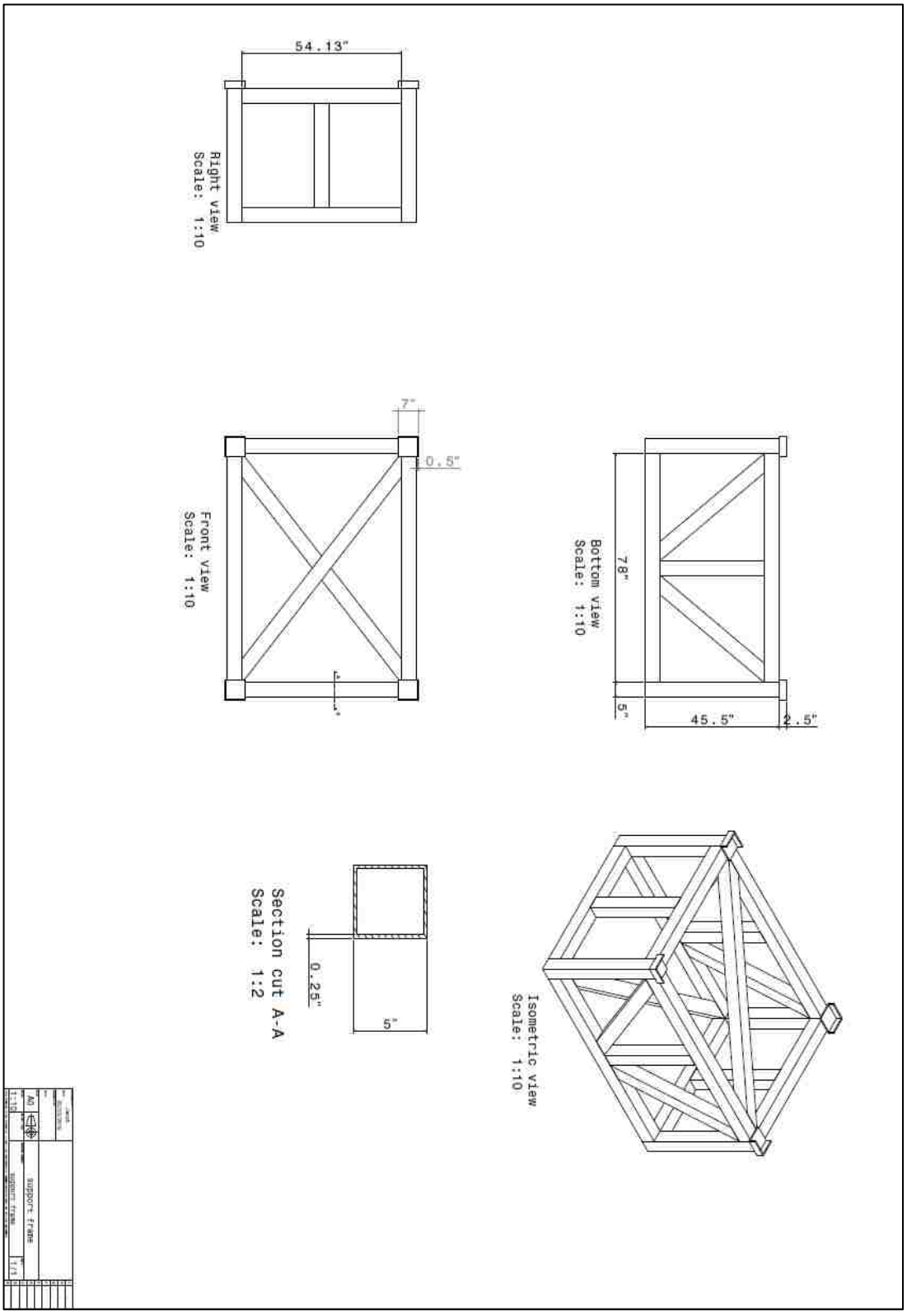

Appendix G: Drawing of the Furnace

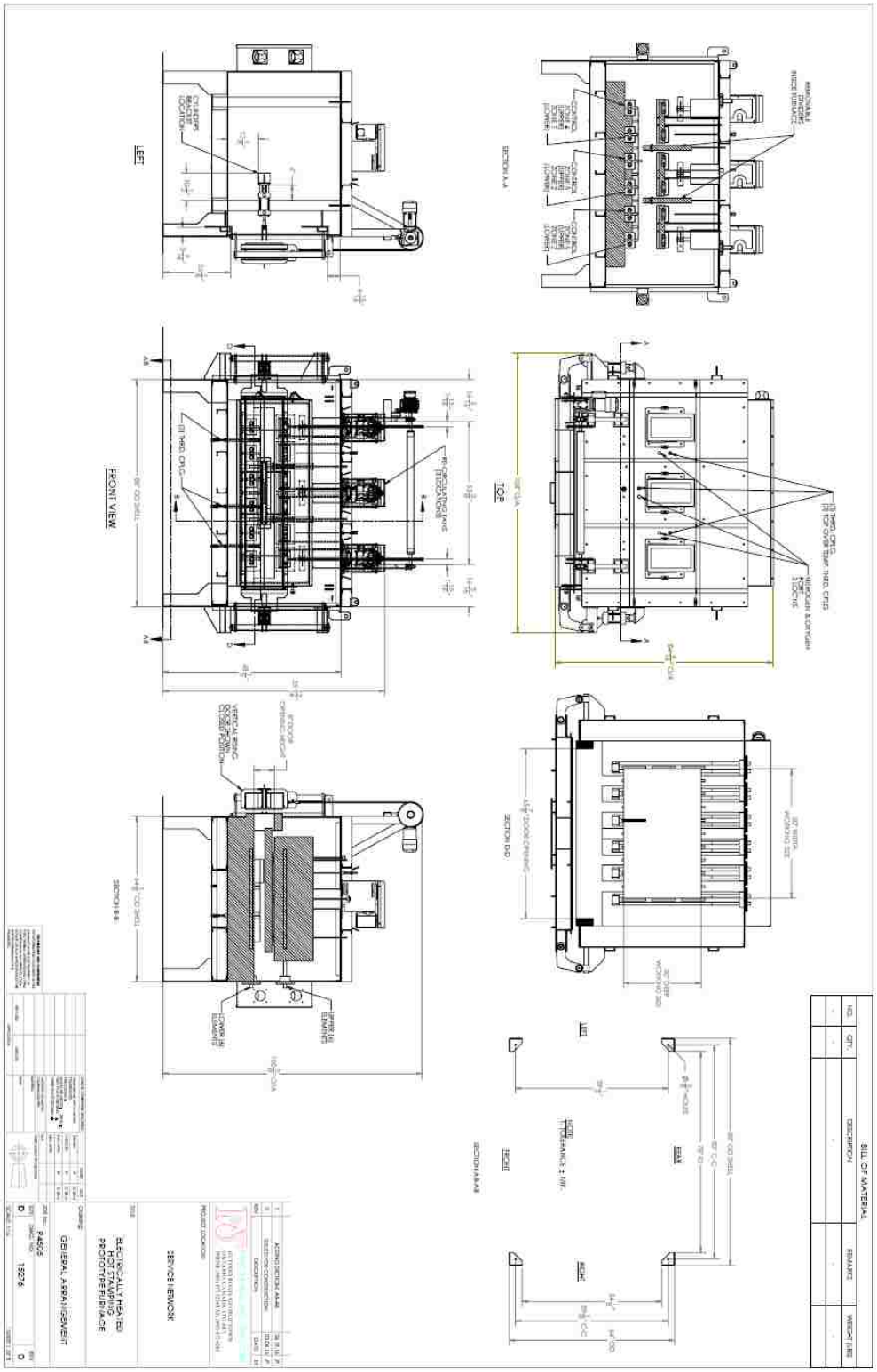

Vita Auctoris

NAME:	Jiakai Shi
PLACE OF BIRTH:	Shanghai, PR China
YEAR OF BIRTH:	1991
EDUCATION:	Chongming High School, Shanghai, China, 2009
	University of Windsor, B.A.Sc., Windsor, ON, 2015
	University of Windsor, M.A.Sc., Windsor, ON, 2018